

## INFORMATION TO USERS

This manuscript has been reproduced from the microfilm master. UMI films the text directly from the original or copy submitted. Thus, some thesis and dissertation copies are in typewriter face, while others may be from any type of computer printer.

The quality of this reproduction is dependent upon the quality of the copy submitted. Broken or indistinct print, colored or poor quality illustrations and photographs, print bleedthrough, substandard margins, and improper alignment can adversely affect reproduction.

In the unlikely event that the author did not send UMI a complete manuscript and there are missing pages, these will be noted. Also, if unauthorized copyright material had to be removed, a note will indicate the deletion.

Oversize materials (e.g., maps, drawings, charts) are reproduced by sectioning the original, beginning at the upper left-hand corner and continuing from left to right in equal sections with small overlaps.

Photographs included in the original manuscript have been reproduced xerographically in this copy. Higher quality 6" x 9" black and white photographic prints are available for any photographs or illustrations appearing in this copy for an additional charge. Contact UMI directly to order.

Bell & Howell Information and Learning  
300 North Zeeb Road, Ann Arbor, MI 48106-1346 USA  
800-521-0600

UMI<sup>®</sup>



**UNIVERSITY OF OKLAHOMA**

**GRADUATE COLLEGE**

**SEMI-ACTIVE STRUCTURAL CONTROL SYSTEMS WITH  
NONLINEAR ACTUATOR DYNAMICS: DESIGN, STABILITY  
ANALYSIS, AND EXPERIMENTAL VERIFICATION**

**A Dissertation**

**SUBMITTED TO THE GRADUATE FACULTY**

**in partial fulfillment of the requirements for the**

**degree of**

**DOCTOR OF PHILOSOPHY**

**By**

**JEFFREY L. KUEHN**

**Norman, Oklahoma**

**2000**

UMI Number: 9994072

UMI<sup>®</sup>

---

UMI Microform 9994072

Copyright 2001 by Bell & Howell Information and Learning Company.

All rights reserved. This microform edition is protected against  
unauthorized copying under Title 17, United States Code.

---

Bell & Howell Information and Learning Company  
300 North Zeeb Road  
P.O. Box 1346  
Ann Arbor, MI 48106-1346

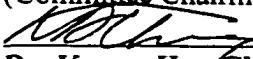
**SEMI-ACTIVE STRUCTURAL CONTROL SYSTEMS WITH  
NONLINEAR ACTUATOR DYNAMICS: DESIGN, STABILITY  
ANALYSIS, AND EXPERIMENTAL VERIFICATION**

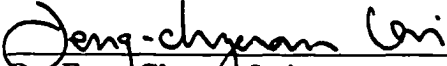
**A DISSERTATION**

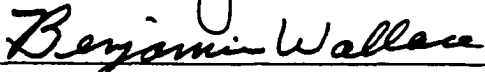
**APPROVED FOR THE SCHOOL OF  
AEROSPACE AND MECHANICAL ENGINEERING**

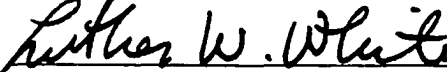
By

  
\_\_\_\_\_  
Dr. Harold L. Stalford  
(Committee Chairman)

  
\_\_\_\_\_  
Dr. Kuang-Hua Chang

  
\_\_\_\_\_  
Dr. Feng-Chyuan Lai

  
\_\_\_\_\_  
Dr. Benjamin Wallace

  
\_\_\_\_\_  
Dr. Luther W. White

**© Copyright by Jeffrey L. Kuehn 2000**

**All Rights Reserved.**

## ACKNOWLEDGEMENTS

This dissertation is dedicated to the memory of Professor William Neff Patten, Ph.D., PE. I will always treasure the time I spent working with him. His groundbreaking research has made a tremendous impact in the field of semi-active control while his work ethic and dedication to his students made a lasting impression on those around him. It is an honor to have him as both a mentor and a friend.

I owe a deep debt of gratitude to Dr. Harold L. Stalford for stepping in and helping me complete this research in spite of his busy schedule. His ideas, guidance and support along with his experience in stability have been invaluable to this work. It has been a pleasure working with him.

I would like to thank Dr. Kuang-Hua Chang, Dr. Feng-Chyuan Lai, Dr. Luther White and Dr. Benjamin Wallace for serving as committee members and for their thorough review and helpful comments on this work. This research would not have been possible without the thoughtful advice and cooperation provided by Dr. Benjamin Wallace and the staff at Fears Structural Engineering Laboratory who graciously allowed us the use of their seismic motion simulator.

It has been a privilege to work with my past and present colleagues in the Controls Laboratory, especially Carlos Borrás, Greg Brock, Derrick Harris, Dr. Jae-Soo Lee, Sarah Leming, Pengfei Ma, Dr. Changki Mo, Dr. Gang Song and Dr. Jinghui Sun. I would also like to thank Ann Patten for her kindness and generosity.

I have thoroughly enjoyed working and discussing technical issues with David Epp over the past few years. His contributions to this work are greatly appreciated. I wish him well with his efforts to extend the results presented in this dissertation.

I also appreciate the contributions of my friends Billy Mays, Greg Williams and their student employees in the AME Shop. Their open door policy and helpfulness is a great benefit to the education and research work within this school.

Finally, I would like to thank my family for their support and encouragement throughout this work. Above all, my wife LeeAnn has stood by me with her love, kindness, thoughtfulness and generosity. I would not have embarked on such a journey without her.

# TABLE OF CONTENT

<b>Acknowledgements .....</b>	<b>iv</b>
<b>List of Figures.....</b>	<b>viii</b>
<b>List of Tables .....</b>	<b>xv</b>
<b>List of Photos .....</b>	<b>xvii</b>
<b>Abstract.....</b>	<b>xviii</b>
<b>Chapter 1: Introduction and Background.....</b>	<b>1</b>
1.1 Introduction.....	1
1.2 Background.....	4
1.3 Organization of the Dissertation .....	11
<b>Chapter 2: Experimental Hardware .....</b>	<b>12</b>
2.1 Seismic Test Structure .....	12
2.2 Electro-hydraulic Seismic Motion Simulator .....	15
2.3 Semi-active Actuators.....	22
2.4 Control Hardware.....	29
<b>Chapter 3: System Modeling and Parameter Identification.....</b>	<b>30</b>
3.1 Structure Modeling and Parameter Identification.....	30
3.2 Semi-active Actuator Model .....	36
3.3 Reduced Order Semi-active Model.....	40

3.4 Semi-active Parameter Identification.....	42
3.5 Valve Parameter Identification .....	44
<b>Chapter 4: Semi-active Control Design .....</b>	<b>46</b>
4.1 Introduction.....	46
4.2 Background.....	47
4.3 General System Model With Nonlinear Semi-active Dynamics .....	50
4.4 Quickest Descent Control Law .....	53
4.5 Lyapunov Stability Analysis.....	54
4.6 Coupled Structure/Actuator System Realization .....	60
4.7 Lyapunov Performance Analysis.....	62
<b>Chapter 5: Experimental Results .....</b>	<b>78</b>
5.1 Introduction.....	78
5.2 Passive Test Results.....	78
5.3 Semi-active Test Results.....	98
<b>Chapter 6: Conclusions and Recommendations .....</b>	<b>117</b>
6.1 Conclusions.....	117
6.2 Recommendations.....	119
<b>References.....</b>	<b>121</b>

## LIST OF FIGURES

<b>Figure 1.1:</b>	Semi-active control devices in the literature.....	7
<b>Figure 2.1:</b>	Three-story test structure .....	13
<b>Figure 2.2:</b>	Test configurations used to determine the performance of the semi-active control system .....	14
<b>Figure 2.3:</b>	Typical accelerometer layout on each floor.....	14
<b>Figure 2.4:</b>	Seismic simulator schematic.....	18
<b>Figure 2.5:</b>	Seismic simulator feedback/feed-forward control block diagram .....	20
<b>Figure 2.6:</b>	Seismic motion simulator acceleration transfer function magnitude with and without a 360-kg test structure.....	20
<b>Figure 2.7:</b>	Seismic motion simulator acceleration transfer function phase with and without a 360-kg test structure.....	21
<b>Figure 2.8:</b>	Seismic motion simulator acceleration tracking response of N-S component of the 1940 El Centro earthquake.....	21
<b>Figure 2.9:</b>	Schematic representation of the variable orifice semi-active actuator .....	22
<b>Figure 2.10:</b>	Dynamic friction of the actuator with no fluid subject to a 10-mm amplitude 0.25-Hz sine wave input .....	24
<b>Figure 2.11:</b>	Valve orifice area vs. valve angle for the Whitey SS-33VF4 ball valve ...	25
<b>Figure 2.12:</b>	Variation of valve opening response time with pressure .....	27
<b>Figure 2.13:</b>	Valve closing response time .....	27
<b>Figure 3.1:</b>	Comparison of experimental and analytical transfer function magnitudes for $x_1/d$ .....	33

<b>Figure 3.2:</b>	Comparison of experimental and analytical transfer function phase responses for $x_1/d$ .....	34
<b>Figure 3.3:</b>	Comparison of experimental and analytical transfer function magnitudes for $x_2/d$ .....	34
<b>Figure 3.4:</b>	Comparison of experimental and analytical transfer function phase responses for $x_2/d$ .....	35
<b>Figure 3.5:</b>	Comparison of experimental and analytical transfer function magnitudes for $x_3/d$ .....	35
<b>Figure 3.6:</b>	Comparison of experimental and analytical transfer function phase responses for $x_3/d$ .....	36
<b>Figure 3.7:</b>	Analytical vs. experimental effective bulk modulus for chamber 1 .....	44
<b>Figure 3.8:</b>	Analytical vs. experimental effective bulk modulus for chamber 2 .....	45
<b>Figure 3.9:</b>	Experimental valve discharge coefficient vs. choke number.....	45
<b>Figure 4.1:</b>	Summary of semi-active structural control design research.....	50
<b>Figure 4.2:</b>	Simulated values of $\ z_1\ _\infty$ for three disturbance cases .....	68
<b>Figure 4.3:</b>	Simulated values of $\ z_2\ _\infty$ for three disturbance cases.....	68
<b>Figure 4.4:</b>	Simulated values of $\ z_3\ _\infty$ for three disturbance cases.....	69
<b>Figure 4.5:</b>	Simulated values of $\ z_4\ _\infty$ for three disturbance cases.....	69
<b>Figure 4.6:</b>	Simulated values of $\ z_5\ _\infty$ for three disturbance cases.....	70
<b>Figure 4.7:</b>	Simulated values of $\ z_6\ _\infty$ for three disturbance cases.....	70
<b>Figure 4.8:</b>	Simulated values of $\ z_7\ _\infty$ for three disturbance cases.....	71

<b>Figure 5.1:</b>	Frequency response function magnitude $z_1 / d$ with actuator operated passively in Position 1. ....	82
<b>Figure 5.2:</b>	Frequency response function magnitude $z_1 / d$ with actuator operated passively in Position 2. ....	82
<b>Figure 5.3:</b>	Frequency response function magnitude $z_2 / d$ with actuator operated passively in Position 1. ....	83
<b>Figure 5.4:</b>	Frequency response function magnitude $z_2 / d$ with actuator operated passively in Position 2. ....	83
<b>Figure 5.5:</b>	Frequency response function magnitude $z_3 / d$ with actuator operated passively in Position 1. ....	84
<b>Figure 5.6:</b>	Frequency response function magnitude $z_3 / d$ with actuator operated passively in Position 2. ....	84
<b>Figure 5.7:</b>	Frequency response function magnitude $\ddot{x}_{11} / d$ with actuator operated passively in Position 1. ....	85
<b>Figure 5.8:</b>	Frequency response function magnitude $\ddot{x}_{11} / d$ with actuator operated passively in Position 2. ....	85
<b>Figure 5.9:</b>	Frequency response function magnitude $\ddot{x}_{12} / d$ with actuator operated passively in Position 1. ....	86
<b>Figure 5.10:</b>	Frequency response function magnitude $\ddot{x}_{12} / d$ with actuator operated passively in Position 2. ....	86
<b>Figure 5.11:</b>	Frequency response function magnitude $\ddot{x}_{21} / d$ with actuator operated passively in Position 1. ....	87

<b>Figure 5.12:</b> Frequency response function magnitude $\ddot{x}_{21} / d$ with actuator operated passively in Position 2. ....	87
<b>Figure 5.13:</b> Frequency response function magnitude $\ddot{x}_{22} / d$ with actuator operated passively in Position 1. ....	88
<b>Figure 5.14:</b> Frequency response function magnitude $\ddot{x}_{22} / d$ with actuator operated passively in Position 2. ....	88
<b>Figure 5.15:</b> Frequency response function magnitude $\ddot{x}_{31} / d$ with actuator operated passively in Position 1. ....	89
<b>Figure 5.16:</b> Frequency response function magnitude $\ddot{x}_{31} / d$ with actuator operated passively in Position 2. ....	89
<b>Figure 5.17:</b> Frequency response function magnitude $\ddot{x}_{32} / d$ with actuator operated passively in Position 1. ....	90
<b>Figure 5.18:</b> Frequency response function magnitude $\ddot{x}_{32} / d$ with actuator operated passively in Position 2. ....	90
<b>Figure 5.8:</b> Frequency response function magnitude $\ddot{y}_1 / d$ with actuator operated passively in Position 1. ....	91
<b>Figure 5.20:</b> Frequency response function magnitude $\ddot{y}_1 / d$ with actuator operated passively in Position 2. ....	91
<b>Figure 5.21:</b> Frequency response function magnitude $\ddot{y}_2 / d$ with actuator operated passively in Position 1. ....	92
<b>Figure 5.22:</b> Frequency response function magnitude $\ddot{y}_2 / d$ with actuator operated passively in Position 2. ....	92

<b>Figure 5.23:</b> Frequency response function magnitude $\ddot{y}_3 / d$ with actuator operated passively in Position 1. ....	93
<b>Figure 5.24:</b> Frequency response function magnitude $\ddot{y}_3 / d$ with actuator operated passively in Position 2. ....	93
<b>Figure 5.25:</b> Frequency response function magnitude $z_1 / d$ with semi-active control in Position 1. ....	101
<b>Figure 5.26:</b> Frequency response function magnitude $z_1 / d$ with semi-active control in Position 2. ....	101
<b>Figure 5.27:</b> Frequency response function magnitude $z_2 / d$ with semi-active control in Position 1. ....	102
<b>Figure 5.28:</b> Frequency response function magnitude $z_2 / d$ with semi-active control in Position 2. ....	102
<b>Figure 5.29:</b> Frequency response function magnitude $z_3 / d$ with semi-active control in Position 1. ....	103
<b>Figure 5.30:</b> Frequency response function magnitude $z_3 / d$ with semi-active control in Position 2. ....	103
<b>Figure 5.31:</b> Frequency response function magnitude $\ddot{x}_{11} / d$ with semi-active control in Position 1. ....	104
<b>Figure 5.32:</b> Frequency response function magnitude $\ddot{x}_{11} / d$ with semi-active control in Position 2. ....	104
<b>Figure 5.33:</b> Frequency response function magnitude $\ddot{x}_{12} / d$ with semi-active control in Position 1. ....	105

<b>Figure 5.34:</b> Frequency response function magnitude $\ddot{x}_{12} / d$ with semi-active control in Position 2. ....	105
<b>Figure 5.35:</b> Frequency response function magnitude $\ddot{x}_{21} / d$ with semi-active control in Position 1. ....	106
<b>Figure 5.36:</b> Frequency response function magnitude $\ddot{x}_{21} / d$ with semi-active control in Position 2. ....	106
<b>Figure 5.37:</b> Frequency response function magnitude $\ddot{x}_{22} / d$ with semi-active control in Position 1. ....	107
<b>Figure 5.38:</b> Frequency response function magnitude $\ddot{x}_{22} / d$ with semi-active control in Position 2. ....	107
<b>Figure 5.39:</b> Frequency response function magnitude $\ddot{x}_{31} / d$ with semi-active control in Position 1. ....	108
<b>Figure 5.40:</b> Frequency response function magnitude $\ddot{x}_{31} / d$ with semi-active control in Position 2. ....	108
<b>Figure 5.41:</b> Frequency response function magnitude $\ddot{x}_{32} / d$ with semi-active control in Position 1. ....	109
<b>Figure 5.42:</b> Frequency response function magnitude $\ddot{x}_{32} / d$ with semi-active control in Position 2. ....	109
<b>Figure 5.43:</b> Frequency response function magnitude $\ddot{y}_1 / d$ with semi-active control in Position 1. ....	110
<b>Figure 5.44:</b> Frequency response function magnitude $\ddot{y}_1 / d$ with semi-active control in Position 2. ....	110

<b>Figure 5.45:</b> Frequency response function magnitude $\ddot{y}_2 / d$ with semi-active control in Position 1. ....	111
<b>Figure 5.46:</b> Frequency response function magnitude $\ddot{y}_2 / d$ with semi-active control in Position 2. ....	111
<b>Figure 5.47:</b> Frequency response function magnitude $\ddot{y}_3 / d$ with semi-active control in Position 1. ....	112
<b>Figure 5.48:</b> Frequency response function magnitude $\ddot{y}_3 / d$ with semi-active control in Position 2. ....	112

## LIST OF TABLES

<b>Table 4.1:</b>	Modal control penalties and resulting gains .....	63
<b>Table 4.2:</b>	State control penalties and resulting gains.....	64
<b>Table 4.3:</b>	Infinity norms for Disturbance Law 1 with valve open.....	72
<b>Table 4.4:</b>	Infinity norms for Disturbance Law 1 with control.....	73
<b>Table 4.5:</b>	Infinity norms for Disturbance Law 2 with control .....	74
<b>Table 4.6:</b>	Infinity norms for white noise acceleration disturbance with control .....	75
<b>Table 4.7:</b>	Theoretical performance index bounds versus maximum simulated values .....	76
<b>Table 4.8:</b>	Attractor set radius versus maximum simulated values.....	77
<b>Table 5.1:</b>	RMS relative displacements and absolute accelerations for passive configurations subjected to a broadband input .....	94
<b>Table 5.2:</b>	Peak relative displacements and absolute accelerations for passive configurations subjected to a broadband input .....	95
<b>Table 5.3:</b>	RMS relative displacements and absolute accelerations for passive configurations subjected to the El Centro earthquake input .....	96
<b>Table 5.4:</b>	Peak relative displacements and absolute accelerations for passive configurations subjected to the El Centro earthquake input.....	97
<b>Table 5.5:</b>	RMS relative displacements and absolute accelerations for semi-active configurations subjected to a broadband input .....	113
<b>Table 5.6:</b>	Peak relative displacements and absolute accelerations for semi-active configurations subjected to a broadband input .....	114

**Table 5.7:** RMS relative displacements and absolute accelerations for passive configurations subjected to the El Centro earthquake input .....115

**Table 5.8:** Peak relative displacements and absolute accelerations for passive configurations subjected to the El Centro earthquake input .....116

## LIST OF PHOTOS

<b>Photo 2.1:</b>	University of Oklahoma seismic motion simulator including test structure.....	17
<b>Photo 2.2:</b>	Semi-active hydraulic actuator assembly.....	22
<b>Photo 2.3:</b>	Ultimag rotary actuator with heat sink and helical coupling .....	26

# ABSTRACT

Semi-active control is emerging as a promising technology for reducing undesirable vibrations in dynamic systems. At present, there is a significant worldwide effort to develop semi-active control systems for structures that resist seismic behavior. To get stability results and performance, however, past efforts have utilized linear control synthesis and analysis techniques, neglecting the nonlinear dynamics of semi-active actuators. An open problem in the literature is establishing the stability of semi-active control systems with nonlinear actuator dynamics. The main focus of this dissertation is on that open stability problem.

We develop and experimentally validate control laws that provide stable closed-loop behavior and good performance for semi-active control systems with nonlinear actuator dynamics. In particular, we treat variable orifice hydraulic semi-active actuators installed on a small-scale seismic structure subjected to seismic motions. First, we design and manufacture an experimental semi-active actuator specifically for the work herein. Next, we develop a new dynamic model for the variable-orifice hydraulic semi-active actuator that accounts for laminar, turbulent and transition flow characteristics. After that, we formulate two general conditions to be met by the nonlinear dynamics of semi-active actuators. This formulation covers a large class of semi-active control systems with nonlinear actuator dynamics. Then, we use the quickest descent Lyapunov method in developing the controller design for this large class. In a theorem, we prove that our controller provides stability for this new class of semi-active control systems with nonlinear actuator dynamics. This provides a solution to the open problem and is one of the major results of this dissertation.

After treating the stability problem, we examine the performance of our controllers. We consider bounded-input/bounded-output (BIBO) stability for multiple bounded excitation disturbances. In a theorem, we establish a ball of ultimate boundedness (stable attractor) whose size is based on the upper bound of the disturbances. The performance of the closed loop semi-active system can be tuned by varying either state or modal penalties in a positive definite performance index  $Q$ . Simulation results using a variety of disturbance inputs are provided to demonstrate the effectiveness of the quickest descent control law for a variety of penalties. The best controller design was derived using a  $Q$  matrix that emphasized the lowest frequency mode of the structure and also the differential pressure state of the semi-active actuator. The system 1-norm and simulation results are used to establish that the guaranteed performance (i.e., bound of the stable attractor) is too conservative by two orders of magnitude for the best performing controller. This part of the work of the dissertation opens up a new problem for future researchers on how to construct guaranteed performance bounds that are less conservative.

The response characteristics of the quickest descent Lyapunov controller are also demonstrated experimentally. A small-scale test structure outfitted with a single variable orifice semi-active actuator is excited using a single axis electro-hydraulic seismic motion simulator. Two seismic inputs are used to excite the test structure. One is band-limited white noise ground acceleration and the other is the North/South component of the 1940 El Centro earthquake. The tracking performance of the simulator is documented herein to assure the validity of the experimental data. The test results are compared to

force/velocity control law used by many semi-active researchers. The experimental work demonstrates that our quickest descent control design technique is a valuable tool for designing stable semi-active control laws that exhibit good performance against realistic seismic inputs. For a band limited white noise input the Lyapunov control law is able to reduce the maximum relative displacement between the ground and first floor of the test structure by 78% compared to a 54% reduction yielded by the force/velocity control law. The Lyapunov controller netted a 38% decrease for a component of the 1940 El Centro earthquake while the force/velocity control provided a 41% reduction.

# CHAPTER 1

## INTRODUCTION AND BACKGROUND

### 1.1 Introduction

Earthquakes are one of the most feared natural forces known to man. They can occur almost anywhere devastating vast areas in a matter of seconds. According to statistics from the United States Geological Survey National Earthquake Information Center, an average of one great earthquake (magnitude greater than 8 on the Richter Scale), 18 major earthquakes (magnitudes 7-8) and 120 strong earthquakes (magnitudes 6-7) occur worldwide each year. There are also more than 9000 minor seismic events (magnitudes 1-3) each day. When large earthquakes strike heavily populated areas, they result in a tremendous amount of property damage and loss of life. The 1989 Loma Prieta earthquake, which registered 7.2 on the Richter Scale, caused 6 billion dollars in damage and 63 deaths while injuring 3,757 others. The 6.7 magnitude Northridge quake in 1994 resulted in 57 deaths, 9,000 injuries and 20 billion dollars in damage. Approximately 9,000 buildings were seriously damaged in the 10-20 seconds of strong shaking which displaced 20,000 people from their homes. The 1995 Kobe earthquake was extremely devastating in terms of structural damage and casualties. The 6.9 magnitude seismic event destroyed 100,000 buildings, killing 5,100 and injuring 27,000.

Civil structures are especially susceptible to the extreme loads resulting from strong seismic motions. Subsequently, many injuries and deaths attributed to earthquakes are caused by structural damage or collapse. While nothing can be done to prevent

earthquakes, researchers are continually striving to better understand how to reduce the effects of seismic motions on structures. The ultimate goal is low cost seismic resistant buildings and bridges, which maintain integrity in the event of an earthquake and prevent excessive acceleration levels that might lead to occupant injuries. A variety of passive structural designs have been developed which provide improved strength and dynamic response characteristics. There are two general passive techniques for reducing seismic damage. The first approach is to isolate the structure from ground motions. Numerous companies around the world manufacture seismic base isolators for such an application. The isolators essentially act as a low-pass filter on ground motions transmitted to the structure and tend to reduce the fundamental oscillatory frequency of the structure. Many seismic isolators incorporate lead cores to tailor the damping characteristics of the devices. Another passive vibration control technique involves adding energy dissipating elements to a structure. Ductile components, which are designed to yield but not fail in the event of an earthquake, are commonly incorporated into buildings to transform vibration energy into heat and noise. A variety of other energy dissipating devices are commercially available for structures including viscous dampers and friction dampers.

Over the past twenty years, there has been considerable research on the use of motion control systems to mitigate structural vibrations. Many promising active, semi-active and hybrid control strategies have been demonstrated as a result of this effort. Of these potential strategies, semi-active devices are well suited to the seismic response control problem because the power required to operate a semi-active actuator is small compared to the achievable control forces. Such devices can operate for several hours on batteries in the event of a power outage during an earthquake. Since large power sources

are not required for semi-active control systems, the hardware is comparable to passive dampers in terms of first cost and maintenance costs. Furthermore, in many cases, semi-active controllers have been shown to exhibit comparable performance to active control systems.

While there has been a significant amount of research in the development and testing of semi-active control devices for civil structures, little emphasis has been placed on tailoring analysis and control synthesis tools to the semi-active control problem. Although many semi-active actuators have nonlinear dynamic characteristics that couple with the structural dynamics, most researchers neglect the actuator dynamics and utilize linear control synthesis techniques. Since the dynamics of the structure and actuator couple, it is also appropriate to consider the coupled system realization for any stability analysis. To date, the stability problem for systems with non-linear semi-active control devices has not been adequately addressed in the literature.

The work presented here describes the development and testing of stable semi-active control laws for seismic response reduction. The dissertation encompasses the design, modeling, construction, control algorithm development, stability analysis and experimental verification of a variable-orifice hydraulic semi-active control system for a small-scale three-story test structure. First, the design and selection of the experimental hardware is presented. Secondly, mechanistic models are developed for the test structure and the semi-active actuator. Next, a method for designing stable bi-state control algorithms based on Lyapunov's direct method is developed for a general class of semi-active control systems. The closed loop semi-active system is shown to provide quadratic convergence to a stable attractor (ball of ultimate boundedness) centered at the origin for

bounded disturbances. The general control law and stability results are applied to a coupled realization of the structure and a single nonlinear semi-active actuator. Simulation results demonstrating the response characteristics of the structure with a variety of control laws and disturbances are presented and compared to the performance bounds generated for each control law. Finally, experimental results obtained with the scale seismic test structure are presented for several cases: a) a semi-active Lyapunov control law, b) a simple collocated energy minimization semi-active control algorithm, c) the semi-active hardware operated passively with the valve open, d) the semi-active hardware operated passively with the valve closed and e) the bare structure with no control hardware. The different test results are used to evaluate the performance of the semi-active Lyapunov control law.

## **1.2 Background**

Yao (1972) introduced the concept of applying active control theory to the design of civil engineering structures. The work suggested that active control systems could be used to improve the safety of civil structures and possibly increase the allowable height of buildings. Since that time, the field of active structural control has gained considerable attention. The variable nature of active control systems would allow structures to adapt to changing load characteristics. Many devices including active tendon control systems (Chung, et al., 1988) and active mass dampers (Dyke, et al, 1996a, Sakamoto, et al, 1994) have been tested in scale laboratory experiments and full-scale structures. Although active control systems have shown exceptional abilities, there are a number of practical issues limiting widespread acceptance of such devices. One of the primary limitations of

active structural control systems is the reliance on tremendous amounts of external power to mitigate vibrations in a massive structure. For instance, since electrical service is often lost in large earthquakes, a local power source, such as a generator would be required to operate the control system, adding to the first cost and upkeep of the installation. The ability to input large amounts of energy into a structure also introduces questions about stability and system behavior in the event of a malfunction. While the United States has been reluctant to implement active control systems in actual structures, active mass dampers have been installed in three buildings in Japan and one in China. (Spencer and Sain, 1997)

Semi-active devices provide a compromise between passive and active control systems. An extensive amount of research has been conducted on applying semi-active control devices to improve the ride and handling characteristics of automobile suspensions since the concept was introduced. (Karnopp, et al. 1974) The work indicated that semi-active force generators could provide substantial performance gains over passive suspensions without the high cost and complexity of active control devices. Hrovat et al. (1983) first proposed the idea of semi-active structural control to mitigate wind-induced vibrations in a single degree of freedom building model using a semi-active tuned mass damper. Simulations, which used a clipped linear quadratic control law and neglected actuator dynamics, indicate the semi-active system provided a 30% reduction in root mean square (RMS) displacement and a 24% reduction in RMS acceleration compared to a passive tuned mass damper system.

Since that initial work, numerous semi-active actuator devices, relying on a variety of technologies, have been proposed, designed and tested. The variety of devices

is illustrated in Figure 1.1. Ehrgott and Masri (1994), Gavin (1994) and Gavin, et al. (1996) investigated the design, modeling and performance of electrorheological (ER) fluid dampers for structural control. Spencer, et al. (1997) developed a model for a prototype magnetorheological (MR) fluid damper. Spencer, et al. (1998) reported the modeling and testing of a 200-kN MR damper designed for controlling full-scale structures. Akbay and Aktan (1990), Feng, et al. (1993), and Dowdell and Cherry (1994) have investigated semi-active variable friction dampers. Nagarajaiah and Mate (1998) developed and tested a continuously variable stiffness device. Harmonic shake table tests indicate the system is capable of effectively reduce the displacement and acceleration of a single degree of freedom test structure. Mo, et al. (1996) and Patten, et al. (1998) developed a model for a variable orifice hydraulic semi-active vibration absorber (SAVA). Symans and Constantinou (1997) described the modeling and extensive testing of a semi-active device with variable linear damping characteristics. There are a variety of different hardware configurations for each type of semi-active actuator as well as a variety of methods to incorporate the devices in a structure.

A number of researchers have experimentally demonstrated the performance of semi-active control systems on realistic structures. Kobori, et al. (1993) and Kamagata and Kobori (1994) reported the installation of an active variable-stiffness system on a full-scale three-story test structure. The control system is designed to maintain a non-resonant structural state based on the excitation input to the structure. The system is shown to effectively reduce structural vibration.

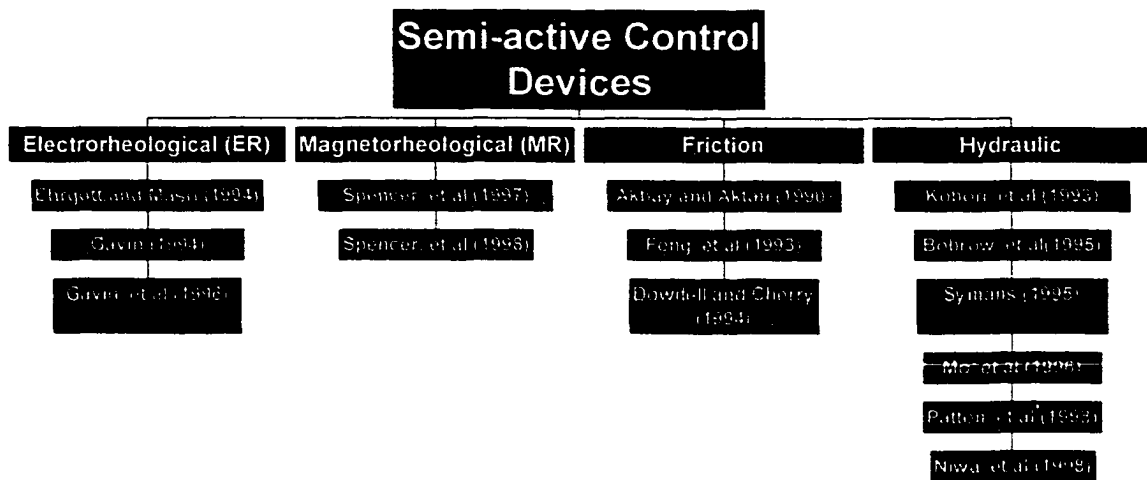


**Figure 1.1:** Semi-active control devices in the literature

Patten, et al. (1994) tested the performance of a variable orifice semi-active damper on a 1/12-scale three-story test structure. A bi-state Lyapunov control algorithm was used for the tests. The device provided a 54% reduction in interstory drift where the actuator was positioned.

Bobrow, et al. (1995) tested the performance of a variable orifice semi-active actuator on a three-story scale test structure. The actuator was filled with air rather than hydraulic oil to prevent large forces on the structure. A maximum energy dissipation algorithm was used to release the stored energy in the actuator by rapidly opening and closing the valve. The structure was excited by an electric motor with an eccentric mass. The system provided approximately a 50% reduction in peak acceleration.

Symans (1995) and Symans and Constantinou (1997) experimentally investigated the performance of a variable-orifice hydraulic semi-active damper on a planar small-scale structure. The dampers were designed to provide adjustable linear viscous damping characteristics. A clipped optimal controller and a sliding mode controller were designed for the structure. The actuator dynamics were not included in the control designs. The

performance of the control algorithms was experimentally obtained and compared to the response of the bare structure and the response of the structure with the dampers operated passively with a minimum damping ratio (4%) and with a maximum damping ratio (14%). The results indicate that both the control algorithms yielded similar performance gains but neither provided any improvement over the passive system configured for maximum damping.

Dyke (1996) and Dyke et al., (1996b) experimentally verified the performance of a MR damper control system on a planar three-story test structure. The system utilized clipped-optimal acceleration feedback controls designed using  $H_2/LQG$  control methods. The test structure was subjected to a scaled component of the 1940 El Centro earthquake with and without the MR damper. The control system provided a 75% reduction in the peak third floor displacement and a 48% reduction in peak third floor acceleration.

Patten (1998) and Patten, et al. (1999) reported experimental results for the first full-scale semi-active structural control system tested in the United States. The control system, installed on an interstate highway bridge near Purcell, Oklahoma, was designed to extend the service life of the bridge by reducing dynamic stresses induced by heavy vehicles. The system was shown to reduce the peak stress reversals in the bridge girders by 40%, extending the safe life of the structure by at least 50 years. Kuehn, et al. (1999) presented test data for a second-generation semi-active bridge stiffener system that does not protrude below the bottom flanges of the bridge beams. Fatigue calculations based on the experimental results indicate that the reduction in stress provided by the non-protruding stiffener system will extend the safe life of the bridge by 40 years.

Niwa, et al. (1998) reported the first installation of a semi-active damper system in an actual building. The five-story structure includes eight actuators on the first four floors (two actuators per floor) oriented along the weak axis of the structure. Analytical results indicate the system provides an 80% reduction in maximum inter-story drift when subjected to a magnitude 8.4, artificial earthquake input. Kurata, et al. (2000) provide test results for the structure which was excited with a 100-kN eccentric mass exciter. The semi-active damper system provided an 80% reduction in peak deflection of the roof floor compared to the uncontrolled structural response.

A comprehensive description of the progress in the development of structural control techniques is provided in a special edition of the *Journal of Engineering Mechanics*. (Housner, et al., 1997) Spencer and Sain (1997) chronicle recent developments in structural control systems including the implementation of such systems in full-scale structures and the different types and characteristics of actuators under investigation. Symans and Constantinou (1999) review the development of semi-active structural control systems with an emphasis on experimental work conducted in this area.

It is well known that stability is an essential characteristic for any active control system. Unfortunately, the stability problem for semi-active control systems is rarely addressed. Dyke, et al. (1998), Spencer, et al. (1998), and Jansen and Dyke (2000) assert that semi-active control systems are inherently stable in the bounded input - bounded output sense without proof. Corless and Leitmann (1997) proved that a variable stiffness controller could destabilize a system if the control logic is improperly selected. Leitmann (1994) investigated the stability of control laws for a semi-active device with both variable linear damping and variable linear stiffness characteristics. One of the control

laws was developed using Lyapunov stability theory. The Lyapunov controller was shown to be stable to a ball about the origin for a bounded excitation. The work treated both the case in which damping and stiffness could be regulated independently and the case where the stiffness and damping are regulated jointly. Neither paper included nonlinear actuator dynamics.

Although many complex actuator models have been developed for semi-active devices, researchers have not utilized these models for proving stability of the closed-loop systems. In fact, only a few researchers consider the actuator dynamics for the control synthesis. Patten et al. (1994, 1999) utilizes a control law aimed at minimizing the first derivative of a quadratic Lyapunov function. While the control law development incorporates nonlinear semi-active actuator dynamics, the resulting controller does not guarantee asymptotic stability because the system matrix used in the design has a zero eigenvalue.

The work herein presents a technique for designing quickest descent semi-active controllers based on quadratic Lyapunov functions. The resulting control laws are shown to provide quadratic convergence to a ball of ultimate boundedness for bounded disturbance inputs for a general class of semi-actively controlled systems. The performance of these control laws is demonstrated with simulation and experimental results for a small-scale three story seismic structure controlled with a single variable orifice semi-active actuator. This is the first work to establish stability for systems that incorporate nonlinear semi-active actuator dynamics.

### **1.3 Organization of the Dissertation**

First, the experimental hardware used in the experiments is described in detail in Chapter 2. The test structure, shake table, semi-active actuator, sensors and related electronics are included. The third chapter provides the development of detailed models for the semi-active actuator and test structure and the procedures used to identify the model parameters. A simplified nonlinear model of the semi-active actuator that accounts for laminar, transition and turbulent flow is also developed to assist in control synthesis. The fourth chapter includes the development of a quickest descent Lyapunov control design technique for coupled systems with nonlinear actuator dynamics. Stability is established for this control law provided the uncontrolled structure is stable provided the semi-active actuator satisfies two general conditions. Numerous simulation results for the three-story structure with a single semi-active actuator are also presented. The fifth chapter describes the experimental procedures and provides a comparison of experimental results for the following cases: a) no semi-active actuator, b) the semi-active actuator valve fixed in the open position, c) the semi-active actuator valve fixed in the closed position, d) with a simple collocated force/velocity semi-active control law and e) with a quickest descent Lyapunov control law. The dissertation closes with conclusions on the analytical and experimental results and recommendations for future work.

# **CHAPTER 2**

## **EXPERIMENTAL HARDWARE**

The objective of the research reported here is to design, implement and test stable semi-active seismic response control systems for a small-scale structure within a laboratory setting. To insure the success of the experiment, each hardware component was carefully designed or selected to satisfy its specified function. This chapter provides a detailed description of the experimental hardware. Most of the components discussed herein were designed and manufactured at OU. First, the characteristics of the fully instrumented small-scale 3-story test structure used to validate the control performance are outlined. Second, the electro-hydraulic seismic motion simulator used to subject the test specimen to reference seismic motions is described in detail. (Kuehn, et al., 1999) (Brock, 2000) A complete description of the hydraulic semi-active control actuator and related sensory hardware is provided next. Finally, the control electronics including the control computer, the interface hardware and signal conditioning circuitry are described.

### **2.1 Seismic Test Structure**

A three-story test structure depicted in Figure 2.1 is used to demonstrate the effectiveness of the semi-active structural control system. The structure is a ¼ scale single bay steel moment-resisting frame utilizing artificial mass simulation. The structure was designed to have the same frequency content as the model described by Soong, et al (1987) and a total weight within the capacity of the seismic shake table. The design of the test specimen allows the addition of stiffeners and mass elements to obtain a variety

of structural configurations. The structure includes fixtures to mount control actuators diagonally between each of the floors in the  $x$ - $z$  plane and between the ground and first floor in the  $y$ - $z$  plane. The actuator configurations for the experimental results provided herein are oriented along the  $x$ - $z$  plane and are indicated in Figure 2.2. As shown in Figure 2.1, the motion of the structure was unconstrained except for a diagonal truss rod placed between the base and first floor to couple bending in the  $y$ -axis with torsion about the  $z$ -axis. The coupling provided a slight increase in the  $y$ -axis natural frequencies to offset them from the  $x$ -axis frequencies. For the experiments here, the total mass of the structure was 360-kg with each floor having an equal mass of 120-kg. The acceleration of each floor of the structure was sensed with three ICS model 3028-002 piezo-resistive accelerometers. The accelerometer layout typical of each floor is shown in Figure 2.3. The relative  $x$ -axis (control axis) displacements of the structure were measured using RDP Electrosense DC/DC LVDTs positioned diagonally between the floors.

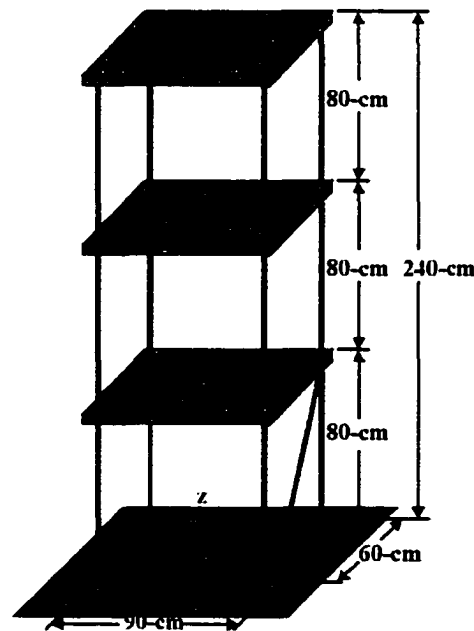


**Figure 2.1:** Three-story test structure

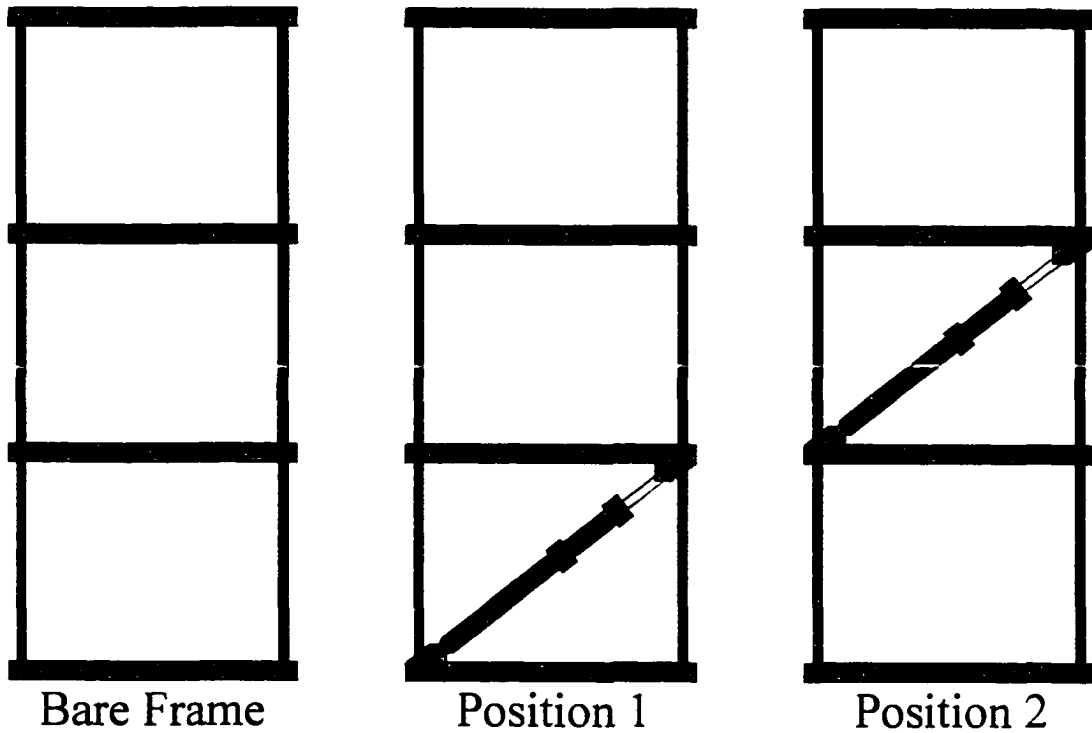


**Figure 2.2:** Test configurations used to determine the performance of the semi-active control system.

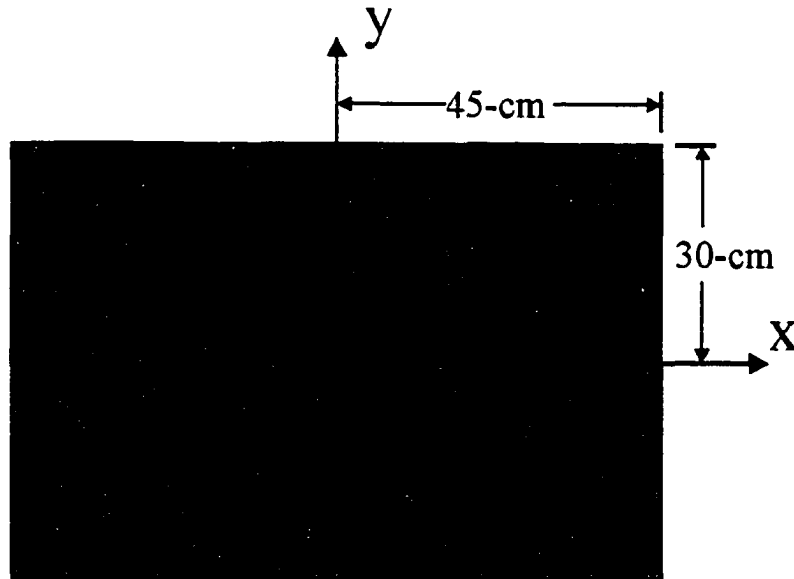


**Figure 2.3:** Typical accelerometer layout for each floor (red dots denote accelerometers) for  $i=1^{\text{st}}, 2^{\text{nd}}$  and  $3^{\text{rd}}$  floor

## **2.2 Electro-hydraulic Seismic Motion Simulator**

Experimental demonstration of seismic protection methods requires a means of subjecting a test structure to reference seismic inputs. Seismic motion simulators (shake tables) are commonly used to generate such motions within a laboratory setting. Even though many researchers have conducted work to improve the tracking fidelity of seismic simulators, the total problem has not been addressed. For any experimental data obtained using a seismic shake table to be meaningful, it is essential that the shaker precisely replicate the desired trajectory (both magnitude and phase) over the frequency spectrum of the reference input with the dynamic test structure installed on the table. Blondet and Esparza (1988) analytically investigated coupling effects between a seismic simulator and test structure. The work indicated the coupling degraded simulator tracking performance near the fundamental frequencies of the test structure and reduced stability margins of the shake table. A recent ASCE conference included two sessions devoted to the design and control of small-scale seismic motion simulators. Symans and Twitchell (1998) developed a linearized model of the coupled uniaxial shake table and single story test structure at Washington State University. That work failed to present phase data for the simulator. Trombetti, et al (1998) generated a transfer function realization for the 1-degree-of-freedom (DOF) simulator at Rice University to assist in tuning the simulator control gains. No closed loop performance data was provided. Spencer and Yang (1998) incorporated a transfer function iteration technique to improve the tracking response of the shake table at the University of Notre Dame. That work did not include a test structure on the simulator during testing.

Since hydraulic systems typically exhibit nonlinear behavior, electro-hydraulic shake table controllers must either treat or be robust to the nonlinear dynamics. Newell, et al (1995) experimentally verified a Kalman filter based feedback controller by linearizing the simulator dynamics about a reference trajectory to obtain a time varying control gain set. The controller utilized an optimal reference trajectory obtained by minimizing acceleration tracking error but the experiment did not include a test structure. Dai, et al (1997) designed a nonlinear simulator control system based on a tensor formulation of a nonlinear regulator design. That work also neglected the test structure. Unfortunately, none of the aforementioned experimental work provided both magnitude and phase response characteristics for seismic simulators exciting a dynamic test specimen.

Regardless of the control or model identification technique, the simulator system must have sufficient authority to overcome the effects of reactive loads imparted by the test structure. To accurately replicate desired seismic motions, the simulator control system must either exhibit exceptional tracking performance and stability robustness in the presence of such disturbances or must include the dynamics of the test structure. The latter approach is less desirable for a simulator used to verify structural control systems because the dynamic characteristics of the controlled structure change each time the control system is modified and are often nonlinear. Therefore the shake table control would need to be tuned each time the structural control is varied. Work by Kuehn, et al (1998,1999) and Brock (2000) provides a detailed description of the development and testing of a robust, high fidelity control algorithm for the seismic simulator located in Fears Laboratory at the University of Oklahoma. The results obtained using the OU

simulator for the tests presented herein are reliable since the previous work referenced above demonstrated that the shake table could accurately reproduce both the magnitude and phase of a reference input with the same three-story structure.

The University of Oklahoma seismic shake table shown in Photo 2.1 and in Figure 2.4 consists of a 635-kg welded steel motion platform (A) with a 1.8-m × 1.2-m

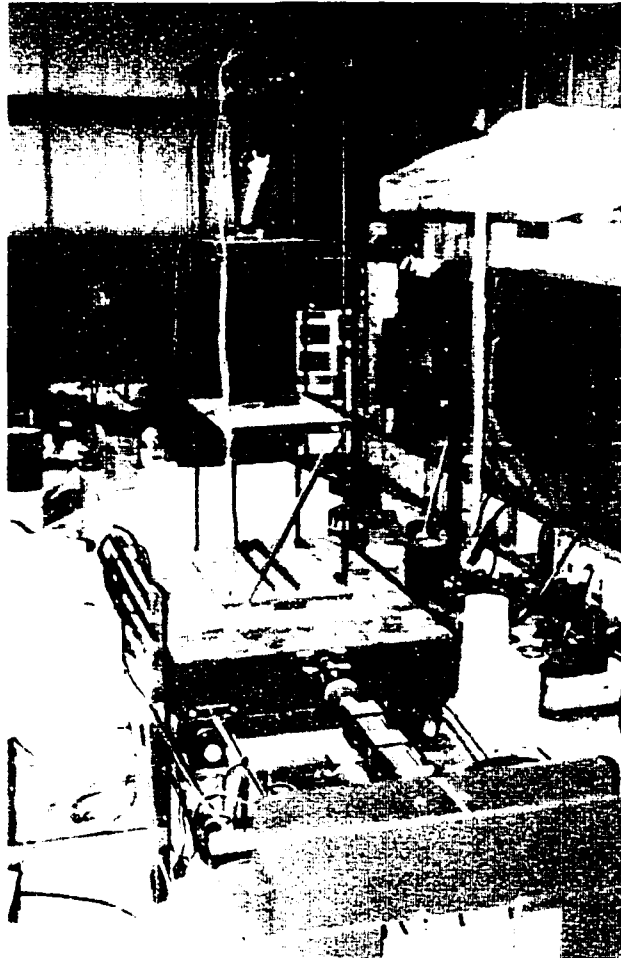


**Photo 2.1:** University of Oklahoma seismic motion simulator including test structure

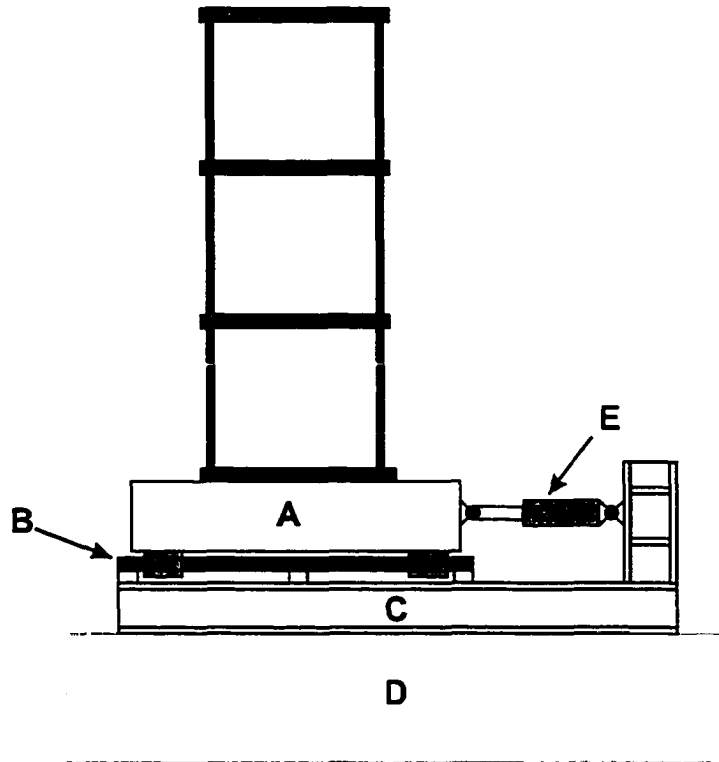


**Figure 2.4:** Seismic simulator schematic

horizontal footprint. The motion of the table is constrained to a single horizontal axis with Thomson 75-mm extra rigid precision linear bearings (B). The support frame (C) is constructed from W12×65 wide flange I-beam that is bolted to reaction mass (D). The table is actuated with a fatigue rated 50-kN MTS hydraulic cylinder (E). The actuator has an effective piston area of  $2.5 \times 10^3$ -mm<sup>2</sup> and  $\pm 75$ -mm dynamic stroke.

Hydraulic flow to the actuator is regulated with dual MTS 252 servo-valves. Each valve has a 57-lpm maximum flow rate at 21-MPa operating pressure. The hydraulic power unit for the simulator consists of a 37-kW 3-phase AC motor, which drives a Parker variable displacement piston pump with maximum flow rate of 95-lpm at 21-MPa. The system includes 1-liter hydraulic accumulators mounted on the supply and

return ports of the servovalve manifold as well as 0.5-liter and 7.6-liter accumulators at the pump to stabilize the supply pressure.

A variety of sensors are required to control and monitor the performance of the simulator system. The differential pressure between actuator chambers is monitored with an MTS differential pressure transducer with a bandwidth of DC to 1-kHz. The platform displacement is measured with an RDP Electrosense DC/DC LVDT that has a bandwidth of DC to 200-Hz. The table accelerations are sensed with ICS model 3028-002 piezo-resistive accelerometers. The accelerometers have flat frequency responses from DC to 1-kHz.

The shake table was controlled with a personal computer (PC) based control system utilizing a Real Time Device's ADA3100 data acquisition module with 12-bit differential A/D and D/A for analog interfacing. Each A/D channel was outfitted with a second order low pass Butterworth filter to prevent aliasing. The break frequency of each filter was set at 500-Hz. The control system utilized a closed loop feedback/feed-forward algorithm obtained by the optimization of a receding-horizon tracking performance index. The resulting digital control was implemented with a 2000-Hz update rate. The block diagram of the simulator control algorithm is depicted in Figure 2.5. The seismic simulator tracking performance and robustness to test structure dynamics were experimentally verified. Figures 2.6 and 2.7 indicate the frequency response magnitude and phase of the simulator with and without a 360-kg flexible test structure for a banded white noise acceleration input. The time domain acceleration tracking response of the motion simulator with the test structure attached is shown in Figure 2.8. The reference input was the North/South component of the 1940 El Centro

earthquake scaled by 50%. The results of Figures 2.6-2.8 were obtained before adding semi-active control devices to the structure.

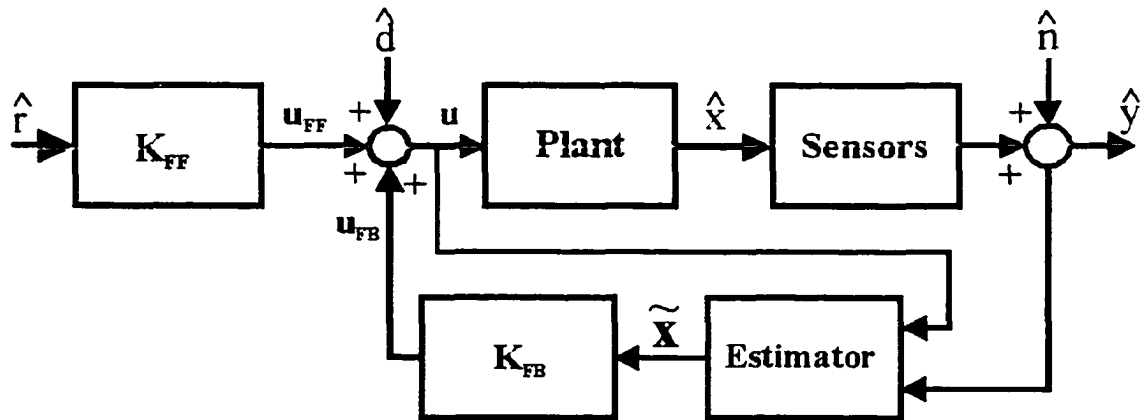


Figure 2.5: Seismic simulator feedback/feed-forward control block diagram

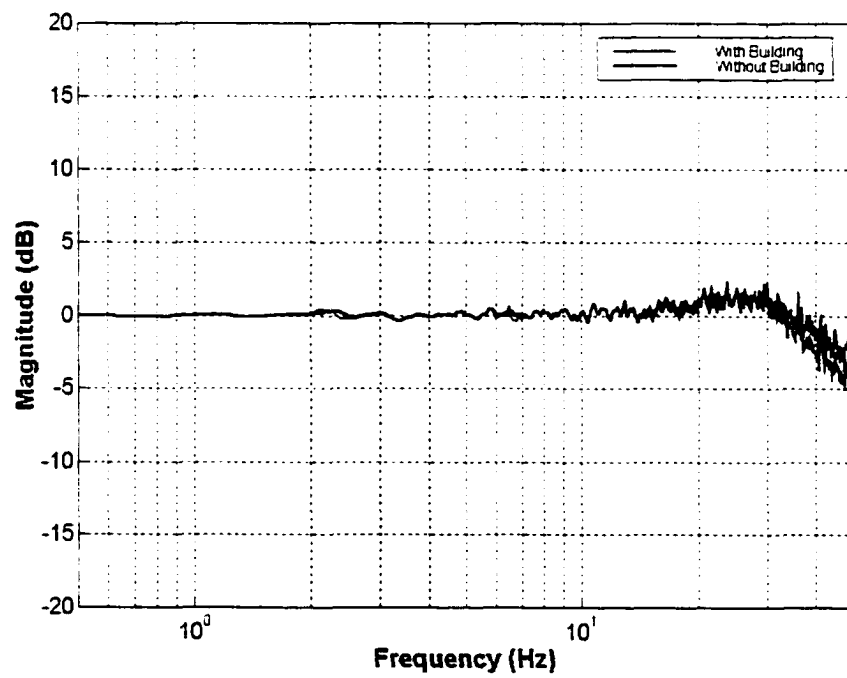
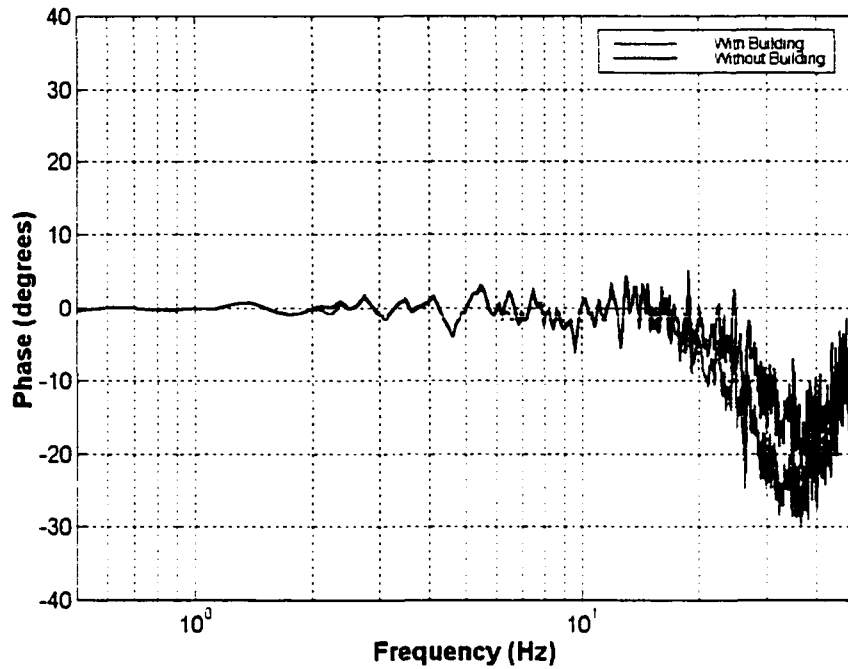
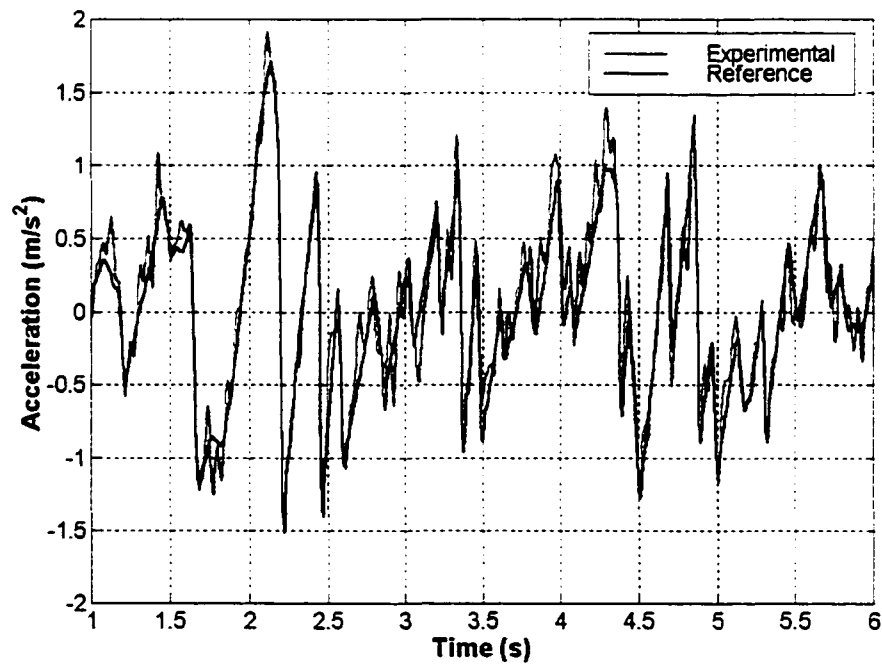


Figure 2.6: Seismic motion simulator acceleration frequency response magnitude with and without a 360-kg test structure



**Figure 2.7:** Seismic motion simulator acceleration frequency response phase with and without a 360-kg test structure



**Figure 2.8:** Seismic motion simulator acceleration tracking response of N-S component of the 1940 El Centro earthquake

### 2.3 Semi-Active Actuators

The variable orifice hydraulic semi-active control device used for the work here is shown in Photo 2.2 and a cross section is depicted in Figure 2.9. The hardware consists of a hydraulic actuator (A), control valve (B), absolute pressure sensors (C), LVDT (D),

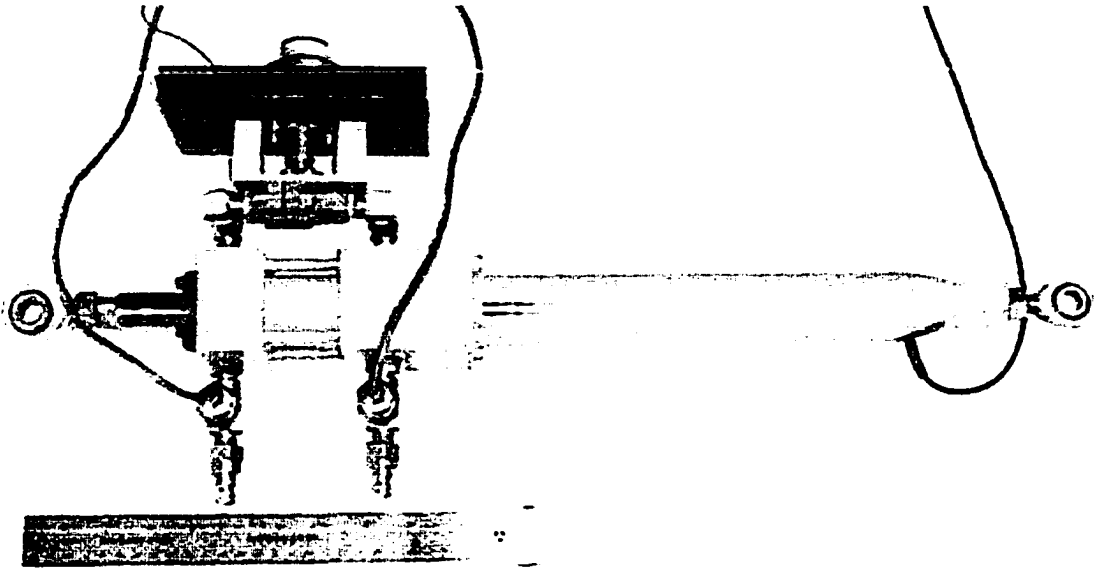


Photo 2.2: Semi-active hydraulic actuator assembly

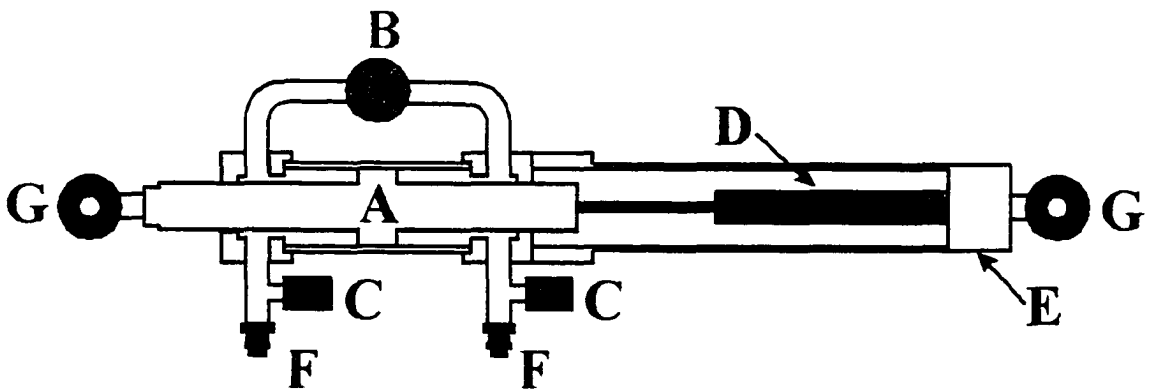


Figure 2.9: Schematic representation of the variable orifice semi-active actuator

extension housing (E), quick disconnects (F) and spherical rod ends (G). The actuator (A) was designed and fabricated at OU specifically for the research presented herein. Design optimization studies conducted at the CSC (Cao, 1999, and Zhuang, 1999) have

shown that semi-active control performance can vary significantly with variations in hardware parameters including piston area, actuator stroke, minimum valve orifice area and maximum valve orifice area.

The characteristics of the hydraulic actuator are critical to the performance of the semi-active control system. To objectively evaluate the performance of the semi-active hardware, the influence of actuator friction on the structural dynamics must be small. This is especially problematic for small-scale testing because the amount of friction is linearly proportional to the piston and rod diameters, not the effective piston area, which determines load capacity. For example, Parker Hannafin predicts its 125-kN rated “low friction” actuator to have approximately 550-N dynamic friction at 7-Mpa operating pressure while a 13-kN rated “low friction” actuator is predicted to have 250-N dynamic friction under the same conditions. The friction of the smaller actuator, which has the same bore and rod diameter as the actuators used for the work reported here, would clearly dominate the dynamics of the test structure. Several small-scale experiments at the CSC (Mo, 1996, Lee, 1998) have relied on low friction actuators intended for pneumatic and low-pressure hydraulic applications. Such actuators have desirable friction characteristics but are limited to peak pressures of 2-MPa. Rather than refine a commercially available product, the semi-active actuators were custom designed and fabricated by the author. The resulting double rod actuators have a dynamic stroke of  $\pm 25$ -mm, a 38-mm diameter bore and a 25-mm diameter piston rod providing an effective area of 633-mm<sup>2</sup>. The piston seal is a Parker P808 polytetrafluoroethylene (PTFE) piston ring with a nitrile o-ring energizer, while the rod seals are shore A-70 cast polyurethane o-rings with 2.4-mm diameter cross-section. The actuator was designed for a peak

pressure of 10-MPa. Cyclic tests (10-mm amplitude 0.25-Hz sine wave) with no hydraulic oil in the semi-active device indicate the actuator provided a maximum 75-N of friction. (Figure 2.10)

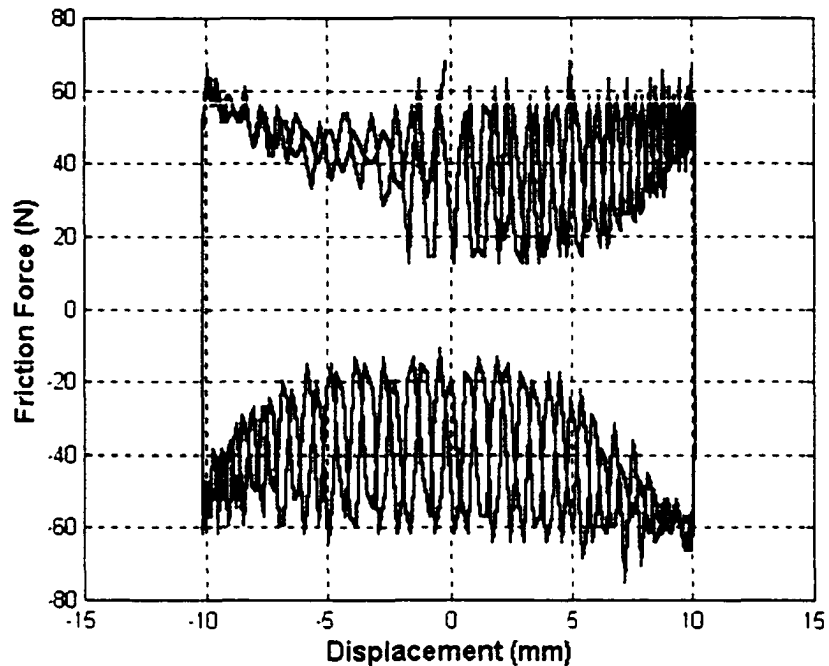


**Figure 2.10:** Dynamic friction of the actuator with no fluid subject to a 10-mm amplitude 0.25-Hz sine wave input

Flow between the two chambers of the semi-active actuator is controlled by a Whitey Model SS-33VF4 ball valve. The valve has PTFE seats and a polished stainless steel ball to reduce actuating torque. The valve is rated at 40-MPa maximum pressure. A mapping of the valve orifice area as a function of rotation angle is provided in Figure 2.11.

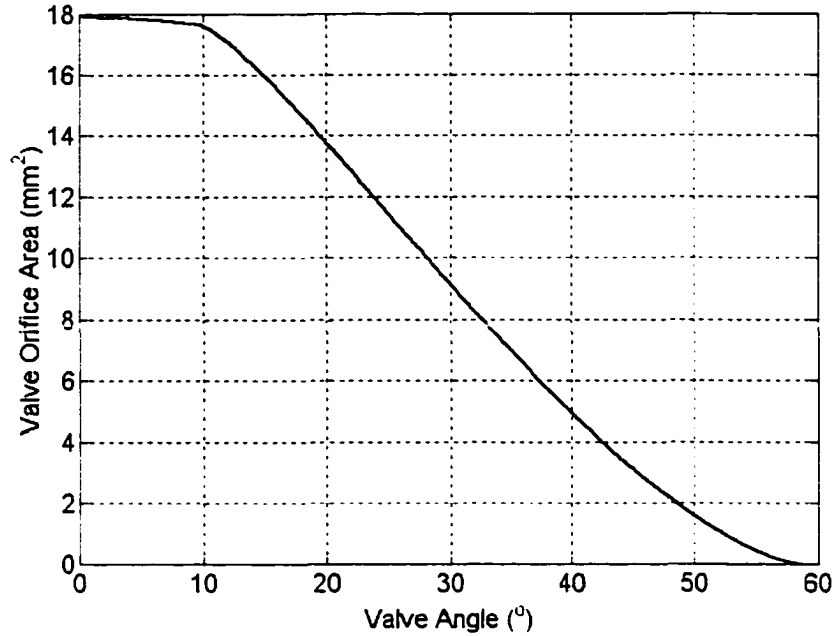


**Figure 2.11:** Valve orifice area vs. valve angle for the Whitey SS-33VF4 ball valve

Previous semi-active devices developed at the CSC used high performance DC motors to drive the semi-active control valves. Such systems require feedback control hardware to regulate the valve position. The work reported here utilized a Lucas Ledex Ultimag rotary actuator, model 1944644-027, to drive the valve. The Ultimag is a DC powered high-speed high-torque rotary actuator with  $\pm 22.5^\circ$  of stroke. The operating characteristics of the actuator are ideal for bi-state control of the valve, which ranges from maximum orifice area to fully closed in  $45^\circ$ . The cost of the device is comparable to a high performance DC motor and does not require feedback control. The Ultimag also provides better performance than rotary solenoids and since it is a double acting device, it does not require return springs which would tend to increase the actuation torque. The device is connected to the valve with a Helical Products flexible stainless steel coupling which allows  $5^\circ$  angular misalignment and 0.25-mm parallel offset

between the actuator and valve shafts. The position of the actuator is monitored with a BEI shaft mounted incremental optical encoder. The actuator assembly, which is fitted with a heat sink, the helical coupling and optical encoder is shown in Photo 2.3. The actuator is driven with a National Semiconductor LMD18200 H-bridge rated at 3-A and a 24-V DC power supply. The output of the LMD18200 is controlled with TTL inputs. The valve system responses are indicated in Figures 2.11 and 2.12 for a variety of loads.

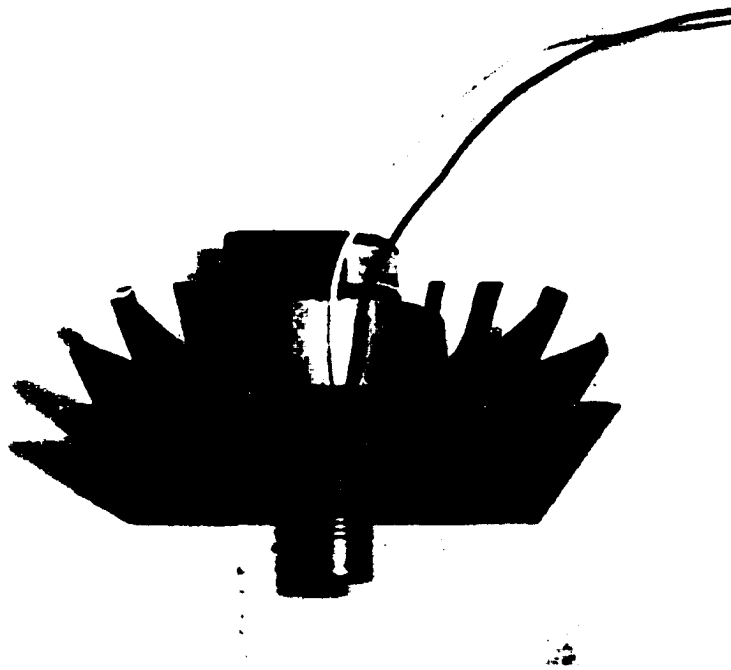


**Photo 2.3:** Ultimag rotary actuator with helical coupling

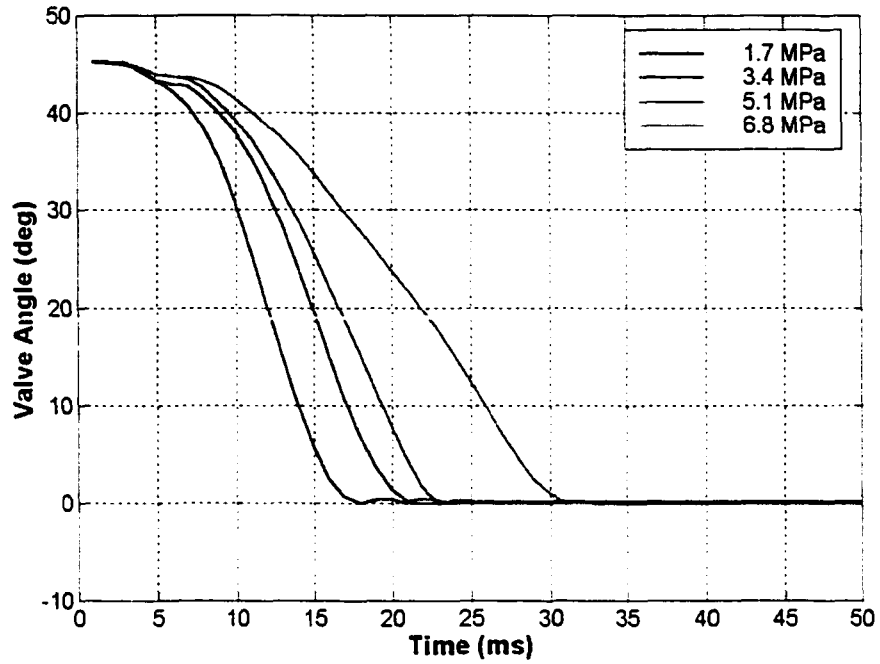


**Figure 2.12:** Variation of valve opening response time with pressure

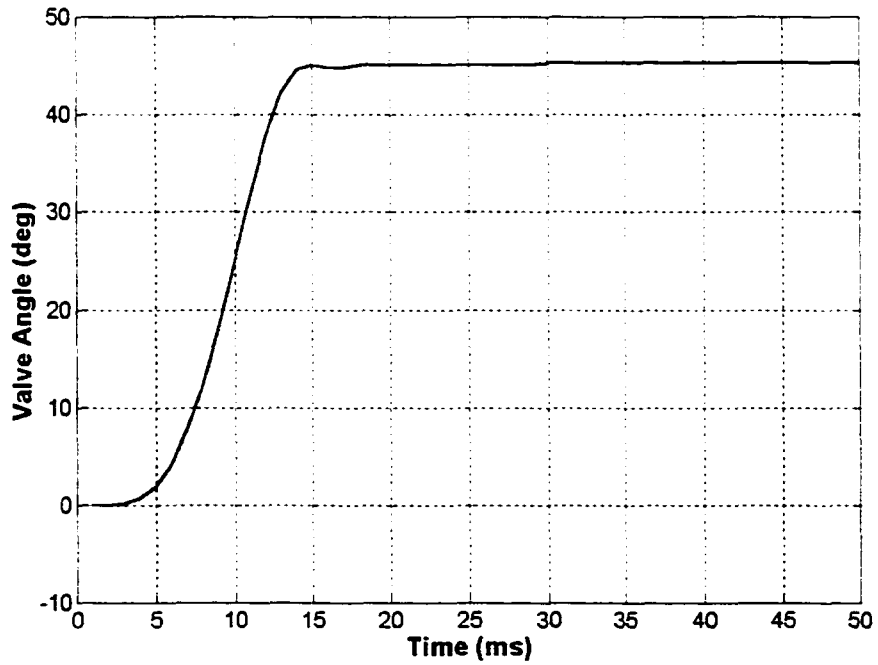


**Figure 2.13:** Valve closing response time

The pressure in each semi-active actuator chamber is sensed with a Measurement Specialties MSP-300 pressure transducer. The low cost sensors have a pressure range of 0 to 7-MPa with an accuracy of  $\pm 70$ -kPa, a bandwidth from DC to 1-kHz and are temperature compensated from 0° to 55° C. The displacement of the actuator piston relative to the actuator body is measured with an RDP Electrosense DC/DC LVDT with  $\pm 25$ -mm stroke. The LVDT has a bandwidth of DC to 200-Hz with 30-mV peak-to-peak output ripple. The LVDT is mounted inside the actuator extension housing.

The stiffness of the hydraulic fluid and subsequently, the effectiveness of the semi-active actuator are dictated by the amount of air mixed with the hydraulic fluid in the actuator. It is therefore advantageous to eliminate as much of the air from the device as possible. A gravitational bleeding assembly, which is connected to the actuator quick disconnects, was designed to fill the actuator with hydraulic fluid and bleed air from the system. The actuator was charged to a nominal pressure using a hydraulic accumulator that is connected to a quick disconnect on the actuator. The accumulator was disconnected from the system during testing. Actuator testing indicated the quick disconnects can be problematic if the pressure in either chamber becomes lower than atmospheric pressure. Under such conditions, the pressure imbalance will tend to force open the quick disconnect check valve, allowing outside air to infiltrate the chamber. Therefore, the quick disconnects should be capped to prevent unwanted air from entering the system.

The actuator is connected to mounting brackets on the test structure using Aurora spherical rod ends. The rod ends are lined with a PTFE fabric to eliminate backlash and

reduce friction. The spherical connections also allow for up to 12° of angular misalignment.

## **2.4 Control Hardware**

The semi-active structural control system was implemented digitally with a 200-MHz PC. A Real Time Device's ADA3110 data acquisition board with 16 single-ended 12-bit A/D channels was used to digitize the analog sensor data. The ADA3110 was used to digitize the outputs of ten accelerometers, two pressure sensors and three LVDTs. The outputs of the pressure sensors and LVDTs were filtered with second-order low-pass active Butterworth filters. The accelerometer outputs were amplified with custom-made signal conditioning circuits utilizing Analog Devices AD524 precision instrumentation amplifiers. A Hewlett-Packard HCTL-2020 was used to decode the output of the optical encoder used to sense the position of the Ultimag actuator. A Computer Board's CIO-DIO24 digital input/output board was used to import the digital output of the decoder circuit into the PC. The digital I/O channels on the ADA3110 were used to output TTL commands to the H-bridge circuit that drives the valve actuator.

The control software was designed to scan and save data from all the sensors as well as control the semi-active actuator. The control logic utilized LVDT and Pressure sensor data to determine the desired state of the semi-active valve and is discussed in Chapter 4. The software was written in Borland C and was compiled with a Phar-Lap DOS extender to allow multiple large arrays to be stored in high memory. The analog and digital inputs were sampled at 2000-Hz per channel using burst mode for the A/D conversions while the control was updated at 200-Hz.

# CHAPTER 3

## SYSTEM MODELING AND PARAMETER IDENTIFICATION

In order to design an effective structural control system, it is necessary to have an understanding of the dynamic characteristics of both the structure and the control actuator. Much of the structural control work in the literature neglects the dynamic coupling between the structure and the control actuator. The objective of this chapter is to develop dynamic models for both the test structure and the semi-active actuator, which can be coupled together for the control design process.

### 3.1 Structure Modeling and Parameter Identification

The three-story test structure is idealized as a lumped mass system with three degrees of freedom for each floor: displacement in the  $x$ -direction, displacement in the  $y$ -direction and rotation about the  $z$ -axis. Since only the  $x$ -axis degrees of freedom are controllable for the actuator configurations considered in this dissertation (Figure 2.2), the control model developed for the structure includes only three degrees of freedom in the  $x$ -direction.

The planar equations of motion for the three-story structure are expressed in terms of relative displacements between the floors as

$$M_s \ddot{x}_s + C_s \dot{x}_s + K_s x_s = B_{i0} \Delta p_i + D_0 d \quad (3.1)$$

where  $x_s$  is a  $3 \times 1$  vector of floor-to floor relative displacements in the  $x$ -axis.  $\Delta p_i$  is the semi-active actuator differential pressure and  $d$  is a scalar disturbance input representing a uniaxial ground acceleration. The mass, damping and stiffness matrices for the structure are represented by  $M_s$ ,  $C_s$  and  $K_s$  respectively. The two  $3 \times 1$  differential pressure influence coefficient vectors  $B_{1_0}$  and  $B_{2_0}$  correspond to the two semi-active actuator positions depicted in Figure 2.2. The values of  $B_{1_0}$  and  $B_{2_0}$  were calculated from the actuator installation geometry and the effective piston area of the actuators. For the work presented herein, only one actuator is enabled for any given test and the other actuator differential pressure is set to zero.  $D_s$  is the  $3 \times 1$  ground acceleration influence coefficient vector.

The structural stiffness parameters were determined by static tests. A hydraulic actuator was used to apply constant loads between floors of the structure. The forces were measured with a Transducer techniques 9-kN load cell model SWO-2K. The relative displacements between floors were measured with RDP Electrosense LVDTs. The resulting floor-to-floor stiffness is 180-kN/m for the first floor, 184-kN/m for the second floor and 222-kN/m for the third floor.

Shake table tests were performed on the instrumented bare frame to determine the remaining model parameters. The structure was subjected to a 0.5-50-Hz band limited white noise ground acceleration input directed along the  $x$ -axis of the structure. The time histories for each channel of data were recorded and used to compute frequency response functions for the structure. A least-squares algorithm was employed to identify the remaining model parameters from the frequency response data. The resulting system matrices are as follows:

$$M_s = \begin{bmatrix} 168 & 0 & 0 \\ 177 & 177 & 0 \\ 193 & 193 & 193 \end{bmatrix} kg \quad (3.2)$$

$$C_s = \begin{bmatrix} 267 & -76 & 0 \\ 0 & 76 & -74 \\ 0 & 0 & 74 \end{bmatrix} \frac{N \cdot s}{m} \quad (3.3)$$

$$K_s = \begin{bmatrix} 180 & -184 & 0 \\ 0 & 184 & -222 \\ 0 & 0 & 222 \end{bmatrix} \frac{N}{mm} \quad (3.4)$$

$$B_{1_0} = [485 \ 0 \ 0]^T \frac{N}{MPa} \quad (3.5)$$

$$B_{2_0} = [-485 \ 485 \ 0]^T \frac{N}{MPa} \quad (3.6)$$

$$D_0 = -[168 \ 177 \ 193]^T kg \quad (3.7)$$

Next, the system (3.1) is transformed into state space format

$$\dot{x} = A_s x + B_{1_s} y_i + D_s d \quad (3.8)$$

where

$$A_s = \begin{bmatrix} 0 & 0 & 0 & 1 & 0 & 0 \\ 0 & 0 & 0 & 0 & 1 & 0 \\ 0 & 0 & 0 & 0 & 0 & 1 \\ -1070 & 1100 & 0 & -1.59 & 0.46 & 0 \\ 1070 & -2130 & 1250 & 1.59 & -0.86 & 0.41 \\ 0 & 1030 & -2400 & 0 & 0.43 & -0.80 \end{bmatrix} \quad (3.9)$$

$$B_{1_s} = [0 \ 0 \ 0 \ 2.89 \ -2.89 \ 0]^T \quad (3.10)$$

$$B_{2_s} = [0 \ 0 \ 0 \ -2.89 \ 5.62 \ -2.73]^T \quad (3.11)$$

$$D_s = [0 \ 0 \ 0 \ -1 \ 0 \ 0]^T \quad (3.12)$$

States  $x_1$ - $x_3$  represent the relative displacements between floors in  $mm$  and states  $x_4$ - $x_6$  are the corresponding relative velocities in  $mm/s$ . The actuator differential pressures  $\Delta p_i$  are in  $MPa$  and the disturbance input  $d$  is in  $m/s^2$ . The state space system model (3.9) is used to approximate the structural dynamics throughout the work presented here. Magnitude and phase transfer functions of the system model (3.8) are compared to the experimentally obtained frequency response functions in Figures 3.1-3.6. The plots indicate that in spite of the simplifying assumptions, the model provides a reasonable approximation of the data obtained from the test structure.

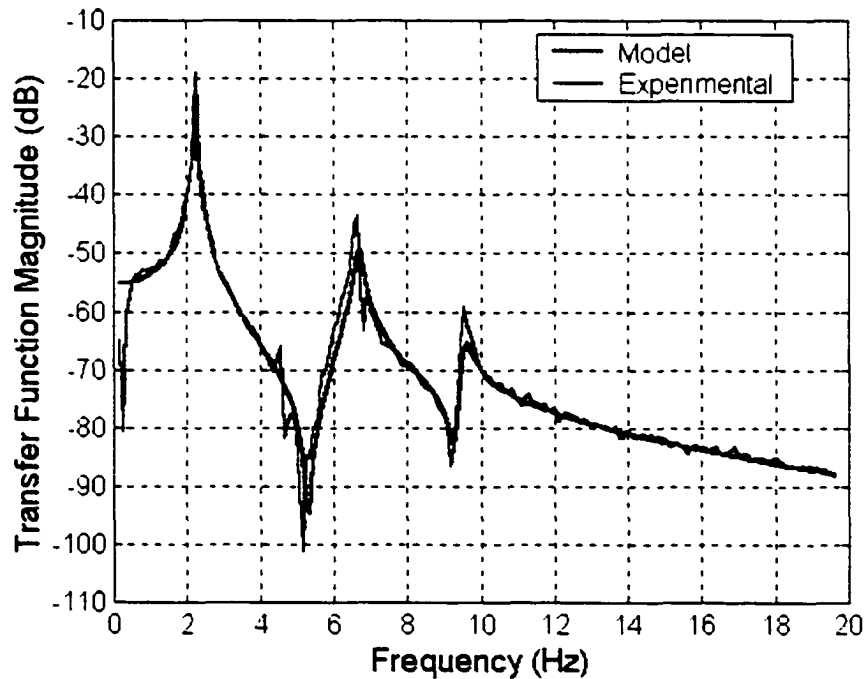


**Figure 3.1:** Comparison of experimental and analytical transfer function magnitudes for  $x_1/d$

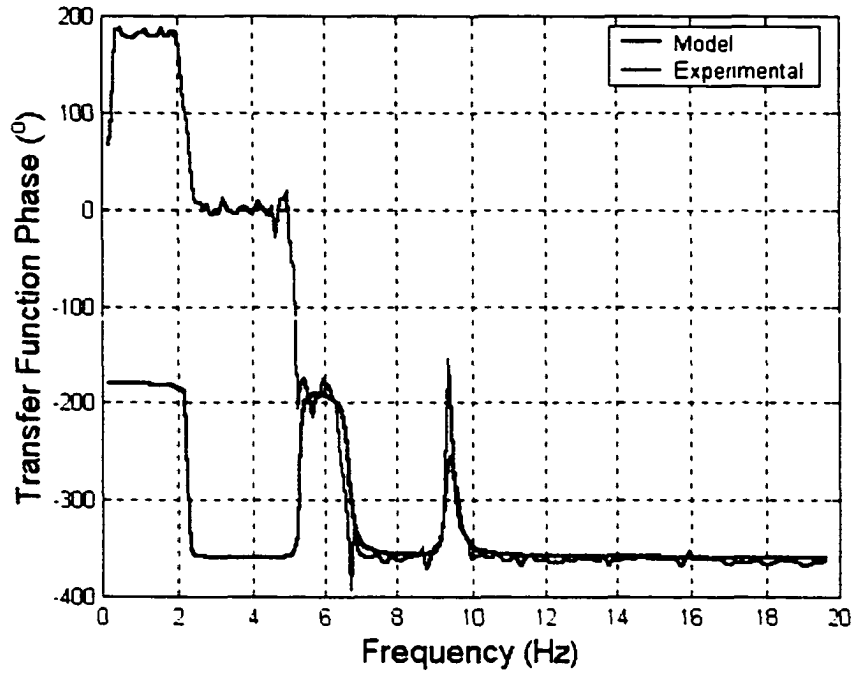


Figure 3.2: Comparison of experimental and analytical transfer function phase response  $x_1 / d$ .

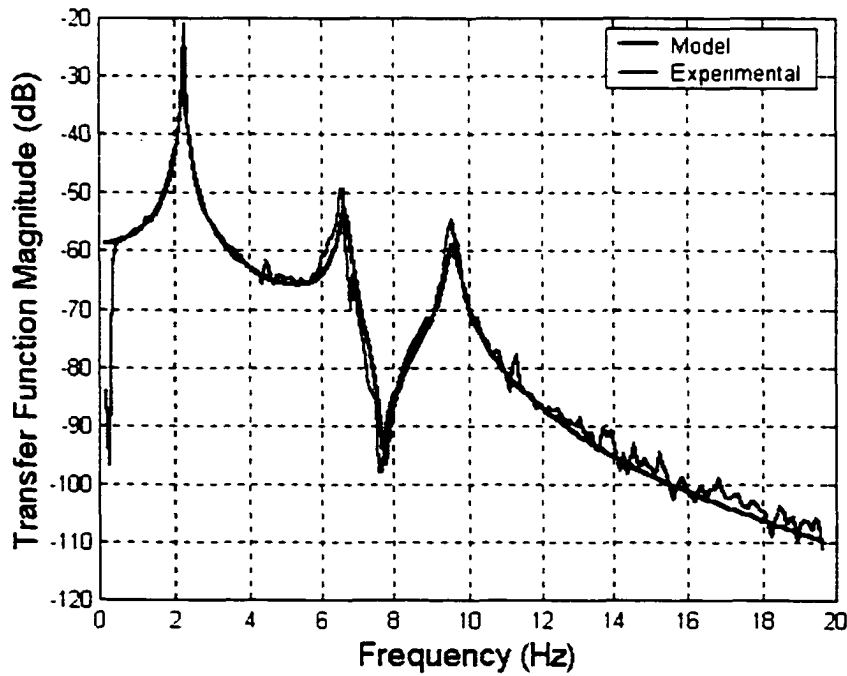


Figure 3.3: Comparison of experimental and analytical transfer function magnitudes for  $x_2 / d$

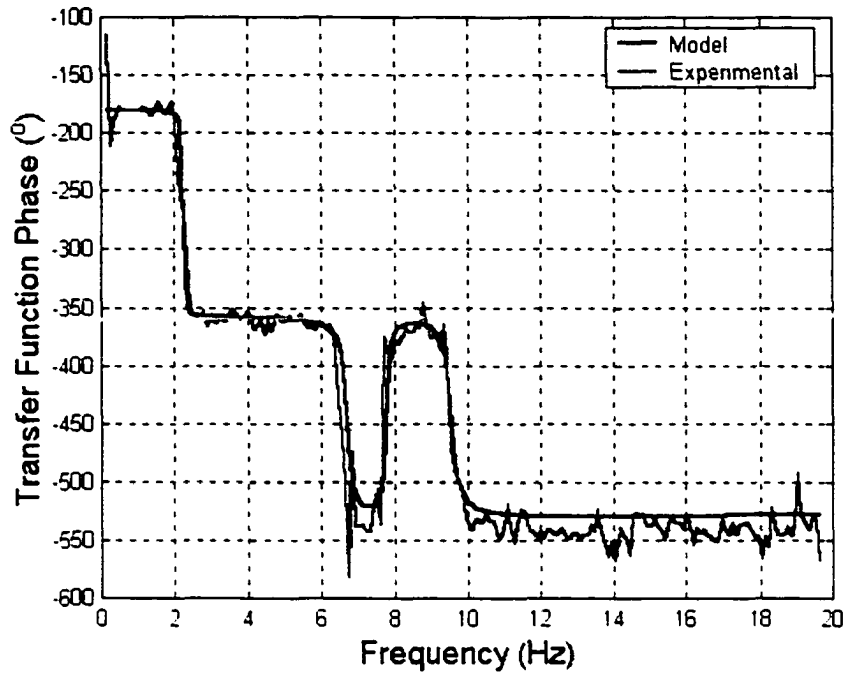


Figure 3.4: Comparison of experimental and analytical transfer function phase responses for  $x_2/d$ .

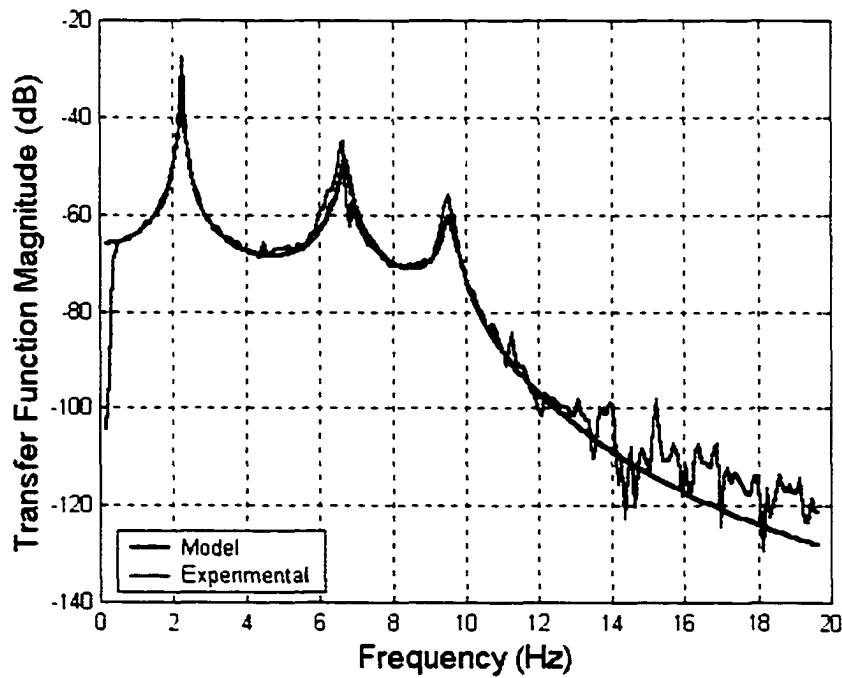
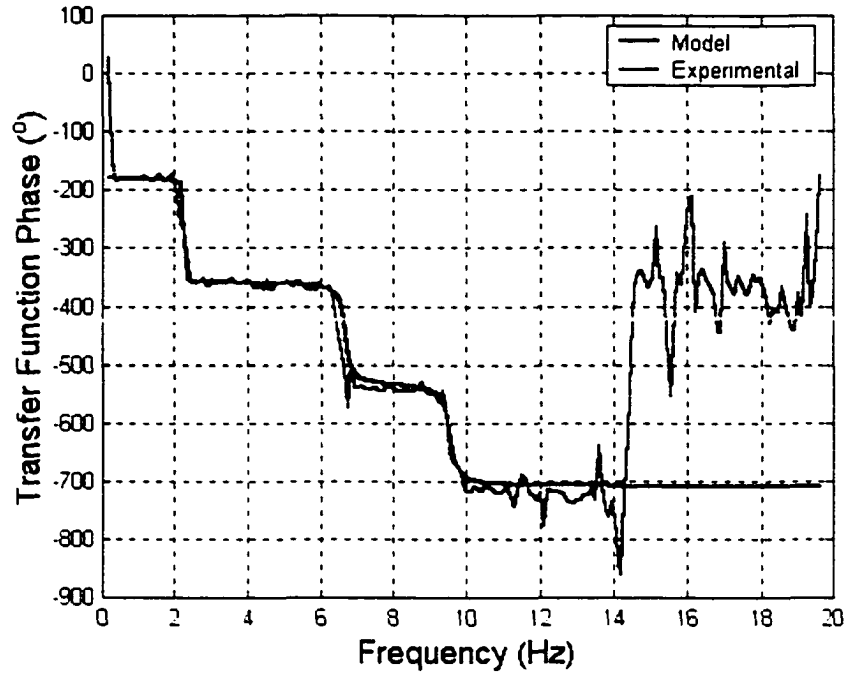


Figure 3.5: Comparison of experimental and analytical transfer function magnitudes for  $x_3/d$ .



**Figure 3.6:** Comparison of experimental and analytical transfer function phase responses for  $x_3/d$ .

### 3.2 Semi-Active Actuator Model

The following section presents a detailed development of a lumped parameter dynamic model for the variable orifice hydraulic semi-active actuator. The semi-active actuator is represented schematically in Figure 2.9. It is assumed that the fluid in each actuator chamber is slightly compressible. The equation of state relating fluid density to variations in pressure and temperature in each chamber  $i=1,2$  is approximated by a first order Taylor Series (Merritt, 1967)

$$\rho_i = \rho_0 + \left( \frac{\partial \rho_i}{\partial p_i} \right)_{T_i} (p_i - p_0) + \left( \frac{\partial \rho_i}{\partial T_i} \right)_{p_i} (T_i - T_0) \quad (3.13)$$

where  $\rho_i$ ,  $p_i$  and  $T_i$  are the density, pressure and temperature respectively of the fluid in chamber  $i$  and  $\rho_0$ ,  $p_0$  and  $T_0$  are nominal values of the density, pressure and temperature for the fluid. The isothermal bulk modulus of the fluid in each chamber is defined as

$$\beta_i \equiv \rho_0 \left( \frac{\partial p_i}{\partial \rho_i} \right)_{T_i} = -V_i \left( \frac{\partial p_i}{\partial V_i} \right)_{T_i} \quad (3.14)$$

Assuming the temperature in each actuator chamber is constant and the nominal values are at atmospheric pressure, Equation (3.13) can be reduced to the form

$$\rho_i = \rho_0 \left( 1 + \frac{1}{\beta_i} (p_i - p_{atm}) \right) \quad (3.15)$$

Since it is impossible to extract all the air from the semi-active actuator, the fluid in the actuator is a mixture of hydraulic oil and air. Neglecting the elasticity of the actuator, the effective isothermal bulk modulus of the mixture in chamber  $i$  is defined as

$$\beta_i = \frac{1}{\frac{v_{oil}}{v_{tot} \beta_{oil}} + \frac{v_{air}}{v_{tot} \beta_{air}(p_i)}} \quad (3.16)$$

where  $v_{oil}$  and  $v_{air}$  are the respective volumes of oil and air in the actuator at atmospheric pressure,  $v_{tot}$  is the nominal volume of the actuator and  $\beta_{oil}$  and  $\beta_{air}$  are the bulk moduli of the oil and air respectively. Assuming the bulk modulus of the oil is constant and the air in the system behaves as an ideal gas, Equation (3.16) can be simplified as

$$\beta_i = \frac{1}{\frac{v_{oil}}{v_{tot} \beta_{oil}} + \frac{v_{air}}{v_{tot} p_i}} \quad (3.17)$$

Substituting Equation (3.17) into (3.15) yields the state relation

$$\rho_i = \rho_0 \left( 1 + (p_i - p_{atm}) \left( \frac{v_{oil}}{v_{tot} \beta_{oil}} + \frac{v_{air}}{v_{tot} p_i} \right) \right) \quad (3.18)$$

Equation (3.18) can be differentiated with respect to time to obtain

$$\frac{d\rho_i}{dt} = \rho_i \frac{\left( \frac{v_{oil}}{v_{tot}\beta_{oil}} + \frac{v_{air}P_{atm}}{v_{tot}P_i^2} \right)}{\left( 1 + \frac{P_i - P_{atm}}{\beta_i} \right)} \frac{dp_i}{dt} \quad (3.19)$$

Since the system pressure is typically much smaller than the effective bulk modulus, (3.19) is approximated as

$$\frac{d\rho_i}{dt} = \rho_i \left( \frac{v_{oil}}{v_{tot}\beta_{oil}} + \frac{v_{air}P_{atm}}{v_{tot}P_i^2} \right) \frac{dp_i}{dt} \quad (3.20)$$

Assuming there is no leakage from either chamber, the continuity relations for each chamber of the actuator can be expressed as (Merritt, 1967)

$$\frac{dm_i}{dt} = \rho_i \frac{dv_i}{dt} + v_i \frac{d\rho_i}{dt} \quad (3.21)$$

where  $m_i$  is the mass of fluid in chamber  $i$ ,  $\rho_i$  is the fluid density in chamber  $i$ , and  $v_i$  is the volume of chamber  $i$ . Equations (3.20) and (3.21) are combined to yield flow relations for each actuator chamber

$$-q_1 = \frac{dv_1}{dt} + \frac{v_1}{\beta_1^*} \frac{dp_1}{dt} \quad (3.22)$$

$$q_2 = \frac{dv_2}{dt} + \frac{v_2}{\beta_2^*} \frac{dp_2}{dt} \quad (3.23)$$

where  $q_1$  is the volumetric flow rate out of actuator chamber 1,  $q_2$  is the volumetric flow rate into chamber 2 and  $\beta_i^*$  is defined as

$$\beta_i^* \equiv \frac{1}{\frac{v_{oil}}{v_{tot}\beta_{oil}} + \frac{v_{air}P_{atm}}{v_{tot}P_i^2}} \quad (3.24)$$

The volume for each actuator chamber is defined as:

$$v_1 = \frac{1}{2} v_t + A_p x_{sa} \quad (3.25)$$

$$v_2 = \frac{1}{2} v_t - A_p x_{sa} \quad (3.26)$$

where  $v_t$  is the total actuator volume,  $A_p$  is the effective piston area, and  $x_{sa}$  is the displacement of the actuator piston from the mid-stroke point. Differentiating equations (3.25) and (3.26) with respect to time yields

$$\dot{v}_1 = A_p \dot{x}_{sa} \quad (3.27)$$

$$\dot{v}_2 = -A_p \dot{x}_{sa} \quad (3.28)$$

where

$$\dot{x}_{sa} \equiv \frac{dx_{sa}}{dt} \quad (3.29)$$

Equations (3.22), (3.23), (3.27), and (3.28) can be combined to obtain flow equations for each chamber

$$-q_1 = A_p \dot{x}_{sa} + \frac{v_1}{\beta_1^*} \dot{p}_1 \quad (3.30)$$

$$q_2 = -A_p \dot{x}_{sa} + \frac{v_2}{\beta_2^*} \dot{p}_2 \quad (3.31)$$

Assuming there is no leakage from the valve, the mass flow rate through the valve must equal the mass flow rate out of one actuator chamber and the mass flow rate into the other chamber

$$\rho_1 q_1 = \rho_v q_v \quad (3.32)$$

$$\rho_2 q_2 = \rho_v q_v \quad (3.33)$$

Assuming (1) that the valve acts as a symmetric thin-plate orifice, (2) the flow through the valve is incompressible and (3) the flow is steady, the energy loss through the valve can be expressed by the Torricelli equation (Dulay, 1988)

$$q_v = C_d(Re)A_v(t)\text{sgn}(p_1 - p_2)\sqrt{\frac{2|p_1 - p_2|}{\rho_v}} \quad (3.34)$$

where  $C_d$  is the valve discharge coefficient which is a function of the Reynolds number  $Re$ , the variable valve orifice area  $A_v(t)$  is the control input and the signum function is defined as

$$\text{sgn}(a) \equiv \begin{cases} 1 & \text{if } a > 0 \\ 0 & \text{if } a = 0 \\ -1 & \text{if } a < 0 \end{cases} \quad (3.35)$$

Assuming the peak chamber pressures are small compared to the bulk modulus of the hydraulic oil and the amount of entrained air in the system is small, equation (3.18) indicates that variations in fluid density are small. Therefore, the density of the fluid at the valve is assumed to be the density of the fluid at equilibrium and equation (3.34) can be approximated as

$$q_v = C_d(Re)A_v(t)\text{sgn}(p_1 - p_2)\sqrt{\frac{2|p_1 - p_2|}{\rho_{eq}}} \quad (3.36)$$

Equations (3.18), (3.30)-(3.33) and (3.36) are used to simulate the behavior of the variable orifice hydraulic semi-active actuator.

### 3.3 Reduced Order Semi-Active Model

Assuming the density of the hydraulic fluid in the semi-active actuator is constant

$$\rho_1 = \rho_2 = \rho_v = \rho \quad (3.37)$$

Equations (3.30)-(3.34) and (3.37) can be combined to yield a reduced order model for the semi-active actuator

$$\dot{p}_1 = -\frac{\beta_1^*}{v_1} \left( A_p \dot{x}_{sa} + C_d A_v \operatorname{sgn}(p_1 - p_2) \sqrt{\frac{2|p_1 - p_2|}{\rho}} \right) \quad (3.38)$$

$$\dot{p}_2 = \frac{\beta_2^*}{v_2} \left( A_p \dot{x}_{sa} + C_d A_v \operatorname{sgn}(p_1 - p_2) \sqrt{\frac{2|p_1 - p_2|}{\rho}} \right) \quad (3.39)$$

Also, assuming the bulk modulus is constant and that the discharge coefficient can be expressed as a function of differential pressure. Equations (3.38) and (3.39) are combined to form a single equation in terms of the actuator differential pressure

$$\Delta \dot{p} = -\alpha A_p \dot{x}_{sa} - \alpha C_d (\Delta p) A_v \operatorname{sgn}(\Delta p) \sqrt{\frac{2|\Delta p|}{\rho}} \quad (3.40)$$

where

$$\alpha = \beta^* \frac{v_1 + v_2}{v_1 v_2} \quad (3.41)$$

Letting  $u = A_v$ , assuming that variations in actuator chamber volumes from nominal values are small and noting that the actuator relative velocity is a function of the structural state variable  $x$ . Equation 3.40 can be rewritten as

$$\dot{y} = A_{sa} x - B_{sa}(\Delta p) \Delta p u \quad (3.42)$$

where

$$A_{sa} = \alpha_0 A_p T \quad (3.43)$$

$$B_{sa}(\Delta p) = \alpha_0 C_d (\Delta p) \sqrt{\frac{2}{\rho |\Delta p|}} \quad (3.44)$$

and  $\alpha_0$  is the value for  $\alpha$  about equilibrium. For actuator Position 1 (Figure 2.2)

$$T = [0 \ 0 \ 0 \ 1.31 \ 0 \ 0] \quad (3.45)$$

For actuator Position 2

$$T = [0 \ 0 \ 0 \ 0 \ 1.31 \ 0] \quad (3.46)$$

Research by Mo (1996) and Patten, et al (1998) indicates that Equations (3.38) and (3.39) predict slow decays in nominal chamber pressures, which is inconsistent with experimental results. Therefore, the reduced order model is not well suited for designing the semi-active actuator. However, that work also indicated that a simplified version of model (3.42) that treats only turbulent flow provides a good fit to experimentally obtained differential pressure data. Since differential pressure is closely related to the control force, model (3.42) is useful for designing the control logic and simulating the response characteristics of the controlled structure. The structural model (3.8) and the semi-active actuator model (3.42) are combined to form a state space realization of the system for the control design.

### **3.4 Semi-Active Parameter Identification**

Several tests were conducted to determine model parameters for the semi-active actuator. A hydrometer was used to measure the specific gravity of the Shell Tellus ISO-46 hydraulic oil used in the semi-active actuator. The tests were conducted at room temperature and atmospheric pressure. The specific gravity of the oil was 0.864. A rotary viscometer was used to determine the viscosity of the oil. The measured kinematic

viscosity of the oil is 42.3-cSt at 40°C compared to the nominal value of 46-cSt provided by the manufacturer.

A uniaxial electro-hydraulic load frame was used to determine the response characteristics of the semi-active actuator to a variety of inputs. A Transducer Techniques load cell with a range of  $\pm 9$ -kN was placed in series with the actuator to measure the applied force. The pressures in each actuator chamber and the displacement of the actuator piston were also measured. The bulk modulus of the air/oil mixture in each actuator chamber was experimentally determined with load frame tests. The actuator was subjected to a 4-Hz  $\pm 0.4$ -mm amplitude sinusoidal input with the actuator control valve fully closed. The chamber pressure and piston displacement data were substituted into Equation (3.14) to calculate the bulk modulus of the air/oil mixture in each chamber. The chamber volume included the volume of oil in the tubing to the control valve. The bulk modulus of the oil and the volume fraction of air at atmospheric pressure were determined by performing a least-squares fit of the model given in equation (3.17) with the calculated the bulk modulus data. The bulk modulus of the oil was identified to be  $9.0 \times 10^2$ -MPa and 0.37% of the volume in chamber 1 consisted of air while 0.26% of the volume in chamber 2 consisted of air. According to the manufacturers data, the bulk modulus of the hydraulic oil should be approximately  $1.4 \times 10^3$ -MPa. The variation might be accounted for by considering the elasticity of the hydraulic actuator body. Figures 3.7 and 3.8 indicate the variation of the bulk modulus with pressure for each actuator chamber.

### 3.5 Valve parameter identification

A flow bench was set up to measure the flow discharge coefficient of the semi-active flow control valve. The system utilized a variable displacement hydraulic pump driven by an electric motor to supply the hydraulic flow. Sensotec model LM/2345-08 pressure sensors were installed to measure the head loss across the valve. A Hoffer turbine flowmeter model HO1/2x1/4-.1-4.5-UB-1MC3PA-MS was used to sense the flow downstream from the valve. The pressures and flows were measured as the flow rate through the valve was slowly varied. Tests were performed with the valve completely open, closed 30° and closed 45°. The test data were substituted into Equation 3.36 to calculate the discharge coefficient, which is plotted in Figure 3.9 as a function of the choke number. The choke number is a function of the Reynolds number  $Re$ , the hydraulic diameter of the orifice  $D_h$  and the length of the orifice  $L$ .

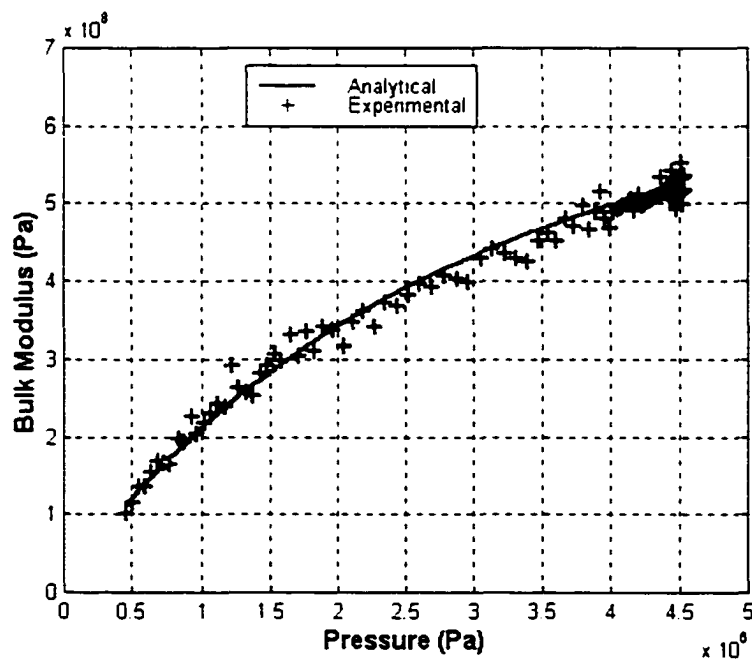
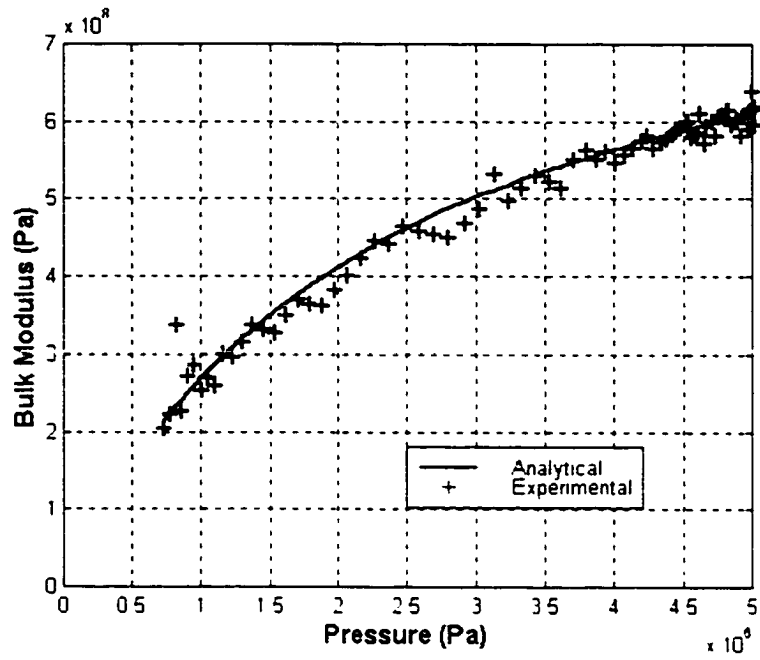
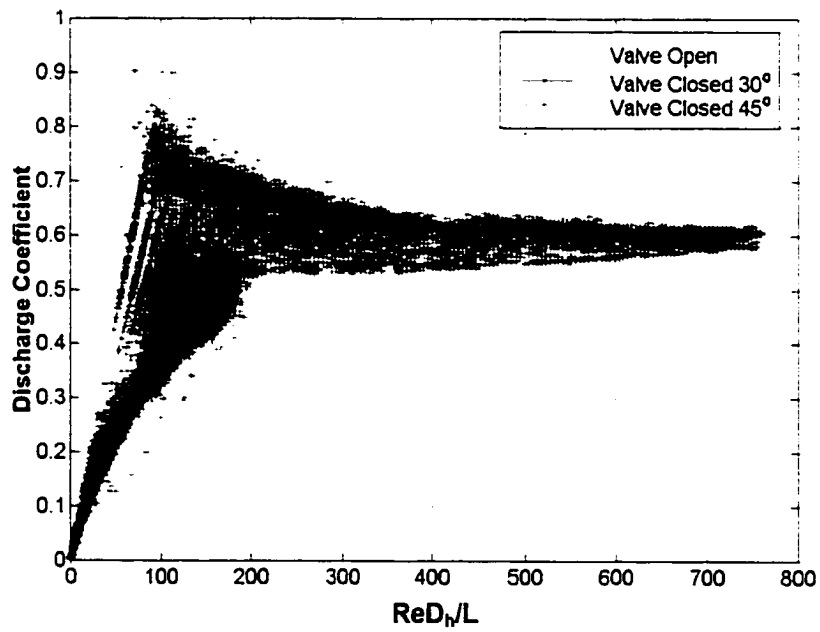


Figure 3.7: Experimental effective bulk modulus vs. model for chamber 1



**Figure 3.8:** Experimental effective bulk modulus vs. model for chamber 2



**Figure 3.9:** Experimental valve discharge coefficient vs. choke number

# CHAPTER 4

## SEMI-ACTIVE CONTROL DESIGN

### 4.1 Introduction

Semi-active devices, like passive elements, (e.g. dampers or springs) generate reaction forces to imposed motions. However, the response characteristics of semi-active actuators can be varied in real time by adjusting certain actuator parameters. (e.g. valve orifice area, magnetic field strength, etc.) The energy required to vary the properties of semi-active actuators is typically small compared to the energy stored or dissipated by the devices. A variety of linear control synthesis techniques have been used to develop semi-active control laws for systems without treating the semi-active actuator dynamics that couple with the structural dynamics and are often nonlinear. Most control designs presented in the open literature either neglect actuator dynamics or treat the actuators as linear, variable parameter devices. Since most designs are based on simplified dynamic realizations, closed loop stability of the coupled semi-active control systems has been an open question.

The objective of this chapter is to address that open question and present a general control design methodology that guarantees stability for system models that include nonlinear semi-active actuator dynamics. First, a brief literature survey is presented that highlights the design techniques and assumptions used to develop semi-active control laws for structures. Second, a quickest descent semi-active control law is developed for a wide class of systems controlled with nonlinear actuators. The control objective is to

instantaneously minimize the time rate of change of a quadratic function of the system state variable, which includes coupled actuator states. The controlled system (structure and actuators) is then shown to provide quadratic convergence to the origin for the undisturbed case and quadratic convergence to a ball of ultimate boundedness (stable attractor) for nonzero bounded disturbances. Finally, simulation results are presented to compare the response of the semi-actively controlled three-story structure for a variety of control gains and to make conclusions regarding the stability bounds obtained for each control.

## **4.2 Background**

The earliest work in designing semi-active control algorithms for structures completely neglected the dynamics of the semi-active actuator. Hrovat, et al (1983) first proposed the use of semi-active control to reduce vibrations in buildings. The work included simulations of a clipped linear quadratic controller aimed at reducing wind-induced vibrations in a single degree of freedom building model using a semi-active tuned mass damper. The analysis assumed that the actuator could provide any desired force up to a maximum value provided the force was dissipative. If the desired force was non-dissipative, the control force was set to zero. Kasturi and Dupont (1998) formulated a constrained optimal control to maximize energy dissipation with a semi-active damper. That work neglected the actuator dynamics also.

Most control designs treat semi-active actuators as instantaneously adjustable linear devices with either variable stiffness parameters, variable damping parameters or

both. A number of researchers have focused on developing control strategies for devices in which only the damping was variable. Sadek and Mohraz (1998) present a variety of control strategies for structures with variable linear damping devices. The algorithms include a clipped LQR design, a generalized clipped LQR design including penalties on the acceleration of each degree-of-freedom, and a displacement-acceleration algorithm. The generalized clipped LQR algorithm provided the best response characteristics of the three algorithms. Symans (1995) and Symans and Constantinou (1997) used clipped LQR and Sliding mode control designs to mitigate seismic vibrations of a three-story structure equipped with linear variable dampers. Tests indicate a passive high damping configuration provided better performance than both of the semi-active controllers did. Symans and Kelly (1999) developed a fuzzy logic controller for a hybrid semi-active control system to seismically isolate a bridge. The semi-active actuators were modeled as linear viscous dampers with bounded variable damping coefficients.

Other researchers have developed controllers for semi-active devices in which only the stiffness was adjustable. Kobori, et al (1993) developed a non-resonant open loop control law for a full-scale model building equipped with variable stiffness actuators. The actuators were regulated between two stiffness states based on the measured seismic excitation to the structure. Nagarajaiah and Mate (1998) utilized a maximum dissipativeness control switching logic for a continuously variable linear semi-active stiffness device.

Leitmann (1994) compared two control strategies for a semi-active device with both variable linear damping and variable linear stiffness characteristics. The first control strategy was aimed at minimizing the rate of change of system energy while the

second was developed using Lyapunov stability theory. The work treated both the case in which damping and stiffness could be regulated independently and the case where the stiffness and damping are regulated jointly. Loh and Ma (1994) investigated the performance of controllers that vary linear damping and stiffness parameters for seismically excited buildings. The work compared the performance of optimal, instantaneous optimal and Lyapunov control strategies. The optimal control strategy provided significantly better reduction in peak floor displacements than the alternate controllers did. Singh, et al (1997) investigated the performance of a sliding mode control algorithm for a structure with variable linear damping and stiffness characteristics. Dyke (1996) and Dyke et al. (1996b) experimentally verified the seismic response characteristics of a planar three-story structure with a MR damper. Clipped-optimal acceleration feedback control algorithms were developed using  $H_2/LQG$  control design methods that did not include the semi-active actuator dynamics. A simple bi-state law on the voltage applied to the MR damper was used to track the desired control force.

In reality, many semi-active devices are characterized by nonlinear dynamics but only a few researchers treat the actuator dynamics in the control design. Patten et al. (1994) utilized a control law aimed at minimizing the first derivative of a quadratic Lyapunov function (Mohler, 1991) (Vincent and Grantham, 1997) to mitigate structural vibrations. The Lyapunov function includes terms weighting the differential pressure state variable associated with the semi-active actuator. The analysis did not prove stability. Lee (1998) tested a variety of semi-active control algorithms, including a Lyapunov control design, on a two degree-of-freedom test structure. That work assumed the force of the semi-active actuator was limited and did not treat the coupled system

dynamics in the subsequent stability analysis. Experimental results indicate that both the Lyapunov controller and a control logic that minimizes the product of the actuator force and the actuator relative velocity are able to significantly reduce the dynamic response of the test structure. Both control algorithms provide similar response reductions compared to the no control case. The semi-active structural control design research in the Literature is categorized in Figure 4.1. None of the work has addressed the stability of systems with coupled nonlinear actuator dynamics.

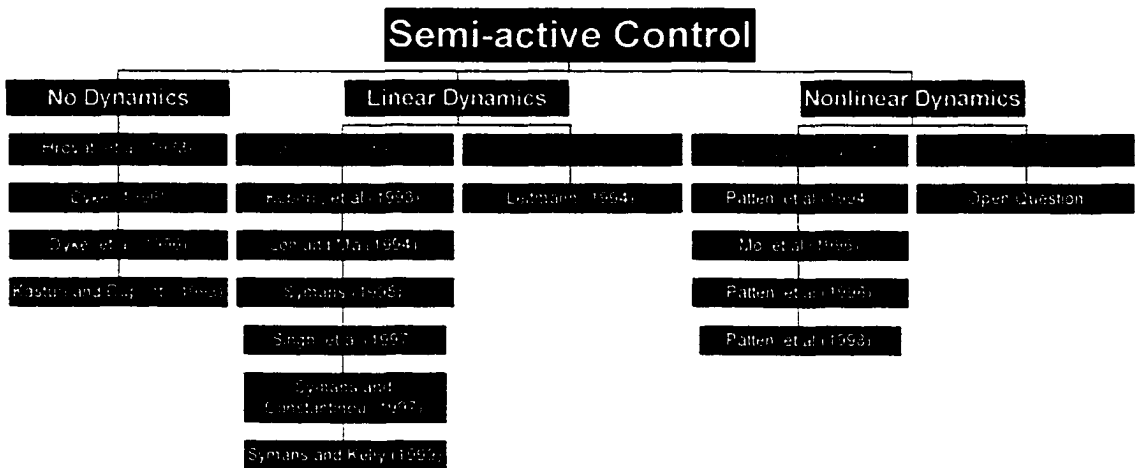


Figure 4.1: Summary of semi-active structural control design research

### 4.3 General System Model with Nonlinear Semi-active Actuator Dynamics

Consider a class of semi-actively controlled linear systems

$$\dot{x} = A_s x + \sum_{i=1}^m B_{s_i} \Delta p_i + D_s d \quad (4.1)$$

with  $m$  semi-active actuators that satisfy nonlinear dynamics of the form

$$\Delta \dot{p}_i = A_{sa_i} x - B_{sa_i}(\Delta p_i) \cdot \Delta p_i u_i, \quad i = 1, 2, \dots, m \quad (4.2)$$

where  $A_s$  is an  $n \times n$  Hurwitz matrix,  $x$  is an  $n \times 1$  state vector,  $\Delta p_i$  is the scalar state of the  $i^{\text{th}}$  semi-active actuator.  $d$  is a Lebesgue-measurable  $r \times 1$  disturbance to the system and  $A_s$  and  $B_s = [B_{s_1}, B_{s_2}, \dots, B_{s_m}]$  form a controllable pair. For  $i = 1, 2, \dots, m$ ,  $A_{sa_i}$  is a  $1 \times n$  vector coupling the  $i^{\text{th}}$  semi-active actuator to the system,  $B_{sa_i}$  is a scalar function of the  $i^{\text{th}}$  actuator state  $\Delta p_i$  and  $u_i$  is a scalar control input to the  $i^{\text{th}}$  actuator. The variables  $\Delta p_i$ ,  $u_i$ ,  $i = 1, 2, \dots, m$ , and  $d_j$ ,  $j = 1, 2, \dots, r$  are bounded.

$$|\Delta p_i(t)| < \Delta p_{i,\max}, \quad \forall t, \quad i = 1, 2, \dots, m \quad (4.3)$$

$$0 \leq u_i(t) \leq u_{i,\max}, \quad \forall t, \quad i = 1, 2, \dots, m \quad (4.4)$$

$$|d_j(t)| \leq d_{j,\max}, \quad \forall t, \quad j = 1, 2, \dots, r \quad (4.5)$$

For  $i = 1, 2, \dots, m$ ,  $B_{sa_i}$  is a scalar function of  $\Delta p_i$ , which satisfies the two conditions

$$\text{Condition I:} \quad \lim_{\Delta p_i \rightarrow 0} B_{sa_i}(\Delta p_i) \Delta p_i = 0 \quad (4.6)$$

$$\text{Condition II:} \quad 0 \leq \delta_i \leq B_{sa_i}(\Delta p_i) \quad \forall \Delta p_i : |\Delta p_i| \leq \Delta p_{i,\max} \quad (4.7)$$

for some  $\delta_i \geq 0$  such that the following matrix  $A$  is Hurwitz

$$A = \begin{bmatrix} A_s & B_s \\ A_{sa} & \Gamma \end{bmatrix} \quad (4.8)$$

where

$$A_{sa} = \begin{bmatrix} A_{sa_1} \\ A_{sa_2} \\ \vdots \\ A_{sa_m} \end{bmatrix}$$

and  $\Gamma$  is a diagonal  $m \times m$  matrix with elements

$$\Gamma_{ii} = -\delta_i u_{i,\max}, \quad i = 1, 2, \dots, m$$

Let  $\delta_i, i = 1, 2, \dots, m$ , be a set of constants such that Condition II is satisfied and (4.8) is Hurwitz. Equation (4.2) is modified by adding and subtracting the term  $\delta_i \Delta p_i u_{i \max}$

$$\Delta \dot{p}_i = A_{sa_i} x - \delta_i \Delta p_i u_{i \max} + (\delta_i u_{i \max} - B_{sa_i}(\Delta p_i) u_i) \Delta p_i, \quad i = 1, 2, \dots, m \quad (4.9)$$

Equations (4.1) and (4.9) are combined to obtain a state space realization of the coupled system.

$$\dot{z} = Az + \sum_{i=1}^m B_i (\delta_i \Delta p_i u_{i \max} - B_{sa_i}(\Delta p_i) \Delta p_i u_i) + Dd \quad (4.10)$$

where

$$B = [B_1 \quad B_2 \quad \dots \quad B_m] = \begin{bmatrix} 0_{n \times m} \\ I_{m \times m} \end{bmatrix} \quad (4.11)$$

$$D = \begin{bmatrix} D_s \\ 0_{m \times r} \end{bmatrix} \quad (4.12)$$

and the augmented state vector is

$$z = \begin{bmatrix} x_{n \times 1} \\ \Delta p_{m \times 1} \end{bmatrix} \quad (4.13)$$

with  $\Delta p^T = [\Delta p_1 \quad \Delta p_2 \quad \dots \quad \Delta p_m]$ . In (4.3) the bound on  $\Delta p$  is due to physical limitations of the semi-active actuator state. For example, the state for the semi-active hydraulic actuator described in Chapter 3 is differential pressure, which is limited to a safe operating limit. For variable orifice hydraulic actuators the limits on  $u$  are due to the geometry of the control valve.

In practice, a set of positive  $\delta_i, i = 1, 2, \dots, m$ , is needed to make  $A$  Hurwitz and  $\delta_i$  is usually selected as the greatest lower bound of  $B_{sa_i}(\Delta p_i)$ .

#### 4.4 Quickest Descent Control Law

The energy in the coupled structure/actuator system is quantified by a quadratic Lyapunov function of the form

$$\dot{V}(z) = z^T P z, z \in R^{n+m} \quad (4.14)$$

where  $P$  is a symmetric positive definite weighting matrix on the augmented state vector that is yet to be specified. ( $P$  is specified later as the solution to (4.22)) The rate of change of energy in the system can be represented as the first derivative of the function  $V$  with respect to time

$$\dot{V} = z^T P \dot{z} + \dot{z}^T P z \quad (4.15)$$

Substituting the coupled state equation (4.10) into (4.15) results in

$$\dot{V}(z) = z^T (PA + A^T P) z + \sum_{i=1}^m 2z^T P B_i \Delta p_i (\delta_i u_i - B_{sa_i}(\Delta p_i) u_i) + 2z^T P D d \quad (4.16)$$

It can be seen that only one term on the right hand side of (4.16) is directly influenced by the control input  $u_i$ . For quickest descent, the goal of the control is to minimize each term

$$2z^T P B_i B_{sa_i}(\Delta p_i) \Delta p_i u_i \quad (4.17)$$

for all  $i = 1, 2, \dots, m$ , subject to the constraints (4.4). Noting that  $B_{sa_i}$  is non-negative, the minimization is achieved by the control law for each input  $u_i$

$$u_i(t) = \begin{cases} 0 & \text{if } z^T P B_i \Delta p_i < 0 \\ u_{i \max} & \text{if } z^T P B_i \Delta p_i \geq 0 \end{cases} \quad (4.18)$$

The resulting bang-bang control algorithm is often referred to in the literature as a quickest descent controller (e.g., Vincent and Grantham, 1997) The following section

provides a straightforward method for determining a matrix  $P$  that guarantees Lyapunov stability of the coupled actuator and structure.

#### 4.5 Lyapunov Stability Analysis

Consider the Lyapunov function (4.14). For the positive definite matrix  $P$  let  $V_1$  denote a positive value and consider the resulting ellipsoid  $E_1$

$$E_1 = \{z \in R^{n+1} : z^T P z = V_1\} \quad (4.19)$$

let  $V_{\max}$  be the largest value of  $V_1$  such that  $E_1$  does not contain a point  $z$  with some component  $y$  that violates the constraint (4.3). Also, define the operating space  $E_{\max}$  as the ellipsoidal region

$$E_{\max} = \{z \in R^{n+1} : z^T P z \leq V_{\max}\} \quad (4.20)$$

The first time derivative of the Lyapunov function (4.16) can be rewritten as

$$\dot{V}(z) = -z^T Q z + \sum_{i=1}^m 2z^T P B_i \Delta p_i \left( \delta_i u_{i,\max} - B_{s_i}(\Delta p_i) u_i \right) + 2z^T P D d \quad (4.21)$$

where  $Q$  is defined as

$$Q = -(PA + A^T P) \quad (4.22)$$

At this point,  $P$  is determined by solving (4.22) for some specified positive definite matrix  $Q$ . For  $A$  stable and  $Q$  positive definite, there is a unique positive definite solution  $P$  to the Lyapunov equation (4.22). This value of  $P$  is used in equations (4.14)-(4.18) to determine the control logic. The matrix  $Q$  is essentially a performance index for the control and can be designed using modal or state penalties. If it can be shown that

$$\dot{V} \leq -z^T Q z, \quad Q > 0 \quad (4.23)$$

then all conditions for Lyapunov stability are satisfied for the system controlled by (4.18). (Kalman and Bertram, 1960) The following lemmas and theorems show that (4.23) holds for the appropriate space.

In Lemma 1, it is shown that the term in the summation on the right hand side of (4.21) is non-positive.

**Lemma 1:** For the control law (4.18), the following inequality holds for all  $|\Delta p_i| \leq \Delta p_{i, \max}, i = 1, 2, \dots, m$ :

$$z^T P B_i \Delta p_i (\delta_i u_{i, \max} - B_{sa_i}(\Delta p_i) u_i) \leq 0 \quad (4.24)$$

**Proof:** Note that if  $\Delta p_i = 0$  then (4.24) holds for any  $B_{sa_i}(\Delta p_i)$  satisfying Condition I.

For the following, assume  $\Delta p_i \neq 0$ .

Case (a):  $z^T P B_i \Delta p_i = 0$

Since  $\Delta p_i \neq 0$ ,  $z^T P B_i = 0$  which satisfies (4.24).

Case (b):  $z^T P B_i \Delta p_i < 0$

For this case  $u_i = 0$ . Therefore,

$$z^T P B_i \Delta p_i (\delta_i u_{i, \max} - B_{sa_i}(\Delta p_i) u_i) = z^T P B_i \Delta p_i \delta_i u_{i, \max} \quad (4.25)$$

Since  $\delta_i$  is non-negative, (4.24) follows.

Case (c):  $z^T P B_i \Delta p_i > 0$  and  $|\Delta p_i| \leq \Delta p_{i, \max}$

For this case  $u_i = u_{i, \max}$ . The left hand side of (4.24) can be rewritten as

$$z^T P B_i \Delta p_i (\delta_i u_{i, \max} - B_{sa_i}(\Delta p_i) u_i) = z^T P B_i \Delta p_i (\delta_i - B_{sa_i}(\Delta p_i)) u_{i, \max} \quad (4.26)$$

From Condition II,  $\delta_i \leq B_{sa_i}(\Delta p_i)$  and (4.24) holds.

This concludes the proof of the lemma.

**Lemma 2:** For the control law (4.18), the following inequality holds for all

$$|\Delta p_i| \leq \Delta p_{i \max}, i = 1, 2, \dots, m :$$

$$\sum_{i=1}^m z^T P B_i \Delta p_i (\delta_i u_{i \max} - B_{sa_i}(\Delta p_i) u_i) \leq 0 \quad (4.27)$$

The proof of this lemma follows directly from Lemma 1.

Incorporating the inequality (4.27) of Lemma 2 into (4.21), it follows that

$$\dot{V} \leq -z^T Q z + 2z^T P D d \quad (4.28)$$

**Theorem 1:** For the case in which the excitation to the system  $d = 0$ , the control law (4.18) provides quadratic asymptotic stability for the system (4.10) in the region  $z \in E_{\max}$ .

**Proof:** From Lemma 2,  $\dot{V} \leq -z^T Q z$  for the case  $d = 0$ . This yields quadratic asymptotic stability since both  $P$  and  $Q$  are positive definite.

For the nonzero disturbance case define

$$z_d = 2Q^{-1} P D d_{\max} \quad (4.29)$$

and substitute into (4.28) to obtain

$$\dot{V} \leq -z^T Q z + z^T Q z_d \quad (4.30)$$

Denote the subspace of disturbance vectors as

$$S_d = \{(d_1, d_2, \dots, d_r) : |d_j| \leq d_{j \max}, j = 1, 2, \dots, r\} \quad (4.31)$$

and make the definitions

$$V_{d \max} = \max\{z_d^T Q z_d : z_d = 2Q^{-1} P D d, d \in S_d\} \quad (4.32)$$

$$E_{V_{d_{\max}}} = \left\{ z \in R^{n+m} : z^T Q z \leq V_{d_{\max}} \right\} \quad (4.33)$$

Let  $V_{\min}$  be the minimum value of  $\sigma$  such that the following condition holds for

$$z \in R^{n+m}$$

$$\text{if } z^T Q z \leq V_{d_{\max}} \text{ then } z^T P z \leq \sigma \quad (4.34)$$

Define the ellipsoid

$$E_{\min} = \left\{ z \in R^{n+m} : z^T P z \leq V_{\min} \right\} \quad (4.35)$$

It is assumed that  $V_{\min} < V_{d_{\max}}$ .

**Theorem 2:** For Lebesgue measurable disturbances  $d_j$ , satisfying  $|d_j(t)| \leq d_{j_{\max}}$ ,

$j = 1, 2, \dots, r$ , the control law (4.18) provides quadratic convergence to the ellipsoid  $E_{\min}$ .

In particular, if  $z \notin E_{V_{d_{\max}}}$  then

$$\dot{V}(z) < -(\lambda - 1)^2 V_{d_{\max}} \quad (4.36)$$

where

$$\lambda = \sqrt{\frac{z^T Q z}{V_{d_{\max}}}} > 1 \quad (4.37)$$

**Proof:** It suffices to show that (4.36) holds. Let  $z$  denote an arbitrary vector that does not

belong to  $E_{V_{d_{\max}}}$  and let  $d$  be some arbitrary disturbance vector in  $S_d$ . Define  $\lambda$  and  $\gamma$

as follows

$$\lambda = \sqrt{\frac{z^T Q z}{V_{d_{\max}}}} \quad (4.38)$$

$$\gamma = \sqrt{\frac{z_d^T Q z_d}{V_{d_{\max}}}} \quad (4.39)$$

Since  $z \notin E_{V_{d_{\max}}}$  and  $z_d \in E_{V_{d_{\max}}}$ , it follows that  $\lambda > 1$  and  $\gamma \leq 1$ .

Since  $Q$  is positive definite, it can be decomposed into positive square root factors  $Q = W^T W$ . Inequality (4.30) can be rewritten as

$$\dot{V}(z) \leq -\lambda^2 V_{d_{\max}} + (Wz)^T (Wz_d) \quad (4.40)$$

Since the second term is the dot product of two vectors, it can be rewritten as

$$(Wz)^T (Wz_d) = \|Wz\|_2 \|Wz_d\|_2 \cos(\theta) \quad (4.41)$$

where  $\theta$  is the angle between  $Wz$  and  $Wz_d$ . Using (4.38) and (4.39), the dot product (4.41) becomes

$$(Wz)^T (Wz_d) = \lambda \gamma V_{d_{\max}} \cos(\theta) \quad (4.42)$$

Substituting (4.42) into (4.40) gives

$$\dot{V}(z) \leq -\lambda^2 V_{d_{\max}} + \lambda \gamma V_{d_{\max}} \cos(\theta) \quad (4.43)$$

Noting that  $\gamma \cos(\theta) \leq 1$  and  $\gamma V_{d_{\max}} > 0$ , (4.43) satisfies

$$\dot{V}(z) \leq -\lambda^2 V_{d_{\max}} + \lambda V_{d_{\max}} < -(\lambda - 1)^2 V_{d_{\max}} \quad (4.44)$$

which gives (4.36).

The ellipsoid  $E_{\min}$  provides a stable attractor (ball of ultimate boundedness) for the semi-actively controlled system (4.10) for disturbances satisfying the bound (4.5). When the disturbance vector is zero, the control law (4.18) provides quadratic asymptotic stability to the origin for any initial condition within the ellipsoidal region  $E_{\max}$ .

Consider the case where the disturbance input is a bounded scalar function of time.

$$|d(t)| \leq d_{\max} \quad (4.45)$$

Let  $V_d$  be the minimum value of  $\sigma$  such that the following condition holds for  $z \in R^{n+m}$

$$\text{if } z^T Qz \leq |2z^T P D d_{\max}| \text{ then } z^T Pz \leq \sigma \quad (4.46)$$

Define the ellipsoid

$$E_d = \{z \in R^{n+m} : z^T Pz \leq V_d\} \quad (4.47)$$

It is assumed that  $V_d < V_{\max}$ .

Define the dipole

$$D_d = \{z : z^T Qz \leq |2z^T P D d_{\max}|\} \quad (4.48)$$

It is apparent that  $D_d \subset E_d$ .

**Lemma 3:** If  $z \notin D_d$  then  $\dot{V} < 0$

**Corollary 1:**  $\dot{V} < 0$  for all  $z \notin E_d$

**Proof of Corollary:** This follows from Lemma 3 since  $D_d \subset E_d$ .

**Proof of Lemma 3:** Rewriting the disturbance as  $d = \gamma d_{\max}$  where  $|\gamma| \leq 1$  and inserting in (4.28) results in

$$\dot{V} \leq -z^T Qz + 2\gamma z^T P D d_{\max} \quad (4.49)$$

Three cases are considered to determine the sign definiteness of the right hand side of (4.49).

Case (a): Suppose  $\gamma z^T P D d_{\max} \leq 0$ . Then  $\dot{V} < 0$  since  $Q$  is positive definite.

Case (b): Suppose  $\gamma z^T P D d_{\max} > 0$  and  $\gamma > 0$ . Then  $z^T P D d_{\max} > 0$  and it follows that since  $z \notin D_d$ ,  $z^T Qz > 2z^T P D d_{\max}$  which is substituted into the right hand side of (4.49) to obtain

$$-z^T Qz + 2\gamma z^T P D d < (\gamma - 1) z^T Qz \quad (4.50)$$

which satisfies  $\dot{V} < 0$  since  $0 < \gamma \leq 1$ .

Case (c): Suppose  $\gamma z^T P D d_{\max} > 0$  and  $\gamma < 0$ . Then  $z^T P D d_{\max} < 0$  and since  $z \notin D_d$ ,

it follows from (4.48) that  $-z^T Qz < 2z^T P D d_{\max}$  which is substituted into the right hand side of (4.49) to obtain

$$-z^T Qz + 2\gamma z^T P D d < -(\gamma + 1) z^T Qz \quad (4.51)$$

which satisfies  $\dot{V} < 0$  since  $-1 \leq \gamma < 0$ .

Since  $z$  was arbitrary for  $z \notin E_d$ , Lemma 3 follows.

#### 4.6 Coupled Structure/Actuator System Realization

The structural model (3.8) and the semi-active actuator model (3.42) are combined to obtain a state space realization of the coupled system

$$\dot{z} = Az + B(\delta \Delta p u_{\max} - B_{sa}(\Delta p) \Delta p u) + Dd \quad (4.52)$$

where

$$z = \begin{bmatrix} x \\ \Delta p \end{bmatrix} \quad (4.53)$$

$$A = \begin{bmatrix} A_s & B_s \\ A_{sa} & \delta u_{\max} \end{bmatrix} \quad (4.54)$$

$$B = [0 \ 0 \ 0 \ 0 \ 0 \ 0 \ 0 \ 1]^T \quad (4.55)$$

$$D = \begin{bmatrix} D_s \\ 0 \end{bmatrix} \quad (4.56)$$

It is assumed that the actuator differential pressure  $\Delta p$  is bounded as well as the valve orifice area  $u$

$$|\Delta p(t)| < \Delta p_{\max} \quad (4.57)$$

$$0 \leq u(t) \leq u_{\max} \quad (4.58)$$

The model can treat laminar, turbulent and transition flow by allowing the discharge coefficient in (3.44) to vary with differential pressure. For laminar flow

$$C_d(\Delta p) = k_1 |\Delta p|^{1/2} \quad 0 \leq |\Delta p| \leq \Delta p_a \quad (4.59)$$

In the transition between laminar and turbulent flow

$$C_{da} \leq C_d(\Delta p) \leq C_{d\max} \quad \Delta p_a \leq |\Delta p| \leq \Delta p_b \quad (4.60)$$

where  $C_{da}$  is obtained from (4.59) with  $\Delta p = \Delta p_a$ . In the turbulent region

$$C_d(\Delta p) = C_{db} \quad \Delta p_b \leq |\Delta p| \leq \Delta p_{\max} \quad (4.61)$$

The value for  $\Delta p_a$  is selected such that  $C_{da} \leq C_{db}$ .

Consider the laminar flow region where  $\Delta p \rightarrow 0$ . Substituting (4.59) into (3.44) it is apparent that  $B_{sa}(\Delta p)$  satisfies Condition I (4.6).  $B_{sa}(\Delta p)$  also satisfies inequality (4.7) of Condition II for a constant  $\delta$  that satisfies

$$0 \leq \delta \leq \delta_{\max} = \alpha_0 \sqrt{\frac{2}{\rho}} \min \left\{ \frac{C_{da}}{\sqrt{\Delta p_b}}, \frac{C_{db}}{\sqrt{\Delta p_{\max}}} \right\} \quad (4.62)$$

For all of the flow regions,  $\delta_{\max}$  is the least upper bound satisfying (4.7).

Since the model satisfies Conditions I and II the stability results in Section 4.5 hold for the coupled system realization (4.52).

## 4.7 Lyapunov Performance Analysis

A variety of control cases were considered in an effort to tune the performance of the Lyapunov controller for a single semi-active actuator installed between the ground and first floor of the scale three-story structure (Position 1 in Figure 2.2). Two techniques were used to determine  $P$  for the control logic in (4.18). The first relied on a modal canonical realization for the coupled system (4.52) with the modes ordered in descending frequency. The second method utilized the system model (4.52) directly. In all cases,  $Q$  was a diagonal matrix and  $P$  was obtained by solving the Lyapunov equation (4.22). For reference, Control Law 1 was a passive control configuration with the semi-active actuator valve completely open. The diagonal elements of  $Q$  and the associated values of  $PB$  used for the control logic (4.18) are provided in Tables 4.1 and 4.2.

The primary objective of the control system is to minimize the peak inter-story drift to prevent the structure from yielding without exceeding the capacity of the semi-active actuator assembly. Two measures were used to assess the performance of each controller. The first method compared the infinity norm of each state obtained with closed loop control with the infinity norms for the open valve case and a theoretical value of the infinity norm of system (4.52) that neglected the nonlinear actuator dynamics. The relative displacements ( $z_1$ ,  $z_2$  and  $z_3$ ) and the differential pressure ( $z_7$ ) were of primary concern and the relative velocities ( $z_4$ ,  $z_5$  and  $z_6$ ) were secondary.

The second metric utilized a scalar performance index defined by

$$PI = \max\left(\sqrt{z^T K z}\right) \quad (4.63)$$

where  $K$  is a positive definite diagonal matrix defined as

which again emphasizes the importance of the relative displacements and the actuator differential pressure.

Numerical simulations were conducted to assess the response characteristics of each controller using three different types of scalar disturbance inputs. The first two disturbance laws are based on the response of the structure and the resulting disturbance inputs are functions of the state vector. The third input is fixed for all the controllers.

**Table 4.1:** Modal control penalties and resulting gains

Test	$Q_{11}$	$Q_{22}$	$Q_{33}$	$Q_{44}$	$Q_{55}$	$Q_{66}$	$Q_{77}$	$PB$
2	1	1	1	1	1	1	1	$[0.899 \ -5.47 \ 7.29 \ 0.161 \ -0.0766 \ 0.0301 \ 0.287]^T$
3	100	1	1	1	1	1	1	$[0.900 \ -5.47 \ 7.29 \ 0.162 \ -0.0766 \ 0.0301 \ 0.369]^T$
4	1	100	1	1	1	1	1	$[1.67 \ -174 \ 328 \ 2.17 \ -3.90 \ 3.11 \ 7.29]^T$
5	1	1	100	1	1	1	1	$[9.23 \ -208 \ 378 \ 2.62 \ -4.12 \ 3.06 \ 8.10]^T$
6	1	1	1	100	1	1	1	$[0.144 \ -47.0 \ 51.9 \ 2.72 \ -1.90 \ -2.13 \ 5.60]^T$
7	1	1	1	1	100	1	1	$[74.9 \ -116 \ 4.12 \ 5.09 \ -1.20 \ -2.77 \ 7.56]^T$
8	1	1	1	1	1	100	1	$[6.52 \ -13.9 \ 2.11 \ 2.39 \ 1.73 \ 1.05 \ 0.792]^T$
9	1	1	1	1	1	1	100	$[1.93 \ -15.2 \ 1.46 \ 1.92 \ 1.34 \ 0.830 \ 0.699]^T$
10	100	1	1	1	1	100	1	$[6.52 \ -13.9 \ 2.11 \ 2.39 \ 1.73 \ 1.05 \ 0.874]^T$
11	100	1	1	1	1	1	100	$[1.93 \ -15.2 \ 1.46 \ 1.92 \ 1.34 \ 0.830 \ 0.781]^T$
12	100	1	1	1	1	100	100	$[7.54 \ -23.7 \ -3.73 \ 4.15 \ 3.15 \ 1.85 \ 1.29]^T$

**Table 4.2:** State control penalties and resulting gains

Test	$Q_{11}$	$Q_{22}$	$Q_{33}$	$Q_{44}$	$Q_{55}$	$Q_{66}$	$Q_{77}$	$PB$
13	1	1	1	1	1	1	1	$[-0.0310 \ -1.35 \ 2.19 \ 0.0451 \ -0.0284 \ 0.0206 \ 0.0885]^T$
14	100	1	1	1	1	1	1	$[0.0238 \ -1.35 \ 2.19 \ 0.0502 \ -0.0249 \ 0.0224 \ 0.0903]^T$
15	1	100	1	1	1	1	1	$[-0.0316 \ -1.40 \ 2.18 \ 0.0484 \ -0.0266 \ 0.0223 \ 0.0902]^T$
16	1	1	100	1	1	1	1	$[-0.0315 \ -1.39 \ 2.24 \ 0.0463 \ -0.0284 \ 0.0207 \ 0.0898]^T$
17	1	1	1	100	1	1	1	$[-0.738 \ 0.740 \ 0.106 \ 1.72 \ 0.00180 \ -0.00350 \ 2.07]^T$
18	1	1	1	1	100	1	1	$[-1.31 \ -45.3 \ 49.8 \ 1.59 \ -1.45 \ 1.74 \ 3.66]^T$
19	1	1	1	1	1	100	1	$[-1.17 \ -93.4 \ 173 \ 1.27 \ -1.45 \ 0.359 \ 3.27]^T$
20	1	1	1	1	1	1	100	$[-0.0310 \ -1.35 \ 2.19 \ 0.0451 \ -0.0284 \ 0.0206 \ 0.108]^T$

The objective of Disturbance Law 1 is to maximize the first time derivative of the Lyapunov function at each point in time.

$$d = \begin{cases} d_{\max} & \text{if } z^T PD \geq 0 \\ d_{\min} & \text{if } z^T PD < 0 \end{cases} \quad (4.65)$$

This logic is essentially the opposite of the quickest descent control law (4.18) and is referred to as a quickest ascent disturbance. This disturbance is not only dependent on the system states  $z$  but also on the matrix  $P$ .

Disturbance Law 2 is also state dependent and is prescribed by the following:

$$d = \max_{\pm d_{\max}} \left( \frac{z^T \dot{z}(d)}{|z| \cdot |\dot{z}(d)|} \right) \quad (4.66)$$

The final disturbance input was a 0.5-50-Hz band limited white noise ground acceleration that was identical for each controller. Each of the disturbance inputs had 1- $\text{m/s}^2$  maximum amplitude.

The infinity norms for states  $z_1$ - $z_7$  are plotted in Figures 4.2-4.8 for each input and each semi-active controller. The figures indicate that modal control laws 8-12 provide consistently lower peak displacements than the other control laws for each disturbance input. State controller 17 provided a small first floor inter-story drift (3.9-mm) but  $z_2$  exceeded 30-mm. Out of the state controllers, laws 14 and 15 had the best overall inter-story drift characteristics but did not provide the same levels of reduction as modal control laws 8-12. Figure 4.8 indicates that the modal controllers provided much lower peak actuator differential pressures than the state controllers except for the white noise input.

The infinity norms for Disturbance 1 are presented in Tables 4.3 and 4.4. Since the disturbance is dependant on the value of  $P$  as well as the state, a different valve open test was conducted for each controller. The valve open test results are provided in Table 4.3 while the closed loop control results are given in Table 4.4. Modal control laws 8 and 10 yielded the lowest maximum relative displacements (3.67-mm) compared to 3.76-mm for controllers 9 and 11. Controller 18 had the best displacement response characteristics of the state controllers with a maximum drift of 6.56-mm but required twice the peak differential pressure as the modal controllers. Modal controller 11 provided at least a 67% reduction in drift and at least a 69% reduction in peak relative velocity over the open valve configuration.

The peak response characteristics for Disturbance Law 2 are summarized in Table 4.5. This disturbance excites the system with the valve open (Control 1) much more than the other disturbance inputs by inputting a square wave at the fundamental frequency of the structure. However, the data indicates that the semi-active controllers were able to

effectively reduce the peak responses. Controller 15 offered the best performance of the state controllers with 5.66-mm peak drift and at least an 82% reduction over the open valve case. Control 11 had the best overall performance with a 3.11-mm maximum inter-story drift and reductions of 96%, 94% and 79% for the first three floors respectively and required 25% less peak differential pressure than the state controller 15.

The Banded White Noise infinity norms are listed in Table 4.6. Control law 11 provided the lowest maximum inter-story drift (1.10-mm) of the modal control laws while controller 14 had the best overall performance (1.02-mm). The state control law also only generated half of the differential pressure as gain set 11. Controller 14 also provided at least a 63% reduction in relative velocity compared to the valve open case while control law 11 netted only an 18% reduction in  $z_6$ .

The second performance metric is summarized in Table 4.7 for each of the disturbances. The theoretical values of the performance index radius are based on the smallest  $K$  ellipsoids that contain the stability ellipsoid  $E_{\text{min}}$  for the general disturbance case and the ellipsoid containing the dipole  $E_d$  for the scalar disturbance input case. The simulated values are much smaller than the theoretical values (more than two orders of magnitude), which are expected since the stability analysis neglects the contribution of the semi-active actuator. The  $K$ -norms indicate that control law 15 has the least  $K$ -norm of the state controllers for Disturbance Laws 1 and 2 (11.5 and 8.00 respectively). Modal control law 11 provides the smallest  $K$ -norm for Disturbance 1 (4.64) and Disturbance 2 (4.95). Controller 14 performs the best for the white noise input with a  $K$ -norm of 1.41 compared to 1.70 for modal control 2.

The theoretical values for the radii of the attractor ellipsoid  $E_{\min}$  for the general disturbance case and the ellipsoid  $E_d$  containing the dipole for the scalar disturbance input case are compared to simulation data in Table 4.8. The data indicate that the radii obtained in the stability analysis are conservative in most cases with values up to five orders of magnitude larger than the values obtained by simulation. However, the theory provides a reasonable approximation for controllers 2 and 3 and differs only by a factor of approximately 3.

The simulation results indicate that a variety of performance gains can be achieved by varying the structure of the  $Q$  matrix in the Lyapunov equation and the performance of each resulting control law depends on the disturbance input. The modal controllers performed considerably better than the state controllers for all disturbances except the white noise input. At present, the best technique for selecting the values of the  $Q$  matrix is a trial-and-error process requiring time consuming numerical simulations to evaluate performance at each step, which is disturbance specific. However, good performance gains can be achieved with a minimal amount of tuning. Control law 11 which placed an emphasis on the highest and lowest modes was able to reduce the maximum relative displacements between floors by at least 61% over the open valve results.

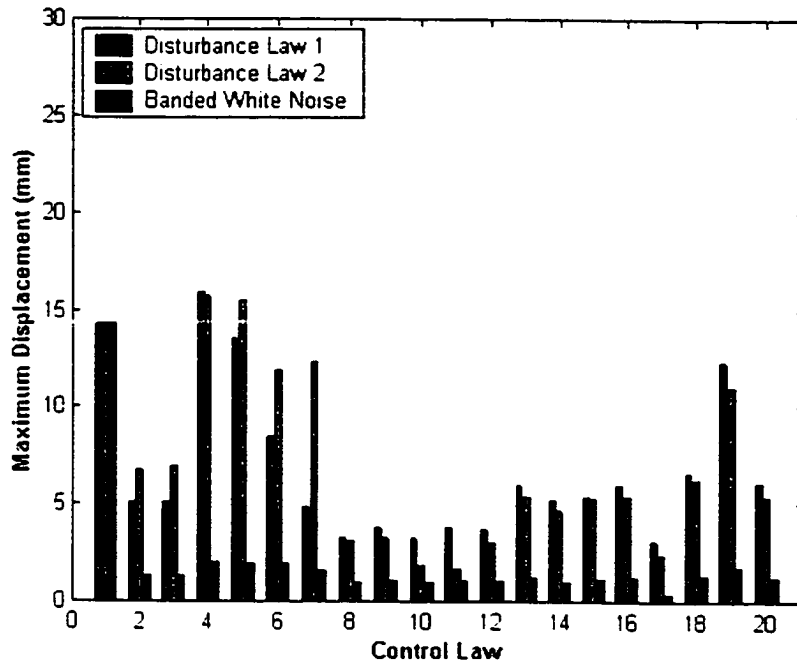


Figure 4.2: Simulated values of  $\|z_1\|_\infty$  for three disturbance cases

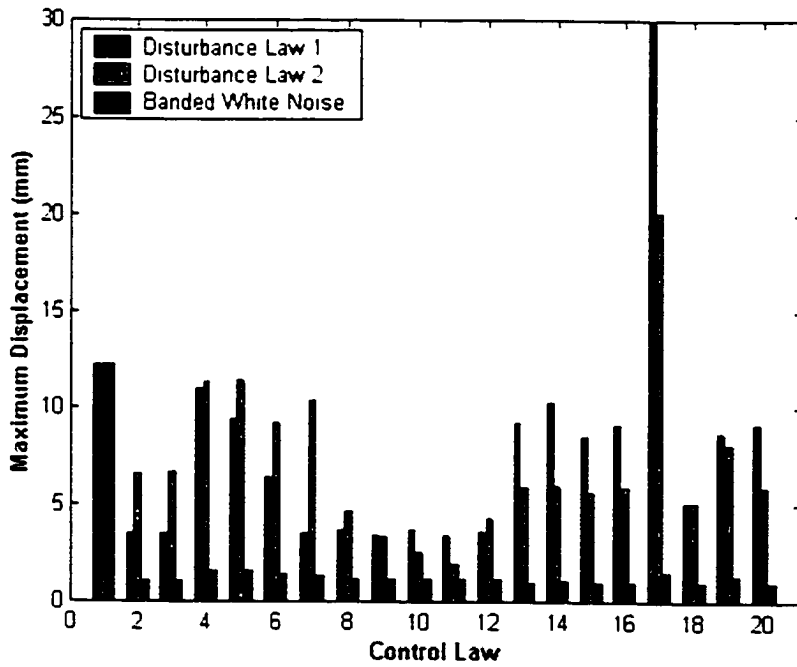


Figure 4.3: Simulated values of  $\|z_2\|_\infty$  for three disturbance cases

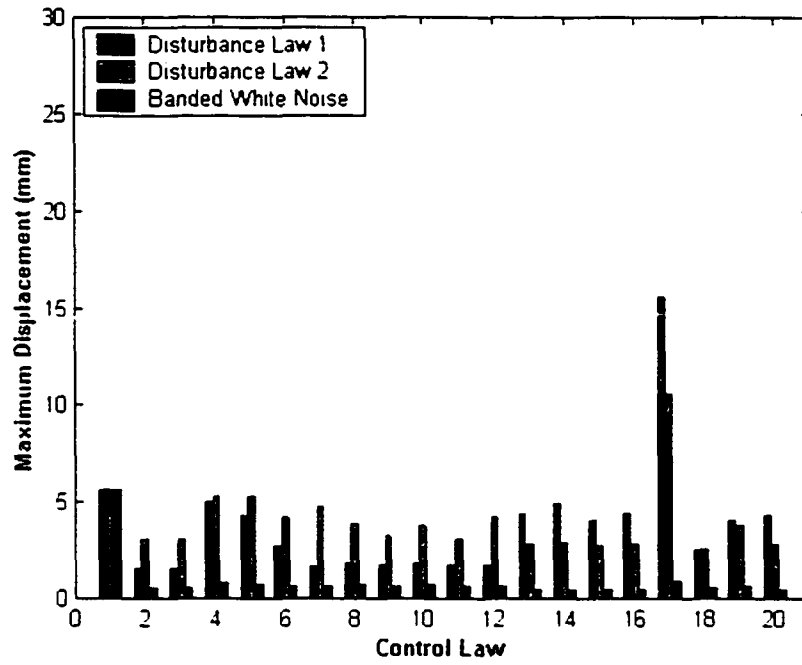


Figure 4.4: Simulated values of  $\|z_3\|_\infty$  for three disturbance cases

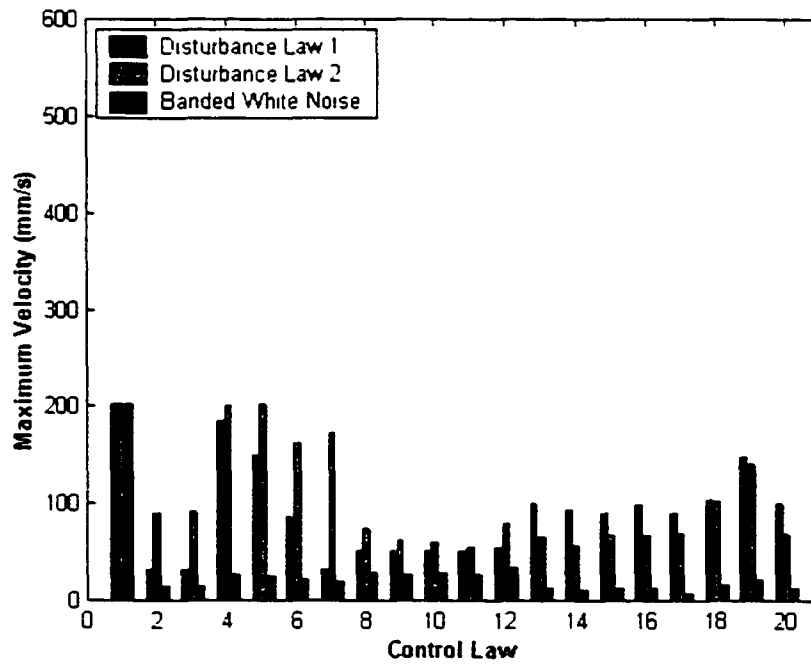


Figure 4.5: Simulated values of  $\|z_4\|_\infty$  for three disturbance cases

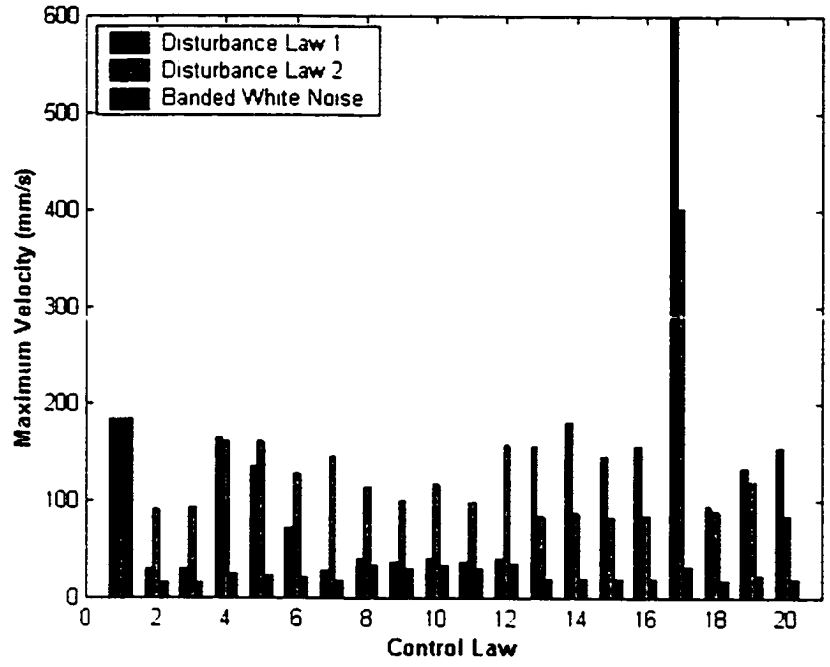


Figure 4.6: Simulated values of  $\|z_5\|_\infty$  for three disturbance cases

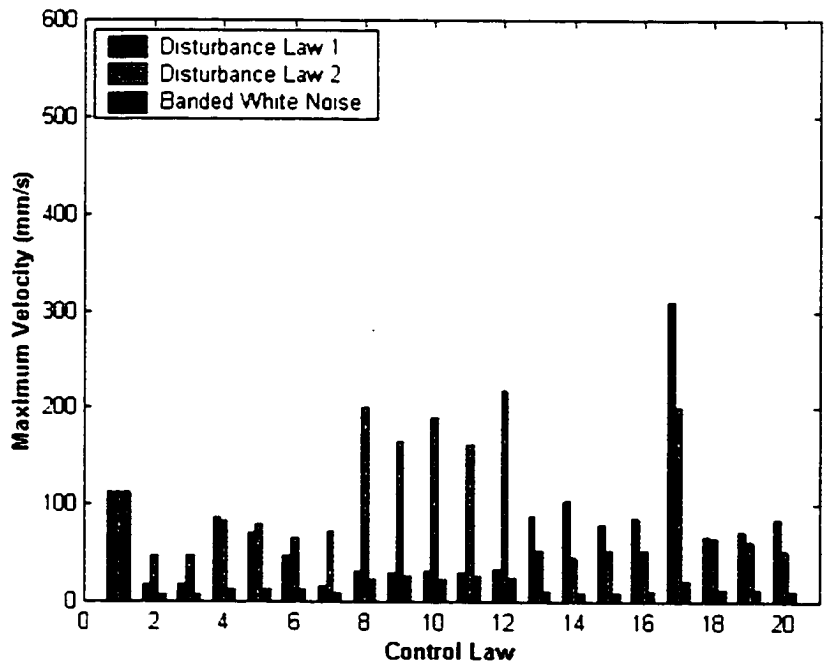
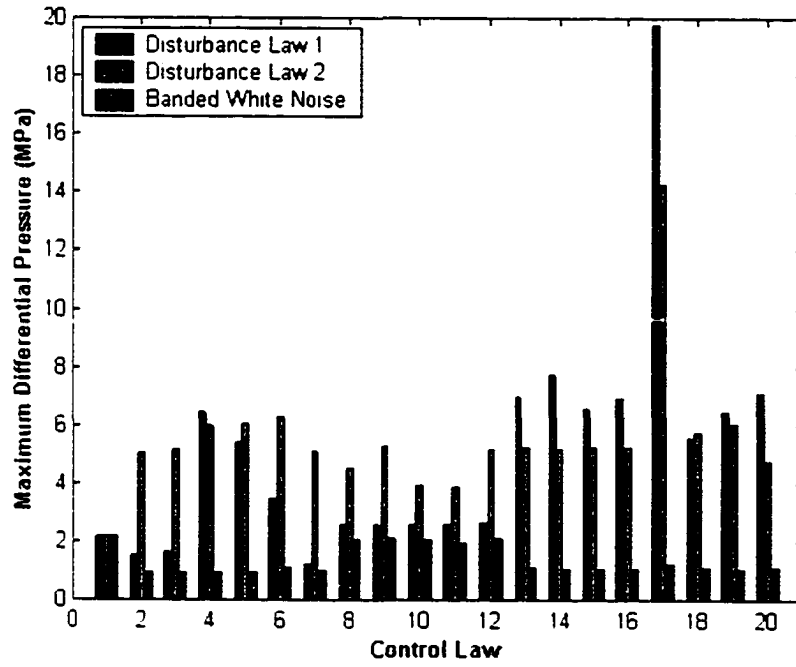


Figure 4.7: Simulated values of  $\|z_6\|_\infty$  for three disturbance cases



**Figure 4.8:** Simulated values of  $\|z_7\|_\infty$  for three disturbance cases

**Table 4.3:** Infinity norms for Disturbance Law 1 with valve open

Control Law	$\ z_1\ _\infty$ (mm)	$\ z_2\ _\infty$ (mm)	$\ z_3\ _\infty$ (mm)	$\ z_4\ _\infty$ (mm/s)	$\ z_5\ _\infty$ (mm/s)	$\ z_6\ _\infty$ (mm/s)	$\ z_7\ _\infty$ (MPa)
Bare Frame	$5.33 \cdot 10^2$	$4.19 \cdot 10^2$	$1.96 \cdot 10^2$	$7.40 \cdot 10^3$	$6.05 \cdot 10^3$	$3.04 \cdot 10^3$	-
Theoretical	$1.43 \cdot 10^1$	$1.22 \cdot 10^1$	$5.61 \cdot 10^0$	$2.02 \cdot 10^2$	$1.85 \cdot 10^2$	$1.12 \cdot 10^2$	$2.18 \cdot 10^0$
2	$1.42 \cdot 10^1$	$1.21 \cdot 10^1$	$5.47 \cdot 10^0$	$1.92 \cdot 10^2$	$1.80 \cdot 10^2$	$9.51 \cdot 10^1$	$2.18 \cdot 10^0$
3	$1.42 \cdot 10^1$	$1.21 \cdot 10^1$	$5.47 \cdot 10^0$	$1.92 \cdot 10^2$	$1.80 \cdot 10^2$	$9.51 \cdot 10^1$	$2.18 \cdot 10^0$
4	$1.29 \cdot 10^0$	$1.53 \cdot 10^0$	$1.33 \cdot 10^0$	$3.79 \cdot 10^1$	$5.48 \cdot 10^1$	$6.94 \cdot 10^1$	$4.32 \cdot 10^{-1}$
5	$1.21 \cdot 10^0$	$1.37 \cdot 10^0$	$1.27 \cdot 10^0$	$3.51 \cdot 10^1$	$5.70 \cdot 10^1$	$6.83 \cdot 10^1$	$3.98 \cdot 10^{-1}$
6	$4.85 \cdot 10^0$	$3.69 \cdot 10^0$	$1.60 \cdot 10^0$	$2.99 \cdot 10^1$	$2.92 \cdot 10^1$	$2.14 \cdot 10^1$	$3.41 \cdot 10^{-1}$
7	$4.85 \cdot 10^0$	$3.69 \cdot 10^0$	$1.60 \cdot 10^0$	$2.99 \cdot 10^1$	$2.92 \cdot 10^1$	$2.14 \cdot 10^1$	$3.41 \cdot 10^{-1}$
8	$1.42 \cdot 10^1$	$1.21 \cdot 10^1$	$5.46 \cdot 10^0$	$1.91 \cdot 10^2$	$1.80 \cdot 10^2$	$9.50 \cdot 10^1$	$2.18 \cdot 10^0$
9	$1.42 \cdot 10^1$	$1.21 \cdot 10^1$	$5.49 \cdot 10^0$	$1.93 \cdot 10^2$	$1.81 \cdot 10^2$	$9.61 \cdot 10^1$	$2.20 \cdot 10^0$
18	$1.42 \cdot 10^1$	$1.21 \cdot 10^1$	$5.46 \cdot 10^0$	$1.91 \cdot 10^2$	$1.80 \cdot 10^2$	$9.50 \cdot 10^1$	$2.18 \cdot 10^0$
19	$1.42 \cdot 10^1$	$1.21 \cdot 10^1$	$5.49 \cdot 10^0$	$1.93 \cdot 10^2$	$1.81 \cdot 10^2$	$9.61 \cdot 10^1$	$2.20 \cdot 10^0$
20	$1.42 \cdot 10^1$	$1.21 \cdot 10^1$	$5.48 \cdot 10^0$	$1.92 \cdot 10^2$	$1.80 \cdot 10^2$	$9.55 \cdot 10^1$	$2.19 \cdot 10^0$
10	$1.41 \cdot 10^1$	$1.21 \cdot 10^1$	$5.53 \cdot 10^0$	$1.95 \cdot 10^2$	$1.82 \cdot 10^2$	$9.82 \cdot 10^1$	$2.22 \cdot 10^0$
11	$1.42 \cdot 10^1$	$1.21 \cdot 10^1$	$5.51 \cdot 10^0$	$1.94 \cdot 10^2$	$1.82 \cdot 10^2$	$9.72 \cdot 10^1$	$2.21 \cdot 10^0$
12	$1.41 \cdot 10^1$	$1.21 \cdot 10^1$	$5.53 \cdot 10^0$	$1.95 \cdot 10^2$	$1.82 \cdot 10^2$	$9.78 \cdot 10^1$	$2.22 \cdot 10^0$
13	$1.41 \cdot 10^1$	$1.21 \cdot 10^1$	$5.53 \cdot 10^0$	$1.95 \cdot 10^2$	$1.82 \cdot 10^2$	$9.81 \cdot 10^1$	$2.22 \cdot 10^0$
14	$1.42 \cdot 10^1$	$1.21 \cdot 10^1$	$5.51 \cdot 10^0$	$1.94 \cdot 10^2$	$1.82 \cdot 10^2$	$9.72 \cdot 10^1$	$2.21 \cdot 10^0$
15	$1.40 \cdot 10^1$	$1.21 \cdot 10^1$	$5.54 \cdot 10^0$	$1.95 \cdot 10^2$	$1.82 \cdot 10^2$	$9.85 \cdot 10^1$	$2.22 \cdot 10^0$
16	$1.38 \cdot 10^1$	$1.20 \cdot 10^1$	$5.53 \cdot 10^0$	$1.95 \cdot 10^2$	$1.82 \cdot 10^2$	$9.86 \cdot 10^1$	$2.22 \cdot 10^0$
17	$1.41 \cdot 10^1$	$1.21 \cdot 10^1$	$5.53 \cdot 10^0$	$1.95 \cdot 10^2$	$1.82 \cdot 10^2$	$9.82 \cdot 10^1$	$2.22 \cdot 10^0$

**Table 4.4: Infinity norms for Disturbance Law 1 with control**

Control Law	$\ z_1\ _\infty$ (mm)	$\ z_2\ _\infty$ (mm)	$\ z_3\ _\infty$ (mm)	$\ z_4\ _\infty$ (mm/s)	$\ z_5\ _\infty$ (mm/s)	$\ z_6\ _\infty$ (mm/s)	$\ z_7\ _\infty$ (MPa)
Bare Frame	$5.33 \cdot 10^{-2}$	$4.19 \cdot 10^{-2}$	$1.96 \cdot 10^{-2}$	$7.40 \cdot 10^3$	$6.05 \cdot 10^3$	$3.04 \cdot 10^3$	-
Theoretical	$1.43 \cdot 10^1$	$1.22 \cdot 10^1$	$5.61 \cdot 10^0$	$2.02 \cdot 10^{-2}$	$1.85 \cdot 10^2$	$1.12 \cdot 10^{-2}$	$2.18 \cdot 10^0$
2	$5.07 \cdot 10^0$	$3.49 \cdot 10^0$	$1.55 \cdot 10^0$	$3.12 \cdot 10^1$	$2.98 \cdot 10^1$	$1.75 \cdot 10^1$	$1.55 \cdot 10^0$
3	$5.09 \cdot 10^0$	$3.50 \cdot 10^0$	$1.55 \cdot 10^0$	$3.12 \cdot 10^1$	$2.99 \cdot 10^1$	$1.75 \cdot 10^1$	$1.63 \cdot 10^0$
4	$1.59 \cdot 10^1$	$1.10 \cdot 10^1$	$5.05 \cdot 10^0$	$1.84 \cdot 10^{-2}$	$1.66 \cdot 10^2$	$8.66 \cdot 10^1$	$6.43 \cdot 10^0$
5	$1.36 \cdot 10^1$	$9.39 \cdot 10^0$	$4.30 \cdot 10^0$	$1.50 \cdot 10^{-2}$	$1.35 \cdot 10^2$	$7.04 \cdot 10^1$	$5.39 \cdot 10^0$
6	$8.45 \cdot 10^0$	$6.42 \cdot 10^0$	$2.71 \cdot 10^0$	$8.67 \cdot 10^1$	$7.27 \cdot 10^1$	$4.75 \cdot 10^1$	$3.46 \cdot 10^0$
7	$4.81 \cdot 10^0$	$3.54 \cdot 10^0$	$1.64 \cdot 10^0$	$3.13 \cdot 10^1$	$2.75 \cdot 10^1$	$1.65 \cdot 10^1$	$1.26 \cdot 10^0$
8	$3.27 \cdot 10^0$	$3.67 \cdot 10^0$	$1.80 \cdot 10^0$	$5.05 \cdot 10^1$	$4.04 \cdot 10^1$	$3.10 \cdot 10^1$	$2.56 \cdot 10^0$
9	$3.76 \cdot 10^0$	$3.42 \cdot 10^0$	$1.79 \cdot 10^0$	$5.16 \cdot 10^1$	$3.77 \cdot 10^1$	$2.98 \cdot 10^1$	$2.57 \cdot 10^0$
10	$3.27 \cdot 10^0$	$3.67 \cdot 10^0$	$1.80 \cdot 10^0$	$5.05 \cdot 10^1$	$4.04 \cdot 10^1$	$3.10 \cdot 10^1$	$2.56 \cdot 10^0$
11	$3.76 \cdot 10^0$	$3.42 \cdot 10^0$	$1.79 \cdot 10^0$	$5.16 \cdot 10^1$	$3.77 \cdot 10^1$	$2.98 \cdot 10^1$	$2.57 \cdot 10^0$
12	$3.70 \cdot 10^0$	$3.62 \cdot 10^0$	$1.80 \cdot 10^0$	$5.52 \cdot 10^1$	$4.09 \cdot 10^1$	$3.31 \cdot 10^1$	$2.64 \cdot 10^0$
13	$5.97 \cdot 10^0$	$9.22 \cdot 10^0$	$4.36 \cdot 10^0$	$1.00 \cdot 10^{-2}$	$1.57 \cdot 10^2$	$8.87 \cdot 10^1$	$7.00 \cdot 10^0$
14	$5.21 \cdot 10^0$	$1.03 \cdot 10^1$	$4.97 \cdot 10^0$	$9.26 \cdot 10^1$	$1.80 \cdot 10^2$	$1.04 \cdot 10^2$	$7.75 \cdot 10^0$
15	$5.35 \cdot 10^0$	$8.51 \cdot 10^0$	$4.08 \cdot 10^0$	$8.99 \cdot 10^1$	$1.46 \cdot 10^2$	$7.95 \cdot 10^1$	$6.57 \cdot 10^0$
16	$5.98 \cdot 10^0$	$9.14 \cdot 10^0$	$4.36 \cdot 10^0$	$9.84 \cdot 10^1$	$1.56 \cdot 10^2$	$8.61 \cdot 10^1$	$6.91 \cdot 10^0$
17	$3.09 \cdot 10^0$	$3.01 \cdot 10^1$	$1.56 \cdot 10^1$	$8.93 \cdot 10^1$	$6.00 \cdot 10^2$	$3.11 \cdot 10^2$	$19.8 \cdot 10^0$
18	$6.56 \cdot 10^0$	$5.10 \cdot 10^0$	$2.58 \cdot 10^0$	$1.04 \cdot 10^{-2}$	$9.46 \cdot 10^1$	$6.71 \cdot 10^1$	$5.59 \cdot 10^0$
19	$1.23 \cdot 10^1$	$8.70 \cdot 10^0$	$4.03 \cdot 10^0$	$1.48 \cdot 10^{-2}$	$1.34 \cdot 10^2$	$7.25 \cdot 10^1$	$6.45 \cdot 10^0$
20	$6.05 \cdot 10^0$	$9.12 \cdot 10^0$	$4.33 \cdot 10^0$	$1.01 \cdot 10^{-2}$	$1.54 \cdot 10^2$	$8.47 \cdot 10^1$	$7.08 \cdot 10^0$

**Table 4.5: Infinity norms for Disturbance Law 2 with control**

Control Law	$\ z_1\ _\infty$ (mm)	$\ z_2\ _\infty$ (mm)	$\ z_3\ _\infty$ (mm)	$\ z_4\ _\infty$ (mm/s)	$\ z_5\ _\infty$ (mm/s)	$\ z_6\ _\infty$ (mm/s)	$\ z_7\ _\infty$ (MPa)
Bare Frame	$5.33 \cdot 10^2$	$4.19 \cdot 10^2$	$1.96 \cdot 10^2$	$7.40 \cdot 10^3$	$6.05 \cdot 10^3$	$3.04 \cdot 10^3$	-
Theoretical	$1.43 \cdot 10^1$	$1.22 \cdot 10^1$	$5.61 \cdot 10^0$	$2.02 \cdot 10^2$	$1.85 \cdot 10^2$	$1.12 \cdot 10^2$	$2.18 \cdot 10^0$
1	$4.47 \cdot 10^1$	$3.32 \cdot 10^1$	$1.48 \cdot 10^1$	$5.26 \cdot 10^2$	$5.28 \cdot 10^2$	$3.06 \cdot 10^2$	$1.71 \cdot 10^0$
2	$6.79 \cdot 10^0$	$6.60 \cdot 10^0$	$3.08 \cdot 10^0$	$8.93 \cdot 10^1$	$9.19 \cdot 10^1$	$4.72 \cdot 10^1$	$5.06 \cdot 10^0$
3	$6.97 \cdot 10^0$	$6.67 \cdot 10^0$	$3.11 \cdot 10^0$	$9.08 \cdot 10^1$	$9.36 \cdot 10^1$	$4.78 \cdot 10^1$	$5.15 \cdot 10^0$
4	$1.57 \cdot 10^1$	$1.13 \cdot 10^1$	$5.24 \cdot 10^0$	$2.01 \cdot 10^2$	$1.63 \cdot 10^2$	$8.24 \cdot 10^1$	$6.00 \cdot 10^0$
5	$1.55 \cdot 10^1$	$1.14 \cdot 10^1$	$5.31 \cdot 10^0$	$2.02 \cdot 10^2$	$1.61 \cdot 10^2$	$7.98 \cdot 10^1$	$6.03 \cdot 10^0$
6	$1.19 \cdot 10^1$	$9.19 \cdot 10^0$	$4.24 \cdot 10^0$	$1.62 \cdot 10^2$	$1.27 \cdot 10^2$	$6.52 \cdot 10^1$	$6.29 \cdot 10^0$
7	$1.23 \cdot 10^1$	$1.04 \cdot 10^1$	$4.76 \cdot 10^0$	$1.72 \cdot 10^2$	$1.46 \cdot 10^2$	$7.27 \cdot 10^1$	$5.12 \cdot 10^0$
8	$3.08 \cdot 10^0$	$4.67 \cdot 10^0$	$3.90 \cdot 10^0$	$7.47 \cdot 10^1$	$1.14 \cdot 10^2$	$2.01 \cdot 10^2$	$4.50 \cdot 10^0$
9	$3.27 \cdot 10^0$	$3.37 \cdot 10^0$	$3.28 \cdot 10^0$	$6.20 \cdot 10^1$	$9.98 \cdot 10^1$	$1.65 \cdot 10^2$	$5.30 \cdot 10^0$
10	$1.87 \cdot 10^0$	$2.52 \cdot 10^0$	$3.82 \cdot 10^0$	$5.98 \cdot 10^1$	$1.19 \cdot 10^2$	$1.90 \cdot 10^2$	$3.91 \cdot 10^0$
11	$1.64 \cdot 10^0$	$1.93 \cdot 10^0$	$3.11 \cdot 10^0$	$5.53 \cdot 10^1$	$9.93 \cdot 10^1$	$1.62 \cdot 10^2$	$3.89 \cdot 10^0$
12	$3.00 \cdot 10^0$	$4.32 \cdot 10^0$	$4.19 \cdot 10^0$	$7.84 \cdot 10^1$	$1.59 \cdot 10^2$	$2.19 \cdot 10^2$	$5.15 \cdot 10^0$
13	$5.36 \cdot 10^0$	$5.89 \cdot 10^0$	$2.81 \cdot 10^0$	$6.55 \cdot 10^1$	$8.43 \cdot 10^1$	$5.21 \cdot 10^1$	$5.24 \cdot 10^0$
14	$4.66 \cdot 10^0$	$5.98 \cdot 10^0$	$2.91 \cdot 10^0$	$5.65 \cdot 10^1$	$8.76 \cdot 10^1$	$4.50 \cdot 10^1$	$5.17 \cdot 10^0$
15	$5.29 \cdot 10^0$	$5.66 \cdot 10^0$	$2.73 \cdot 10^0$	$6.64 \cdot 10^1$	$8.22 \cdot 10^1$	$5.27 \cdot 10^1$	$5.24 \cdot 10^0$
16	$5.37 \cdot 10^0$	$5.87 \cdot 10^0$	$2.81 \cdot 10^0$	$6.64 \cdot 10^1$	$8.38 \cdot 10^1$	$5.26 \cdot 10^1$	$5.24 \cdot 10^0$
17	$2.37 \cdot 10^0$	$2.00 \cdot 10^1$	$1.06 \cdot 10^1$	$6.92 \cdot 10^1$	$4.02 \cdot 10^2$	$2.01 \cdot 10^2$	$1.42 \cdot 10^1$
18	$6.25 \cdot 10^0$	$5.07 \cdot 10^0$	$2.57 \cdot 10^0$	$1.02 \cdot 10^2$	$9.02 \cdot 10^1$	$6.55 \cdot 10^1$	$5.78 \cdot 10^0$
19	$1.10 \cdot 10^1$	$8.11 \cdot 10^0$	$3.75 \cdot 10^0$	$1.40 \cdot 10^2$	$1.19 \cdot 10^2$	$6.23 \cdot 10^1$	$6.06 \cdot 10^0$
20	$5.38 \cdot 10^0$	$5.90 \cdot 10^0$	$2.83 \cdot 10^0$	$6.80 \cdot 10^1$	$8.43 \cdot 10^1$	$5.22 \cdot 10^1$	$4.77 \cdot 10^0$

**Table 4.6: Infinity norms for white noise acceleration disturbance with control**

Control Law	$\ z_1\ _\infty$ (mm)	$\ z_2\ _\infty$ (mm)	$\ z_3\ _\infty$ (mm)	$\ z_4\ _\infty$ (mm/s)	$\ z_5\ _\infty$ (mm/s)	$\ z_6\ _\infty$ (mm/s)	$\ z_7\ _\infty$ (MPa)
Bare Frame	$5.33 \cdot 10^2$	$4.19 \cdot 10^2$	$1.96 \cdot 10^2$	$7.40 \cdot 10^3$	$6.05 \cdot 10^3$	$3.04 \cdot 10^3$	-
Theoretical	$1.43 \cdot 10^1$	$1.22 \cdot 10^1$	$5.61 \cdot 10^0$	$2.02 \cdot 10^2$	$1.85 \cdot 10^2$	$1.12 \cdot 10^2$	$2.18 \cdot 10^0$
1	$4.34 \cdot 10^0$	$3.38 \cdot 10^0$	$1.62 \cdot 10^0$	$6.02 \cdot 10^1$	$5.14 \cdot 10^1$	$3.29 \cdot 10^1$	$2.24 \cdot 10^{-2}$
2	$1.30 \cdot 10^0$	$1.08 \cdot 10^0$	$5.41 \cdot 10^{-1}$	$1.37 \cdot 10^1$	$1.58 \cdot 10^1$	$7.27 \cdot 10^0$	$9.52 \cdot 10^{-1}$
3	$1.30 \cdot 10^0$	$1.08 \cdot 10^0$	$5.42 \cdot 10^{-1}$	$1.37 \cdot 10^1$	$1.57 \cdot 10^1$	$7.27 \cdot 10^0$	$9.50 \cdot 10^{-1}$
4	$2.00 \cdot 10^0$	$1.59 \cdot 10^0$	$7.60 \cdot 10^{-1}$	$2.67 \cdot 10^1$	$2.51 \cdot 10^1$	$1.30 \cdot 10^1$	$9.46 \cdot 10^{-1}$
5	$1.97 \cdot 10^0$	$1.56 \cdot 10^0$	$7.09 \cdot 10^{-1}$	$2.51 \cdot 10^1$	$2.36 \cdot 10^1$	$1.24 \cdot 10^1$	$9.34 \cdot 10^{-1}$
6	$1.90 \cdot 10^0$	$1.40 \cdot 10^0$	$6.07 \cdot 10^{-1}$	$2.18 \cdot 10^1$	$2.12 \cdot 10^1$	$1.21 \cdot 10^1$	$1.09 \cdot 10^0$
7	$1.61 \cdot 10^0$	$1.34 \cdot 10^0$	$6.46 \cdot 10^{-1}$	$2.00 \cdot 10^1$	$1.84 \cdot 10^1$	$9.61 \cdot 10^0$	$1.02 \cdot 10^0$
8	$9.89 \cdot 10^{-1}$	$1.14 \cdot 10^0$	$6.75 \cdot 10^{-1}$	$2.84 \cdot 10^1$	$3.30 \cdot 10^1$	$2.26 \cdot 10^1$	$2.07 \cdot 10^0$
9	$1.09 \cdot 10^0$	$1.10 \cdot 10^0$	$6.23 \cdot 10^{-1}$	$2.67 \cdot 10^1$	$2.94 \cdot 10^1$	$2.70 \cdot 10^1$	$2.10 \cdot 10^0$
10	$9.86 \cdot 10^{-1}$	$1.14 \cdot 10^0$	$6.72 \cdot 10^{-1}$	$2.82 \cdot 10^1$	$3.32 \cdot 10^1$	$2.23 \cdot 10^1$	$2.08 \cdot 10^0$
11	$1.08 \cdot 10^0$	$1.10 \cdot 10^0$	$6.24 \cdot 10^{-1}$	$2.68 \cdot 10^1$	$2.93 \cdot 10^1$	$2.70 \cdot 10^1$	$1.94 \cdot 10^0$
12	$1.05 \cdot 10^0$	$1.16 \cdot 10^0$	$6.44 \cdot 10^{-1}$	$3.30 \cdot 10^1$	$3.61 \cdot 10^1$	$2.50 \cdot 10^1$	$2.13 \cdot 10^0$
13	$1.22 \cdot 10^0$	$9.73 \cdot 10^{-1}$	$4.77 \cdot 10^{-1}$	$1.25 \cdot 10^1$	$1.91 \cdot 10^1$	$9.87 \cdot 10^0$	$1.12 \cdot 10^0$
14	$1.01 \cdot 10^0$	$1.02 \cdot 10^0$	$4.82 \cdot 10^{-1}$	$1.03 \cdot 10^1$	$1.90 \cdot 10^1$	$9.42 \cdot 10^0$	$1.05 \cdot 10^0$
15	$1.14 \cdot 10^0$	$9.24 \cdot 10^{-1}$	$4.53 \cdot 10^{-1}$	$1.15 \cdot 10^1$	$1.94 \cdot 10^1$	$9.48 \cdot 10^0$	$1.04 \cdot 10^0$
16	$1.20 \cdot 10^0$	$9.63 \cdot 10^{-1}$	$4.70 \cdot 10^{-1}$	$1.24 \cdot 10^1$	$1.92 \cdot 10^1$	$9.89 \cdot 10^0$	$1.06 \cdot 10^0$
17	$3.68 \cdot 10^{-1}$	$1.51 \cdot 10^0$	$8.42 \cdot 10^{-1}$	$6.41 \cdot 10^0$	$3.18 \cdot 10^1$	$2.05 \cdot 10^1$	$1.24 \cdot 10^0$
18	$1.33 \cdot 10^0$	$1.00 \cdot 10^0$	$5.09 \cdot 10^{-1}$	$1.52 \cdot 10^1$	$1.77 \cdot 10^1$	$1.16 \cdot 10^1$	$1.14 \cdot 10^0$
19	$1.73 \cdot 10^0$	$1.36 \cdot 10^0$	$6.41 \cdot 10^{-1}$	$2.18 \cdot 10^1$	$2.27 \cdot 10^1$	$1.19 \cdot 10^1$	$1.05 \cdot 10^0$
20	$1.23 \cdot 10^0$	$9.68 \cdot 10^{-1}$	$4.78 \cdot 10^{-1}$	$1.25 \cdot 10^1$	$1.89 \cdot 10^1$	$9.87 \cdot 10^0$	$1.09 \cdot 10^0$

**Table 4.7: Theoretical performance index bounds versus maximum simulated values**

Control Law	Theoretical Performance Index Radius $\sqrt{z^T Kz}$		Simulated $\max(\sqrt{z^T Kz})$		
	Ball	Dipole	Disturbance Law 1	Disturbance Law 2	Random
2	$9.14 \cdot 10^3$	$8.88 \cdot 10^3$	$6.22 \cdot 10^0$	$9.47 \cdot 10^0$	$1.70 \cdot 10^0$
3	$9.15 \cdot 10^2$	$8.88 \cdot 10^2$	$6.23 \cdot 10^0$	$9.64 \cdot 10^0$	$1.71 \cdot 10^0$
4	$7.71 \cdot 10^5$	$7.71 \cdot 10^5$	$1.99 \cdot 10^1$	$1.96 \cdot 10^1$	$2.64 \cdot 10^0$
5	$1.02 \cdot 10^5$	$7.69 \cdot 10^4$	$1.70 \cdot 10^1$	$1.95 \cdot 10^1$	$2.62 \cdot 10^0$
6	$1.44 \cdot 10^5$	$1.43 \cdot 10^5$	$1.10 \cdot 10^1$	$1.51 \cdot 10^1$	$2.44 \cdot 10^0$
7	$1.76 \cdot 10^5$	$1.74 \cdot 10^5$	$6.13 \cdot 10^0$	$1.64 \cdot 10^1$	$2.16 \cdot 10^0$
8	$2.39 \cdot 10^0$	$2.39 \cdot 10^0$	$4.73 \cdot 10^0$	$6.82 \cdot 10^0$	$2.14 \cdot 10^0$
9	$1.80 \cdot 10^0$	$1.79 \cdot 10^0$	$4.65 \cdot 10^0$	$6.97 \cdot 10^0$	$2.24 \cdot 10^0$
10	$2.39 \cdot 10^5$	$2.39 \cdot 10^5$	$4.73 \cdot 10^0$	$5.17 \cdot 10^0$	$2.15 \cdot 10^0$
11	$1.80 \cdot 10^5$	$1.79 \cdot 10^5$	$4.65 \cdot 10^0$	$4.95 \cdot 10^0$	$2.10 \cdot 10^0$
12	$8.43 \cdot 10^3$	$8.43 \cdot 10^3$	$4.71 \cdot 10^0$	$7.11 \cdot 10^0$	$2.22 \cdot 10^0$
13	$2.60 \cdot 10^0$	$2.44 \cdot 10^0$	$1.25 \cdot 10^1$	$8.07 \cdot 10^0$	$1.55 \cdot 10^0$
14	$2.39 \cdot 10^0$	$2.28 \cdot 10^0$	$1.38 \cdot 10^1$	$8.34 \cdot 10^0$	$1.41 \cdot 10^0$
15	$1.50 \cdot 10^0$	$1.36 \cdot 10^0$	$1.15 \cdot 10^1$	$8.00 \cdot 10^0$	$1.45 \cdot 10^0$
16	$1.54 \cdot 10^0$	$1.53 \cdot 10^0$	$1.24 \cdot 10^1$	$8.07 \cdot 10^0$	$1.53 \cdot 10^0$
17	$2.05 \cdot 10^0$	$9.37 \cdot 10^4$	$3.91 \cdot 10^1$	$2.66 \cdot 10^1$	$2.07 \cdot 10^0$
18	$1.42 \cdot 10^8$	$1.35 \cdot 10^8$	$7.84 \cdot 10^0$	$7.88 \cdot 10^0$	$1.72 \cdot 10^0$
19	$9.60 \cdot 10^8$	$8.98 \cdot 10^8$	$1.51 \cdot 10^1$	$1.36 \cdot 10^1$	$2.26 \cdot 10^0$
20	$5.03 \cdot 10^5$	$4.72 \cdot 10^5$	$1.24 \cdot 10^1$	$8.12 \cdot 10^0$	$1.56 \cdot 10^0$

**Table 4.8:** Attractor set radius versus maximum simulated values

Control Law	Theoretical Attractor Set Radius $\sqrt{z^T P z}$		Simulated $\max(\sqrt{z^T P z})$		
	Ball	Dipole	Disturbance Law 1	Disturbance Law 2	Random
2	$2.59 \cdot 10^2$	$2.52 \cdot 10^2$	$5.08 \cdot 10^1$	$7.50 \cdot 10^1$	$1.39 \cdot 10^1$
3	$2.59 \cdot 10^2$	$2.52 \cdot 10^2$	$5.10 \cdot 10^1$	$7.62 \cdot 10^1$	$1.40 \cdot 10^1$
4	$2.18 \cdot 10^4$	$2.18 \cdot 10^4$	$2.43 \cdot 10^2$	$2.25 \cdot 10^2$	$4.40 \cdot 10^1$
5	$2.90 \cdot 10^3$	$2.18 \cdot 10^3$	$1.95 \cdot 10^2$	$1.97 \cdot 10^2$	$3.82 \cdot 10^1$
6	$4.09 \cdot 10^3$	$4.06 \cdot 10^3$	$2.05 \cdot 10^2$	$1.60 \cdot 10^2$	$4.17 \cdot 10^1$
7	$4.98 \cdot 10^3$	$4.95 \cdot 10^3$	$6.30 \cdot 10^1$	$1.39 \cdot 10^2$	$2.12 \cdot 10^1$
8	$6.79 \cdot 10^4$	$6.78 \cdot 10^4$	$2.10 \cdot 10^2$	$1.86 \cdot 10^2$	$6.16 \cdot 10^1$
9	$5.10 \cdot 10^4$	$5.08 \cdot 10^4$	$2.77 \cdot 10^2$	$2.21 \cdot 10^2$	$6.28 \cdot 10^1$
10	$6.79 \cdot 10^4$	$6.78 \cdot 10^4$	$2.10 \cdot 10^2$	$1.31 \cdot 10^2$	$6.15 \cdot 10^1$
11	$5.10 \cdot 10^4$	$5.08 \cdot 10^4$	$2.77 \cdot 10^2$	$1.35 \cdot 10^2$	$6.27 \cdot 10^1$
12	$2.39 \cdot 10^3$	$2.39 \cdot 10^3$	$3.42 \cdot 10^2$	$2.57 \cdot 10^2$	$8.30 \cdot 10^1$
13	$7.27 \cdot 10^4$	$6.82 \cdot 10^4$	$6.90 \cdot 10^1$	$4.26 \cdot 10^1$	$8.68 \cdot 10^0$
14	$6.68 \cdot 10^4$	$6.36 \cdot 10^4$	$8.17 \cdot 10^1$	$4.74 \cdot 10^1$	$9.08 \cdot 10^0$
15	$4.18 \cdot 10^4$	$3.79 \cdot 10^4$	$6.78 \cdot 10^1$	$4.43 \cdot 10^1$	$8.79 \cdot 10^0$
16	$4.31 \cdot 10^4$	$4.26 \cdot 10^4$	$6.97 \cdot 10^1$	$4.35 \cdot 10^1$	$8.71 \cdot 10^0$
17	$3.48 \cdot 10^5$	$1.59 \cdot 10^4$	$1.42 \cdot 10^3$	$9.53 \cdot 10^2$	$7.57 \cdot 10^1$
18	$2.41 \cdot 10^7$	$2.29 \cdot 10^7$	$2.64 \cdot 10^2$	$2.57 \cdot 10^2$	$6.20 \cdot 10^1$
19	$2.72 \cdot 10^7$	$2.54 \cdot 10^7$	$2.76 \cdot 10^2$	$2.50 \cdot 10^2$	$4.75 \cdot 10^1$
20	$7.27 \cdot 10^4$	$6.82 \cdot 10^4$	$6.88 \cdot 10^1$	$4.33 \cdot 10^1$	$8.76 \cdot 10^0$

## **CHAPTER 5**

### **EXPERIMENTAL RESULTS**

#### **5.1 Introduction**

The objective of this chapter is to present experimental results that demonstrate the performance of the semi-active Lyapunov controller developed in the previous chapter. Two seismic inputs were used to excite the test structure. The first input was a 0.15-g RMS 0.5-50 Hz band-limited white noise ground acceleration while the second input was the North/South component of the 1940 El Centro earthquake. The El Centro input amplitude was scaled to 50%. The time scale of the earthquake input was not altered. Shake table tests were conducted on the test structure with three different configurations as indicated in Figure 2.2: 1) the bare frame with no semi-active actuator attached (Bare Frame), 2) with a single semi-active actuator positioned diagonally between the ground and first floor (Position 1) and 3) with a single semi-active actuator located diagonally between the first and second floor (Position 2). Both passive and semi-active test data are compared with the response of the bare frame in the following sections. The results indicate that the semi-active control system can significantly reduce the vibration amplitudes of the seismically excited structure.

#### **5.2 Passive Test Results**

First, shake table tests were performed on the bare structure with no control actuators attached using each of the input histories. The data obtained from the bare

frame tests are plotted in Figures 5.1-5.48 as the “Bare Frame” case and are used as a baseline to assess the effectiveness of the passive and semi-active control configurations.

Next, a single semi-active actuator was added to the test frame. The structural response was obtained with the actuator operated in a passive mode. (constant valve orifice area) Tests were performed with the actuator in Position 1 and Position 2. (Figure 2.2) Two passive cases were investigated for each actuator position. In the first case, the semi-active actuator control valve was fully open. In the second case, the control valve was completely closed. In Figures 5.1-5.24 the “bare frame” case is plotted in blue, the “valve open” case is plotted in green and the “valve closed” case is plotted in red.

The frequency response function magnitudes of the relative floor-to-floor displacements for the broadband input are shown in Figures 5.1-5.6. The damping added by the semi-active actuator in the “valve open” case provides modest reductions in the first mode of the relative displacements. The “valve open” configuration provides at least a 25% reduction in first mode amplitude in Position 1 and an 18% reduction in Position 2. As expected, the actuator provides greater amplitude reductions for the higher modes since the force generated by the actuator is velocity dependent. The “valve open” configuration provides at least a 54% reduction in second mode amplitude in Position 1 and a 40% reduction in Position 2. When the control valve is closed, the actuator increases the stiffness of the structure virtually eliminating any relative motion in the position the actuator is installed in. The “valve closed” frequency response functions have only two clear peaks compared to three peaks for the other cases. The frequencies are slightly higher when the actuator is in Position 1. (3.0-Hz and 8.5-Hz compared to 2.5-Hz and 7.0-Hz for Position 2)

The frequency response function magnitudes of the  $x$ -direction accelerations are plotted in Figures 5.7-5.18. The figures indicate that in the “valve open” case, the damping provided by the semi-active actuator yielded sizeable reductions in acceleration at each natural frequency. In Position 1, the semi-active actuator provided at least a 24% reduction in first mode acceleration compared to the 13% decrease obtained with the actuator in Position 2. For the “valve closed” case, the first mode acceleration amplitude is similar to the “valve open” case when the actuator is in Position 1 but the second mode acceleration is greater than the “no control” case. In Position 2, the first mode acceleration is less than the “valve open” case and the second mode is similar in magnitude to the “no control” case.

The  $y$ -direction accelerations are provided in Figures 5.19-5.24. The frequency response functions indicate that the modes in the  $y$ -direction (which are close in frequency to the  $x$ -axis modes) are excited even though the seismic input is directed along the  $x$ -axis. The damping provided in the “valve open” tests reduced the third floor  $y$ -axis RMS acceleration levels by at least 25% in Position 1 and 18% in Position 2. When the control valve was closed, the  $y$ -axis accelerations were reduced in Position 1 but were magnified in Position 2. This is expected since the fundamental frequency in the  $y$ -axis is 2.5-Hz which coincides with the fundamental frequency in the  $x$ -axis when the semi-active actuator is in Position 2 with the valve closed.

The RMS and peak relative displacements, absolute accelerations and actuator differential pressures from the broadband tests are summarized in Tables 5.1 and 5.2. The data from the El Centro tests are provided in Tables 5.3 and 5.4. For the broadband tests conducted with the valve completely open, the actuator reduces peak inter-story drift

by at least 31% in Position 1 and 25% in Position 2. Likewise, the actuator with the valve completely open provided at least a 12% reduction in peak inter-story drift in Position 1 and a 4% reduction in Position 2. Similar results are obtained when the valve is closed, except that a significant amount of modal leakage to the  $y$ -axis occurs when the actuator is in Position 2. The results also indicate that the additional stiffness in the “closed valve” case provides a tremendous local reduction in displacement but tends to increase acceleration levels throughout the structure.

Both the open valve configuration and the closed valve configuration provide certain desirable characteristics. The open valve configuration attenuates higher frequency modal amplitudes while the closed valve configuration minimizes local displacements. Unfortunately, both configurations have disadvantages as well. The open valve configuration is not particularly well suited to reducing local displacements and tends to amplify out-of-plane accelerations in certain instances. The closed valve configuration amplified both accelerations and relative displacements between floors without actuators. Since neither configuration is capable of both minimizing the maximum inter-story drift and reducing RMS acceleration levels both in and out of plane, it is assumed that better response characteristics can be achieved by modulating the semi-active actuator valve between a maximum and minimum valve orifice area according to some prescribed control logic. The following section presents test results for two control logic candidates.

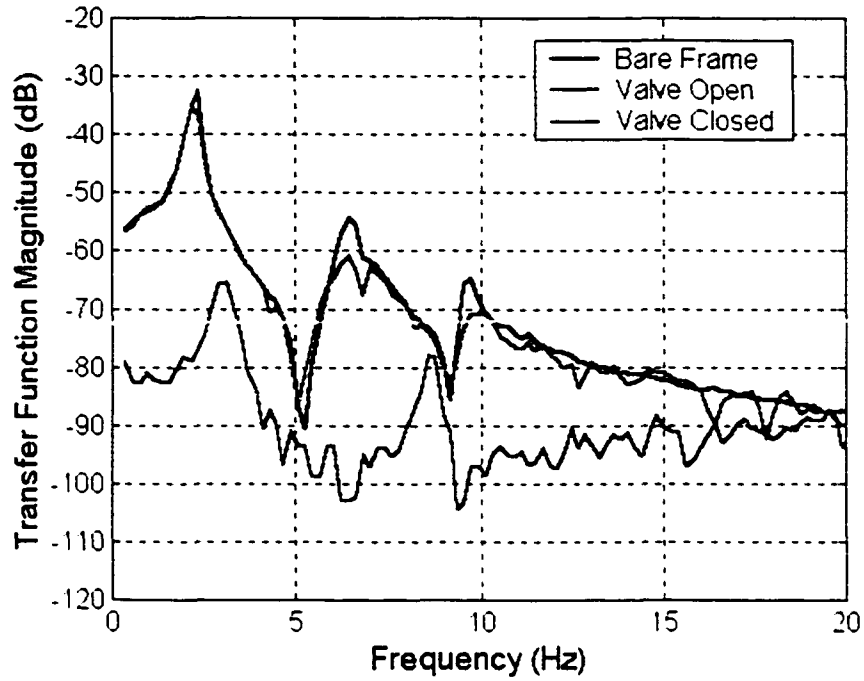


**Figure 5.1:** Frequency response function magnitude  $z_1/d$  with actuator operated passively in Position 1.

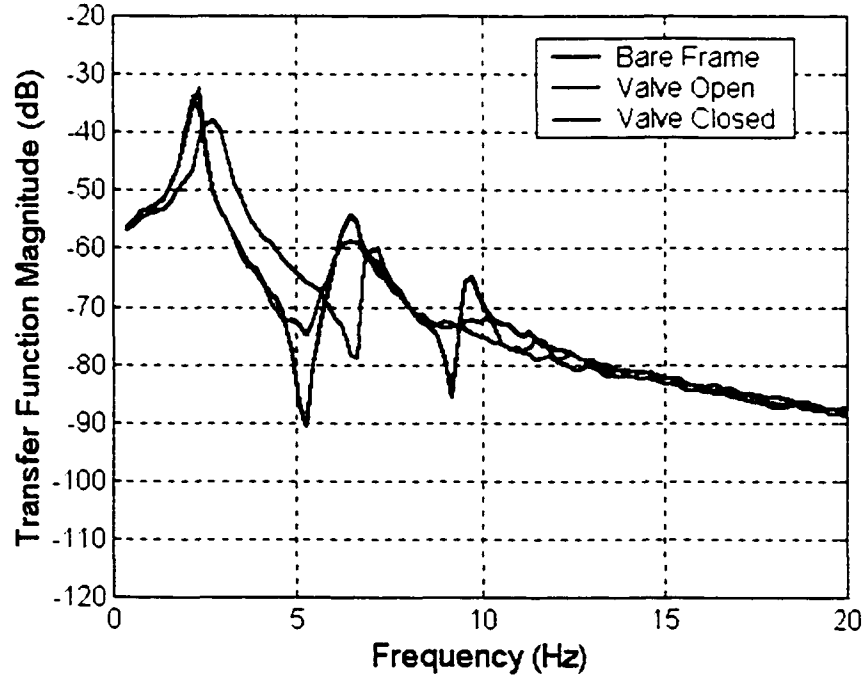


**Figure 5.2:** Frequency response function magnitude  $z_1/d$  with actuator operated passively in Position 2.

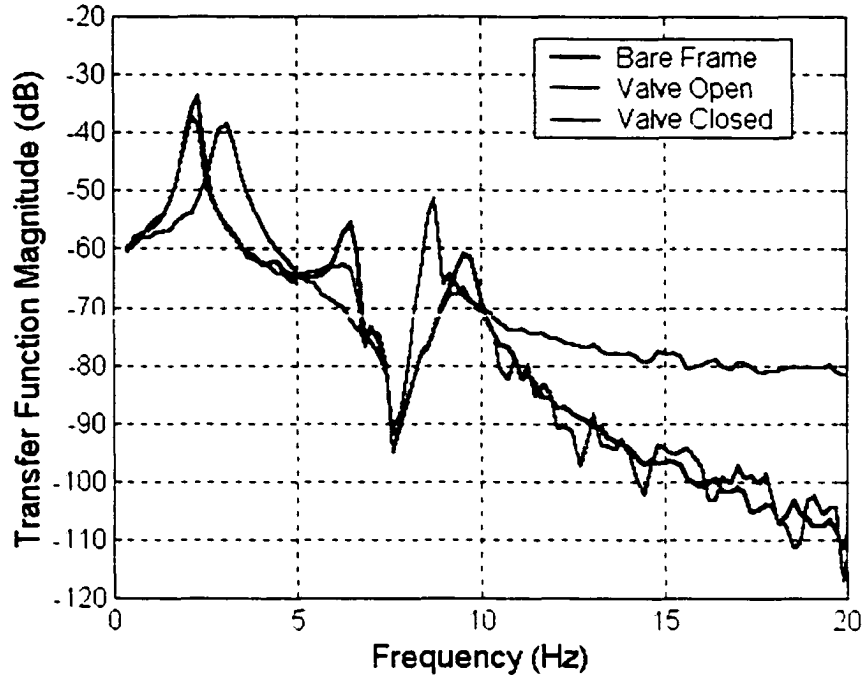


Figure 5.3: Frequency response function magnitude  $z_2/d$  with actuator operated passively in Position 1.

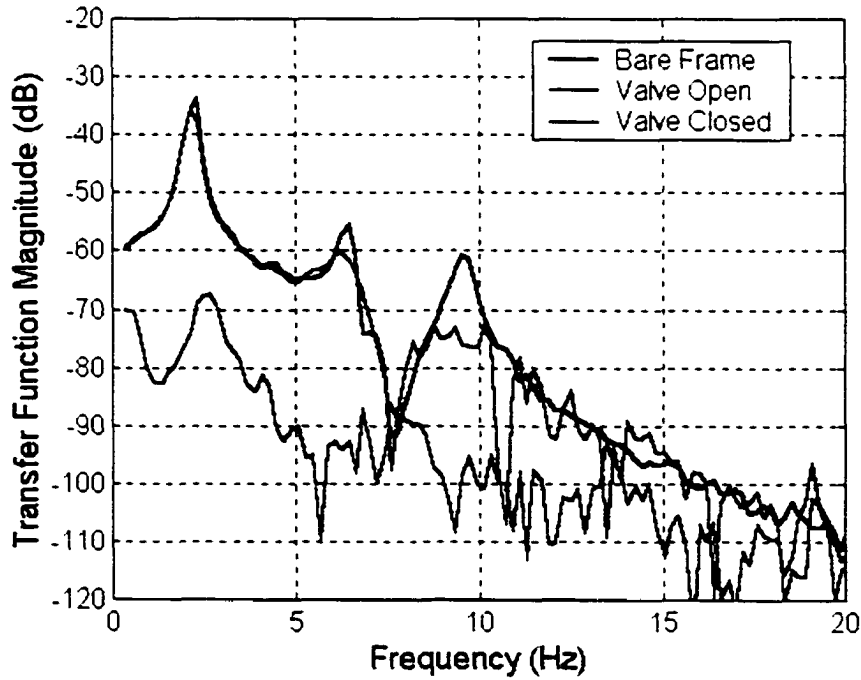
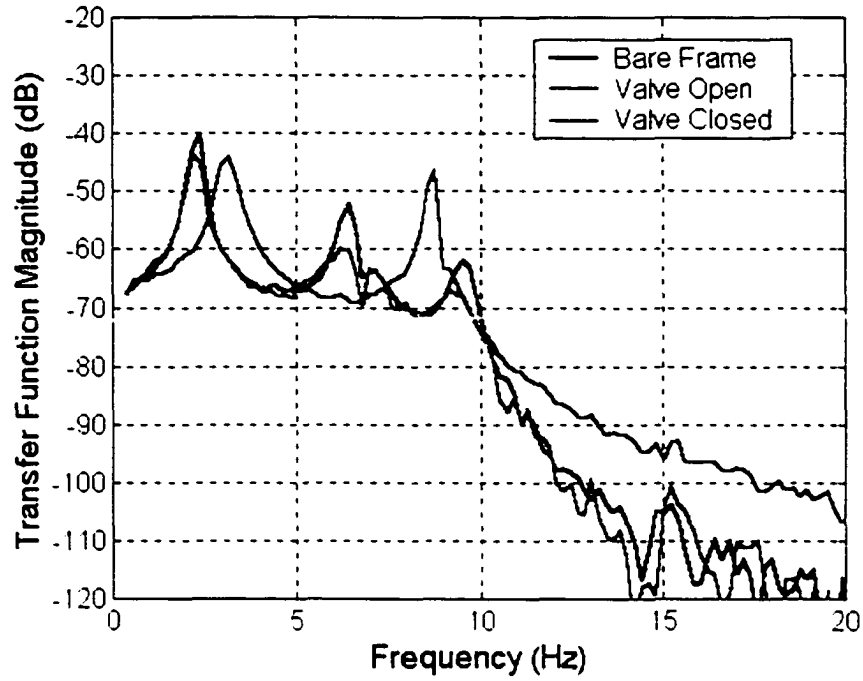
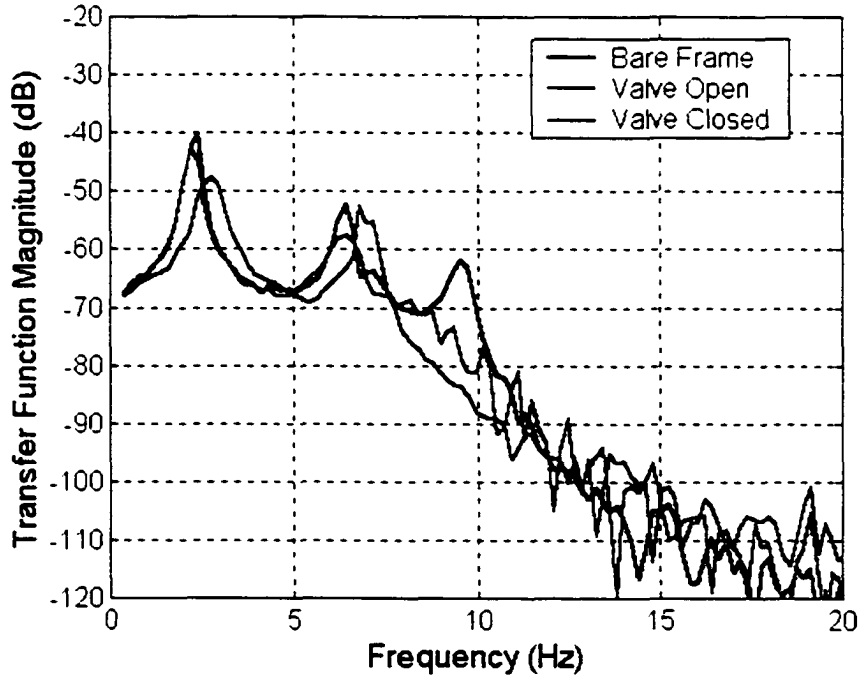


Figure 5.4: Frequency response function magnitude  $z_2/d$  with actuator operated passively in Position 2.



**Figure 5.5:** Frequency response function magnitude  $z_3 / d$  with actuator operated passively in Position 1.



**Figure 5.6:** Frequency response function magnitude  $z_3 / d$  with actuator operated passively in Position 2.

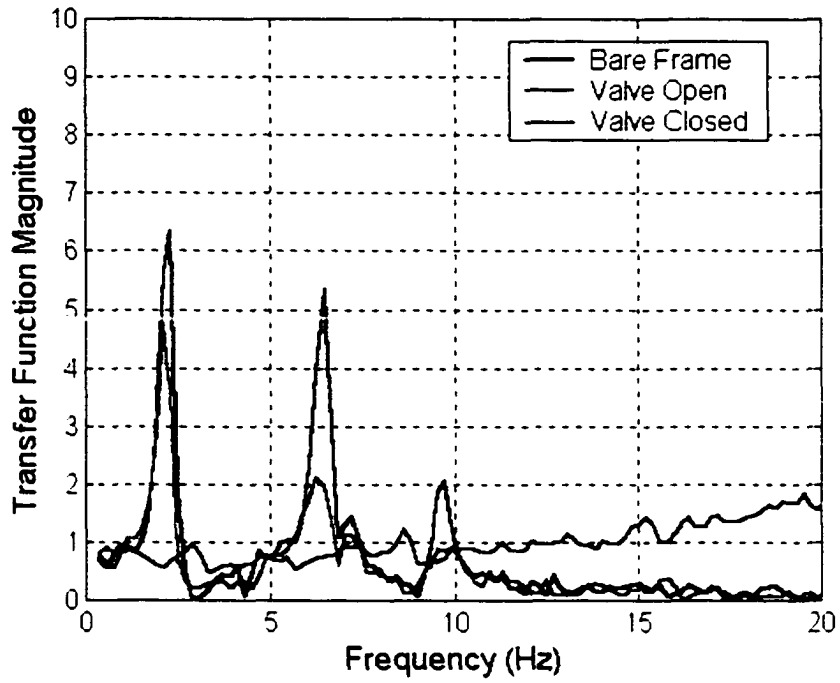


Figure 5.7: Frequency response function magnitude  $\ddot{x}_{11} / d$  with actuator operated passively in Position 1.

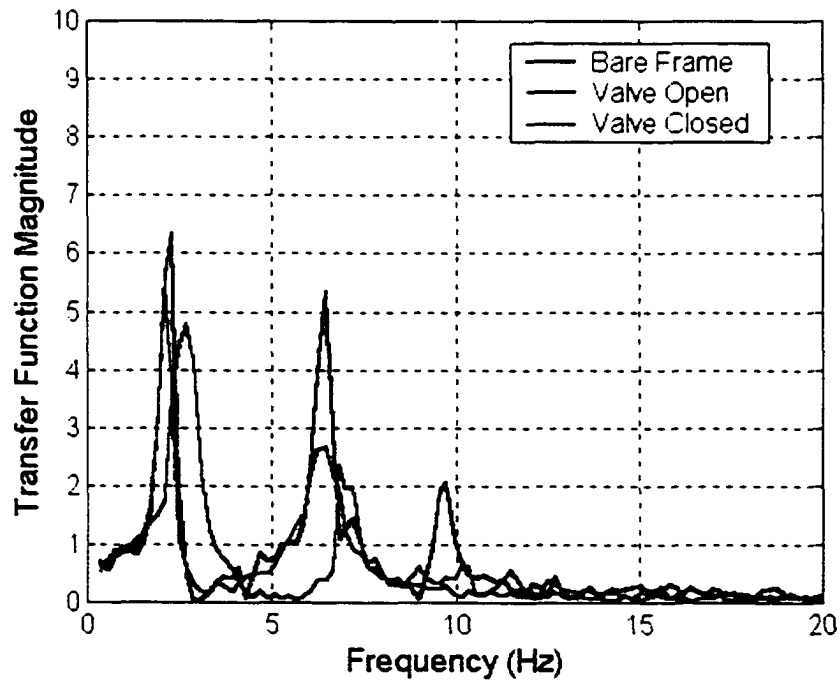
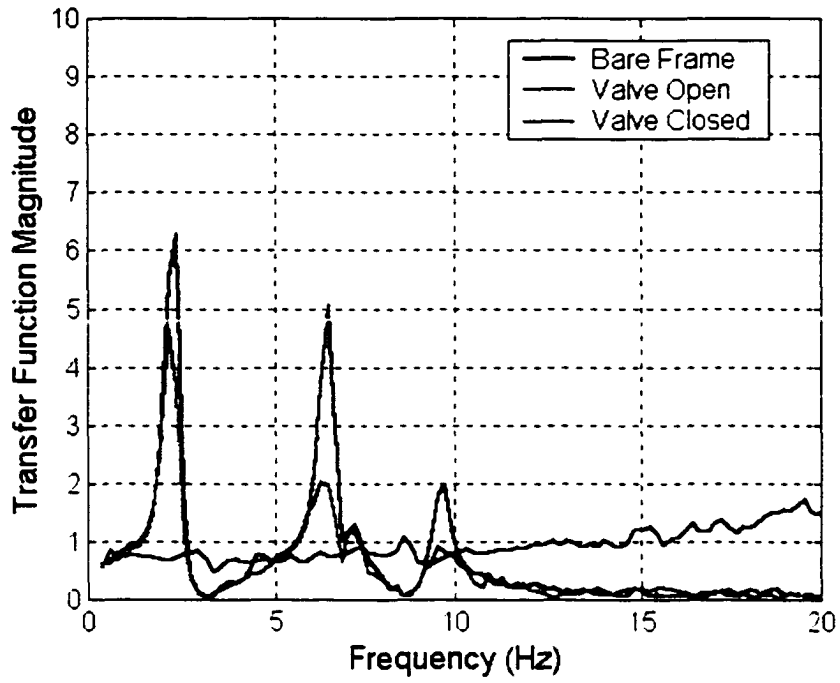
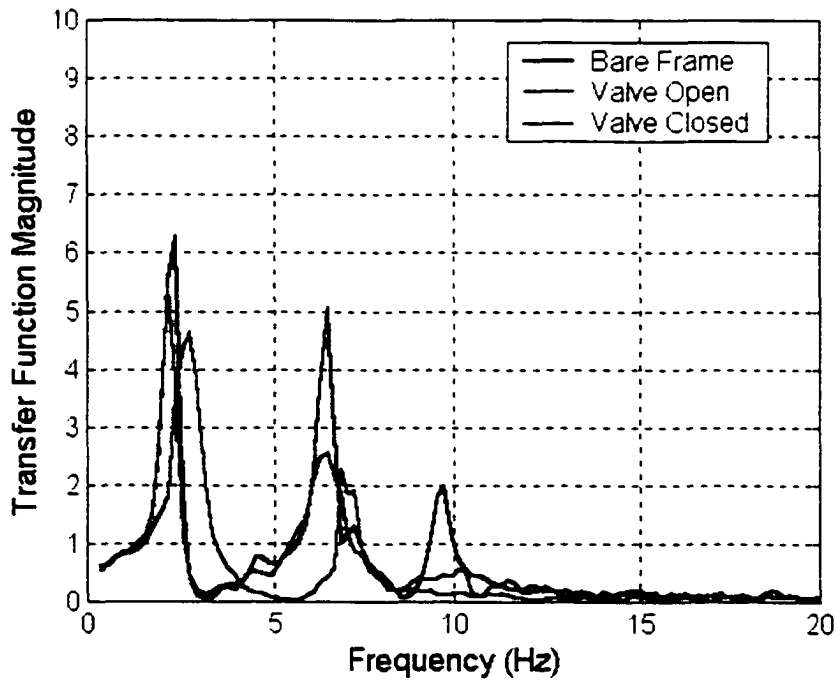


Figure 5.8: Frequency response function magnitude  $\ddot{x}_{11} / d$  with actuator operated passively in Position 2.



**Figure 5.9:** Frequency response function magnitude  $\ddot{x}_{12} / d$  with actuator operated passively in Position 1.



**Figure 5.10:** Frequency response function magnitude  $\ddot{x}_{12} / d$  with actuator operated passively in Position 2.

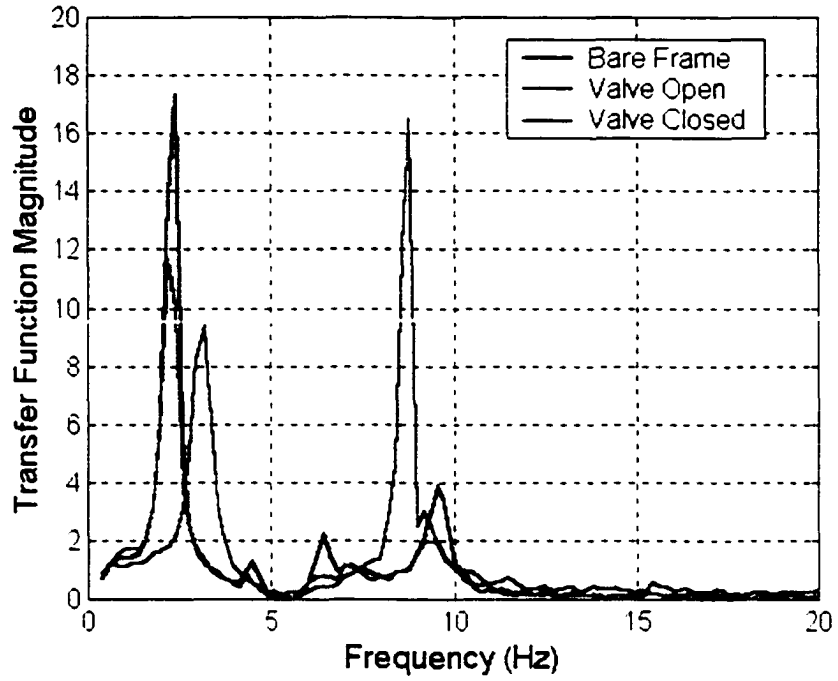


**Figure 5.11:** Frequency response function magnitude  $\ddot{x}_{21} / d$  with actuator operated passively in Position 1.

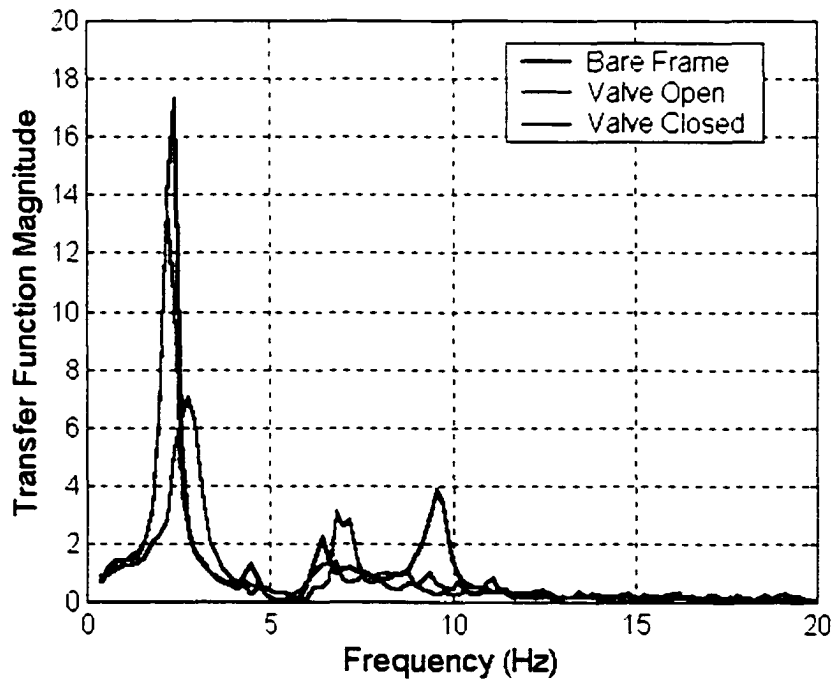


**Figure 5.12:** Frequency response function magnitude  $\ddot{x}_{21} / d$  with actuator operated passively in Position 2.

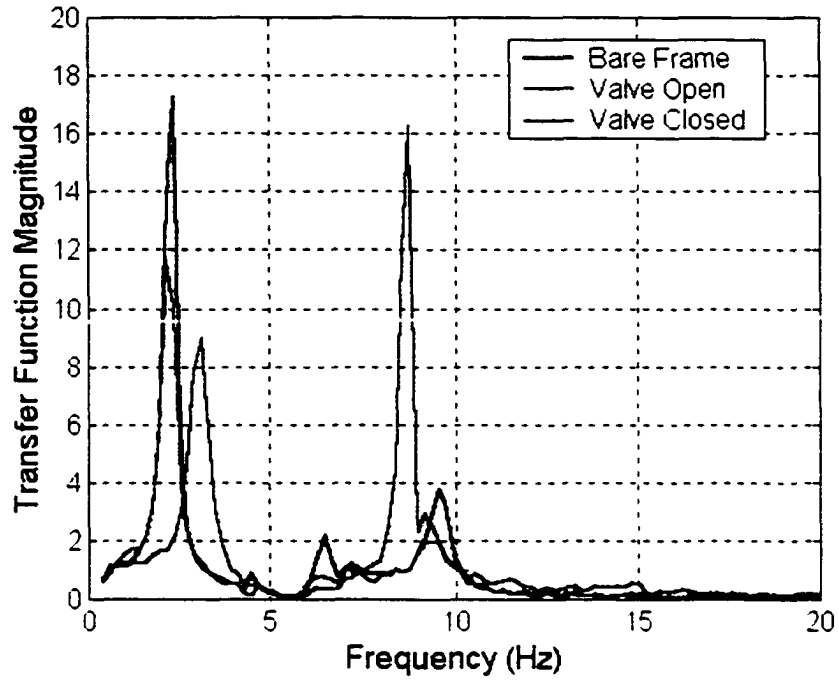


**Figure 5.13:** Frequency response function magnitude  $\ddot{x}_{22}/d$  with actuator operated passively in Position 1.

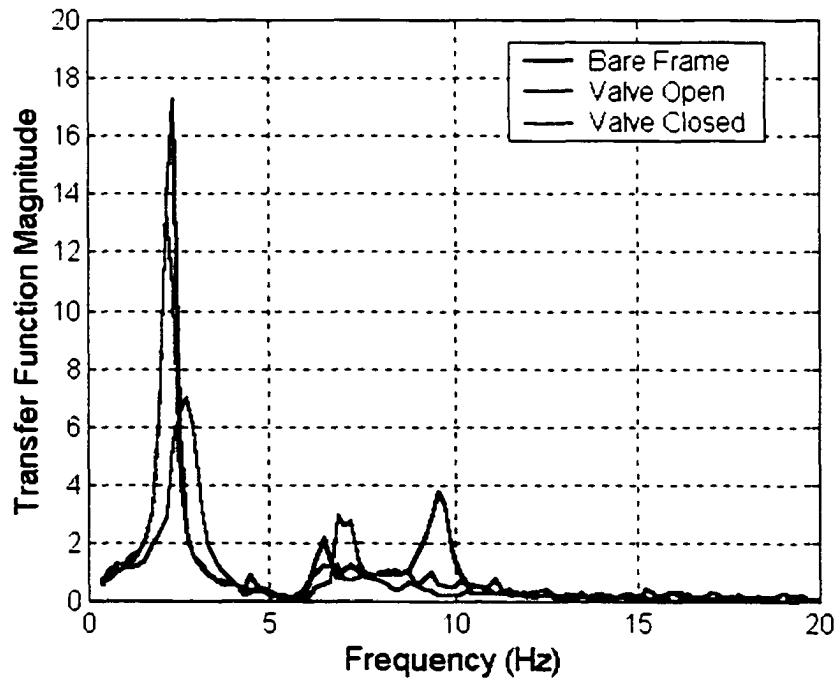


**Figure 5.14:** Frequency response function magnitude  $\ddot{x}_{22}/d$  with actuator operated passively in Position 2.

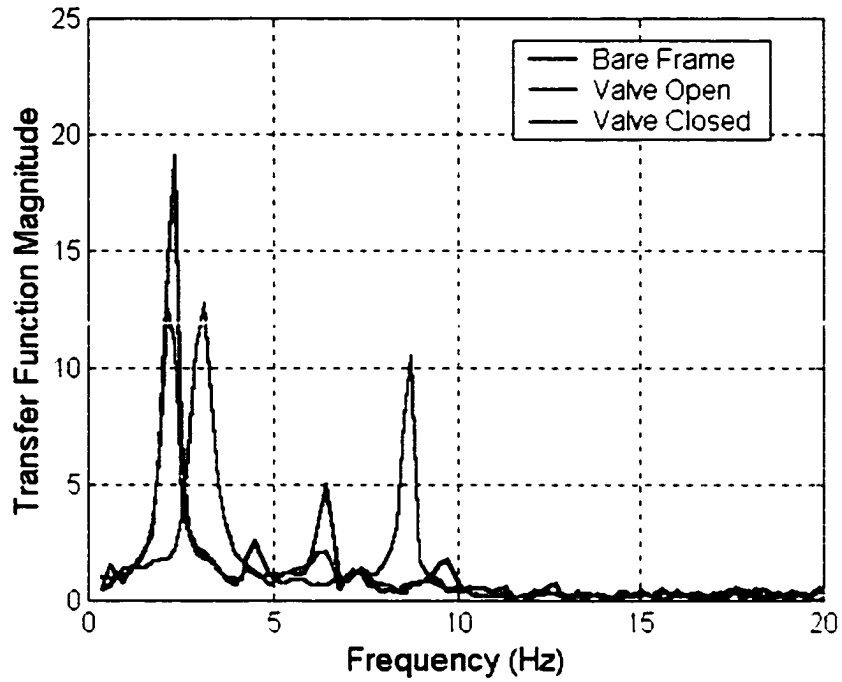


**Figure 5.15:** Frequency response function magnitude  $\ddot{x}_{31} / d$  with actuator operated passively in Position 1.

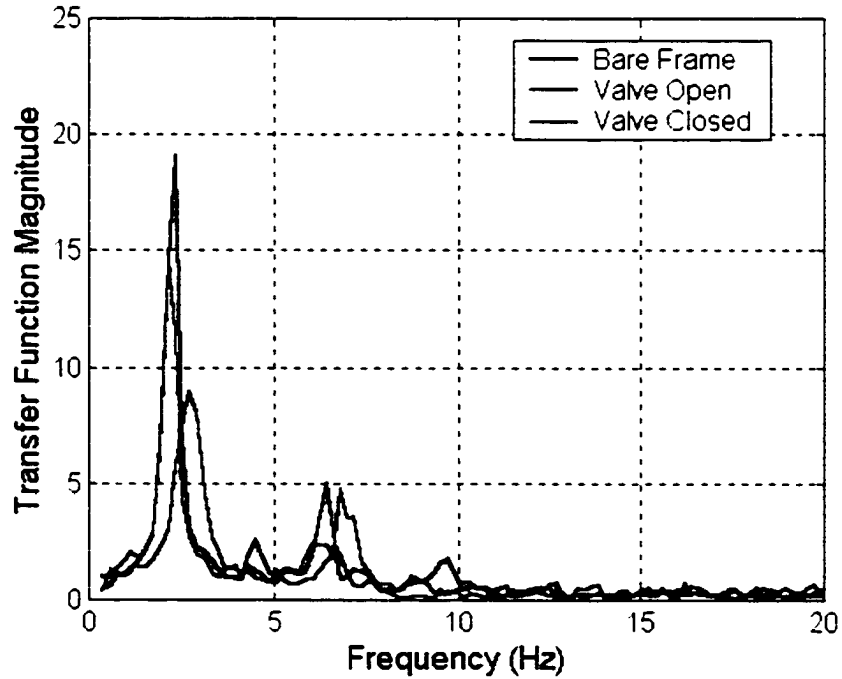


**Figure 5.16:** Frequency response function magnitude  $\ddot{x}_{31} / d$  with actuator operated passively in Position 2.

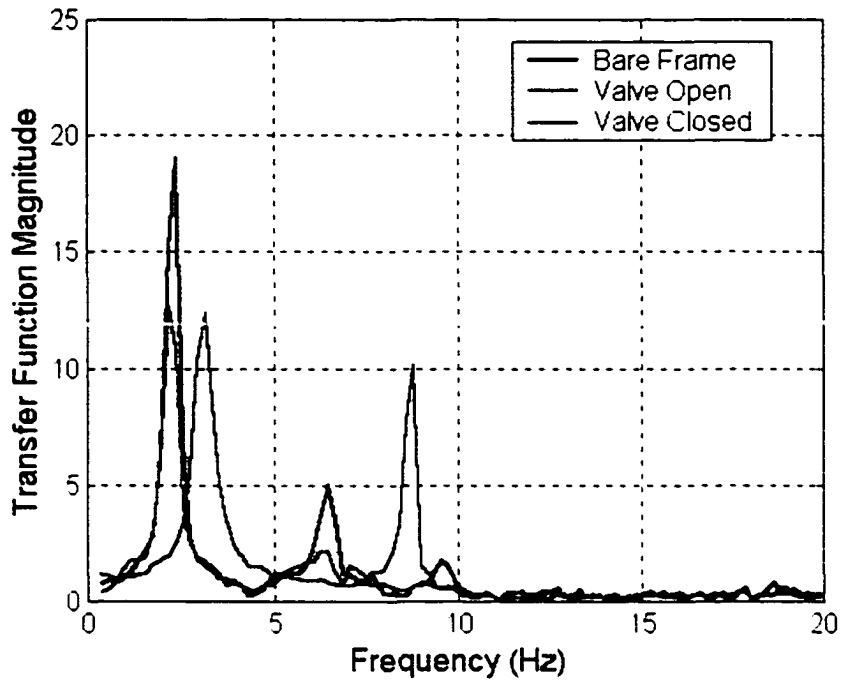


**Figure 5.17:** Frequency response function magnitude  $\ddot{x}_{32}/d$  with actuator operated passively in Position 1.

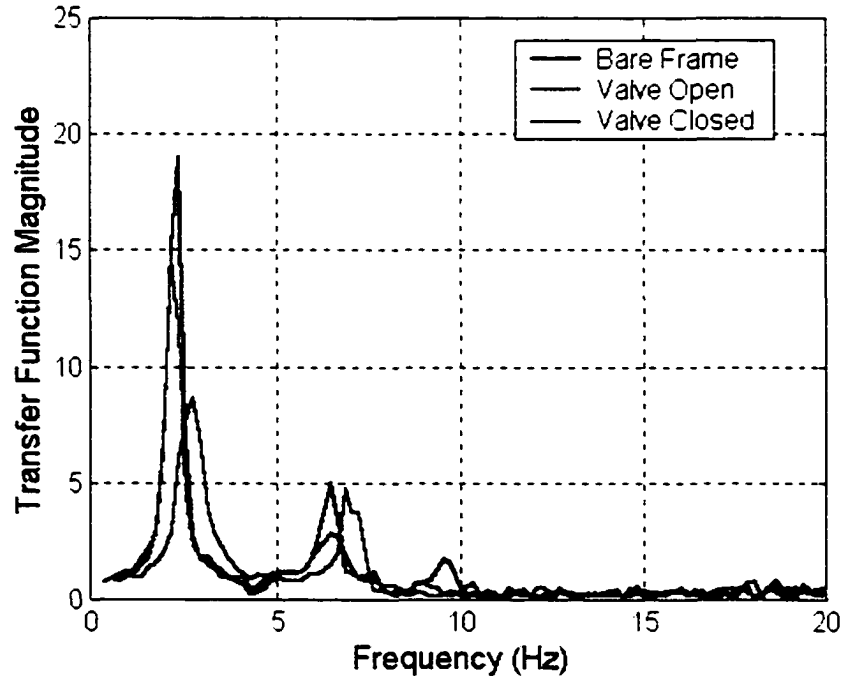


**Figure 5.18:** Frequency response function magnitude  $\ddot{x}_{32}/d$  with actuator operated passively in Position 2.

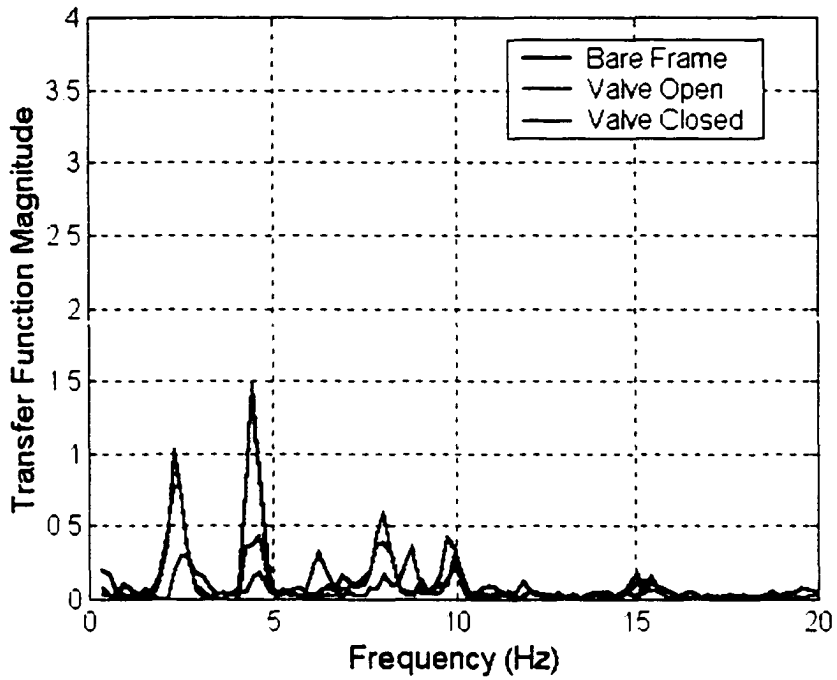


Figure 5.19: Frequency response function magnitude  $\ddot{y}_1/d$  with actuator operated passively in Position 1.

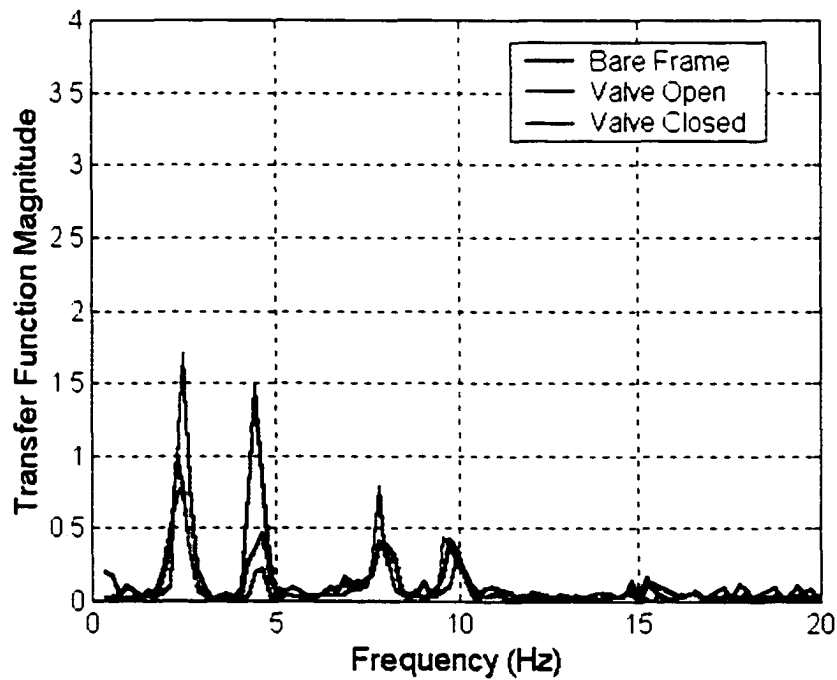


Figure 5.20: Frequency response function magnitude  $\ddot{y}_1/d$  with actuator operated passively in Position 2.

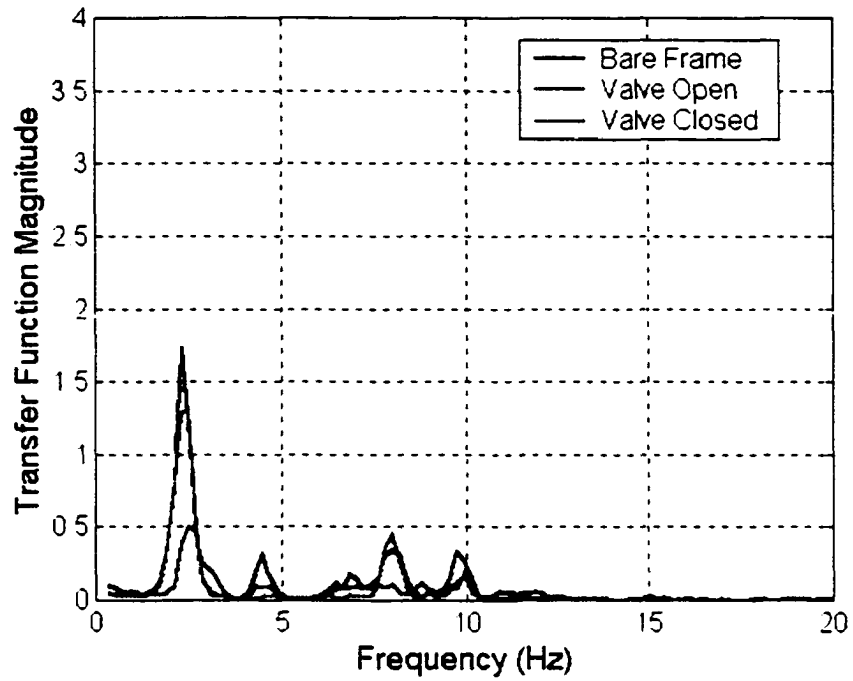


Figure 5.21: Frequency response function magnitude  $\ddot{y}_2/d$  with actuator operated passively in Position 1.

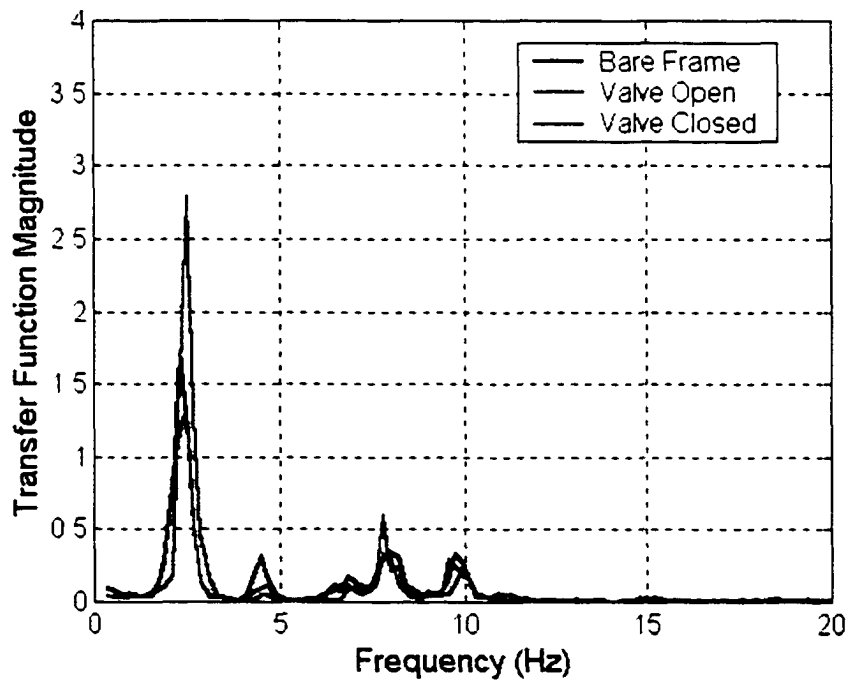


Figure 5.22: Frequency response function magnitude  $\ddot{y}_2/d$  with actuator operated passively in Position 2.

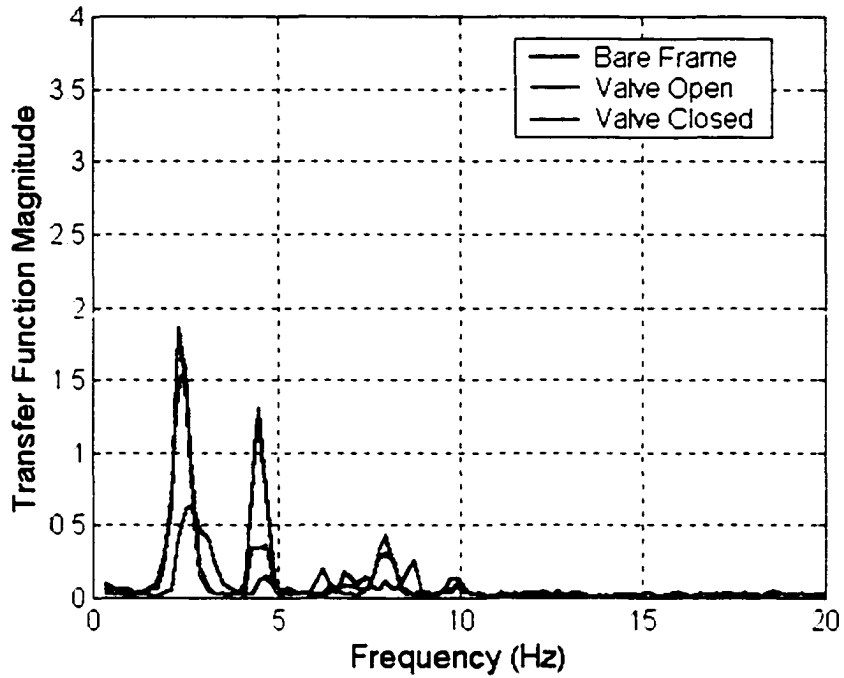


Figure 5.23: Frequency response function magnitude  $\ddot{y}_3/d$  with actuator operated passively in Position 1.

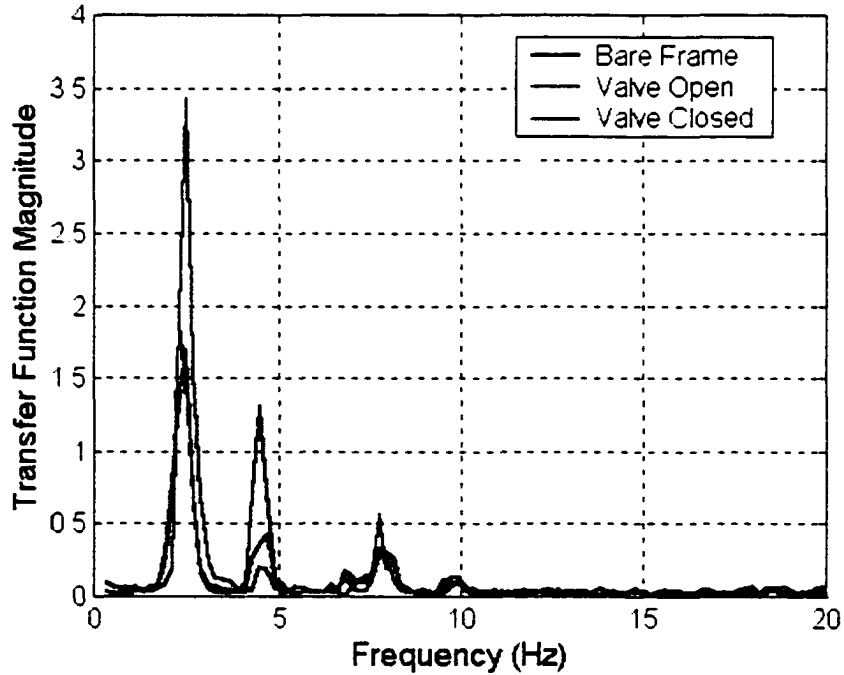


Figure 5.24: Frequency response function magnitude  $\ddot{y}_3/d$  with actuator operated passively in Position 2.

**Table 5.1: RMS relative displacements and absolute accelerations for passive configurations subjected to a broadband input.**

Actuator Position	Bare Frame	Position 1	Position 2	Position 1	Position 2
Valve Configuration	N/A	Open	Open	Closed	Closed
$z_1$ (mm)	3.30	2.00	2.30	0.10	3.80
% change	-	-39.4%	-30.3%	-97.0%	-15.2%
$z_2$ (mm)	2.70	1.60	1.90	2.90	0.20
% change	-	-40.7%	-29.6%	-7.4%	-92.6%
$z_3$ (mm)	1.40	0.80	0.90	1.60	1.30
% change	-	-42.9%	-35.7%	-14.3%	-7.1%
$\ddot{x}_1$ (m/s <sup>2</sup> )	1.92	1.18	1.15	1.95	1.90
% change	-	-38.5%	-40.1%	-1.6%	-1.0%
$\ddot{x}_2$ (m/s <sup>2</sup> )	2.54	1.68	1.79	3.04	2.38
% change	-	-33.9%	-29.5%	-19.7%	-6.3%
$\ddot{x}_3$ (m/s <sup>2</sup> )	2.99	1.92	2.03	3.47	2.95
% change	-	-35.8%	-32.1%	-16.1%	-1.3%
$\ddot{y}_1$ (m/s <sup>2</sup> )	0.46	0.46	0.34	0.41	0.59
% change	-	0.0%	-26.1%	-10.9%	-28.3%
$\ddot{y}_2$ (m/s <sup>2</sup> )	0.31	0.27	0.25	0.20	0.61
% change	-	-12.9%	-19.4%	-35.5%	-96.8%
$\ddot{y}_3$ (m/s <sup>2</sup> )	0.52	0.39	0.37	0.29	0.79
% change	-	-25.0%	-28.8%	-44.2%	-51.9%
$\Delta p$ (MPa)	-	0.02	0.02	1.22	1.00

**Table 5.2: Peak relative displacements and absolute accelerations for passive configurations subjected to a broadband input.**

Actuator Position	Bare Frame	Position 1	Position 2	Position 1	Position 2
Valve Configuration	N/A	Open	Open	Closed	Closed
$z_1$ (mm)	11.20	7.50	8.00	0.50	10.60
% change	-	-33.0%	-28.6%	-95.5%	-5.4%
$z_2$ (mm)	8.20	5.50	6.10	10.50	0.50
% change	-	-32.9%	-25.6%	-28.0%	-93.9%
$z_3$ (mm)	4.10	2.80	3.00	5.20	4.30
% change	-	-31.7%	-26.8%	-26.8%	-4.9%
$\ddot{x}_1$ (m/s <sup>2</sup> )	8.98	5.95	5.21	10.83	7.05
% change	-	-33.7%	-42.0%	-20.6%	-21.5%
$\ddot{x}_2$ (m/s <sup>2</sup> )	9.59	7.31	7.74	13.31	8.47
% change	-	-23.8%	-19.3%	-38.8%	-11.7%
$\ddot{x}_3$ (m/s <sup>2</sup> )	9.87	7.64	8.12	12.93	10.36
% change	-	-22.6%	-17.7%	-31.0%	-5.0%
$\ddot{y}_1$ (m/s <sup>2</sup> )	1.87	2.06	1.38	1.67	2.45
% change	-	-10.2%	-26.2%	-10.7%	-31.0%
$\ddot{y}_2$ (m/s <sup>2</sup> )	1.30	1.20	1.02	0.88	2.10
% change	-	-7.7%	-21.5%	-32.3%	-61.5%
$\ddot{y}_3$ (m/s <sup>2</sup> )	2.12	1.78	1.60	1.32	2.46
% change	-	-16.0%	-24.5%	-37.7%	-16.0%
$\Delta p$ (MPa)	-	0.10	0.10	4.85	3.13

**Table 5.3: RMS relative displacements and absolute accelerations for passive configurations subjected to the El Centro earthquake input.**

Actuator Position	Bare Frame	Position 1	Position 2	Position 1	Position 2
Valve Configuration	N/A	Open	Open	Closed	Closed
$z_1$ (mm)	2.50	1.60	1.80	0.06	2.00
% change	-	-36.0%	-28.0%	-97.6%	-20.0%
$z_2$ (mm)	2.00	1.30	1.30	0.93	0.10
% change	-	-35.0%	-35.0%	-53.5%	-95.0%
$z_3$ (mm)	1.00	0.60	0.70	0.50	0.70
% change	-	-40.0%	-30.0%	-50.0%	-30.0%
$\ddot{x}_1$ (m/s <sup>2</sup> )	1.25	0.82	0.82	0.81	1.04
% change	-	-34.4%	-34.4%	-35.2%	-16.8%
$\ddot{x}_2$ (m/s <sup>2</sup> )	1.81	1.25	1.35	1.04	1.32
% change	-	-30.9%	-25.4%	-42.5%	-27.1%
$\ddot{x}_3$ (m/s <sup>2</sup> )	2.14	1.43	1.60	1.26	1.61
% change	-	-33.2%	-25.2%	-41.1%	-24.8%
$\ddot{y}_1$ (m/s <sup>2</sup> )	0.32	0.33	0.27	0.28	0.34
% change	-	-3.1%	-15.6%	-12.5%	-6.3%
$\ddot{y}_2$ (m/s <sup>2</sup> )	0.19	0.16	0.18	0.13	0.30
% change	-	-15.8%	-5.3%	-31.6%	-57.9%
$\ddot{y}_3$ (m/s <sup>2</sup> )	0.32	0.24	0.26	0.20	0.40
% change	-	-25.0%	-18.8%	-37.5%	-25.0%
$\Delta p$ (MPa)	-	0.02	0.02	0.37	0.53

**Table 5.4:** Peak relative displacements and absolute accelerations for passive configurations subjected to the El Centro earthquake input.

Actuator Position	Bare Frame	Position 1	Position 2	Position 1	Position 2
Valve Configuration	N/A	Open	Open	Closed	Closed
$z_1$ (mm)	12.60	10.60	12.10	0.60	11.30
% change	-	-15.9%	-4.0%	-95.2%	-10.3%
$z_2$ (mm)	10.00	8.80	7.40	6.30	0.50
% change	-	-12.0%	-26.0%	-37.0%	-95.0%
$z_3$ (mm)	5.10	4.30	4.00	3.10	4.10
% change	-	-15.7%	-21.6%	-39.2%	-19.6%
$\ddot{x}_1$ (m/s <sup>2</sup> )	7.52	5.19	6.23	40.78	7.88
% change	-	-31.0%	-17.2%	-442.3%	-4.8%
$\ddot{x}_2$ (m/s <sup>2</sup> )	10.09	10.55	10.75	9.23	8.79
% change	-	-4.6%	-6.5%	-8.5%	-12.9%
$\ddot{x}_3$ (m/s <sup>2</sup> )	11.98	10.93	10.70	12.07	9.54
% change	-	-8.8%	-10.7%	-0.8%	-20.4%
$\ddot{y}_1$ (m/s <sup>2</sup> )	1.69	1.88	1.67	1.35	5.89
% change	-	-11.2%	-1.2%	-20.1%	-248.5%
$\ddot{y}_2$ (m/s <sup>2</sup> )	1.46	1.31	1.29	1.17	1.69
% change	-	-10.3%	-11.6%	-19.9%	-15.8%
$\ddot{y}_3$ (m/s <sup>2</sup> )	1.92	1.82	1.69	1.14	1.96
% change	-	-5.2%	-12.0%	-40.6%	-2.1%
$\Delta p$ (MPa)	-	0.10	0.10	4.85	3.13

### 5.3 Semi-Active Test Results

Semi-active control tests were performed next using the quickest descent Lyapunov control algorithm developed in Chapter 4 and a collocated control designed to minimize the product of the actuator force and the actuator relative velocity. The Lyapunov control logic was based on the actuator differential pressure and the relative displacements and velocities between floors of the structure. Neither control law assumed any knowledge of the seismic disturbance input. Both control laws were tested with a single actuator first in Position 1 and then in Position 2. The control valve was modulated between  $0^\circ$  and  $45^\circ$  based on the control command. The data obtained from the semi-active control tests are plotted in Figures 5.25-5.48. The “bare frame” case is plotted in blue, the “force/velocity” control response is plotted in green and the “Lyapunov” control response is plotted in red.

The frequency response function magnitudes of the relative floor-to-floor displacements for the broadband disturbance input are provided in Figures 5.25-5.30. With the actuator in Position 1, the Lyapunov control provides a 78% reduction in the peak first floor relative displacement compared to a 54% reduction for the force/velocity control. Both controllers decrease peak deflections by at least 46% between the remaining floors. In Position 2, the force/velocity control law yields at least a 39% reduction in peak inter-story drift compared to 48% for the Lyapunov control. The semi-active actuator provides considerable reductions (at least 44%) in the higher frequency modal amplitudes regardless of the control law or actuator position since the force generated by the actuator is velocity dependent. In Position 2, both controllers essentially eliminate the third mode as seen in Figures 5.26, 5.28 and 5.30.

The frequency response function magnitudes of the  $x$ -direction accelerations are plotted in Figures 5.31-5.42. Both controllers provide at least a 43% decrease in  $x$ -axis acceleration at the natural frequencies when compared to the no control case. In Position 1, the force/velocity control law yields at least a 64% reduction in first mode amplitude on each floor compared to 55% for the Lyapunov control. Likewise, in Position 2, the force/velocity control lowered the first mode acceleration by at least 76% compared to 43% with the Lyapunov control law. Figures 5.43-5.48 indicate the acceleration frequency response magnitudes in the  $y$ -direction. All semi-active control laws provided at least a 34% reduction of the third floor  $y$ -axis RMS accelerations over the bare frame case and an 8% reduction from the valve open case.

The RMS and peak relative displacements, absolute accelerations and actuator differential pressures from the broadband tests are summarized in Tables 5.5 and 5.6. The data from the El Centro tests are provided in Tables 5.7 and 5.8. All of the semi-active control configurations provide substantial reductions in maximum floor-to-floor displacements from the passive open valve configurations (at least 35% for the broadband input and 11% for the El Centro input). The semi-active actuator is able to provide more reduction in displacement between floors where the actuator is located. The results for Position 1 also indicate the Lyapunov control is much more effective in reducing relative displacement  $z_1$  than the force/velocity control for the banded white noise input (94% reduction compared to 58%). However, both controls offer comparable performance for the El Centro input, confirming that performance gains are input specific.

Both semi-active control laws have their advantages and disadvantages. The force/velocity control logic is computationally efficient and simple to implement since it

relies on only two sensors per actuator (differential pressure and linear velocity). Since the actuator and sensors are collocated, the entire system including the control electronics can be incorporated into a single self-contained unit greatly simplifying the installation of the system. There are no parameters to tune for this simple control law and performance depends entirely on the control device parameters and the structure. However, Leitmann (1994) showed that such a control scheme for a linearly variable stiffness and damping controller did not guarantee stability of the closed loop system. The stability of the force/velocity controller has not been addressed for the actuator dynamics presented herein.

The Lyapunov control system is much more complicated than the force/velocity controller in that it requires full state information on the structure and the actuator to generate the control command. The state information must be directly measured or estimated on-line adding to the sensory hardware costs, the control processor capabilities and the number of data acquisition channels. The Lyapunov control also requires a suitable control model for designing a candidate Lyapunov function and estimating the system states. For large or complex structures a reduced order control model would be required to prevent the control synthesis and implementation from becoming unwieldy. The primary benefit to the Lyapunov control law is that stability has been established for the controller in Chapter 4. Likewise, the performance of the controller can be tuned by tailoring the Lyapunov function to the application without varying actuator parameters. The variability of the Lyapunov control law allows the semi-active control system to be optimized for a wide range of disturbance inputs.

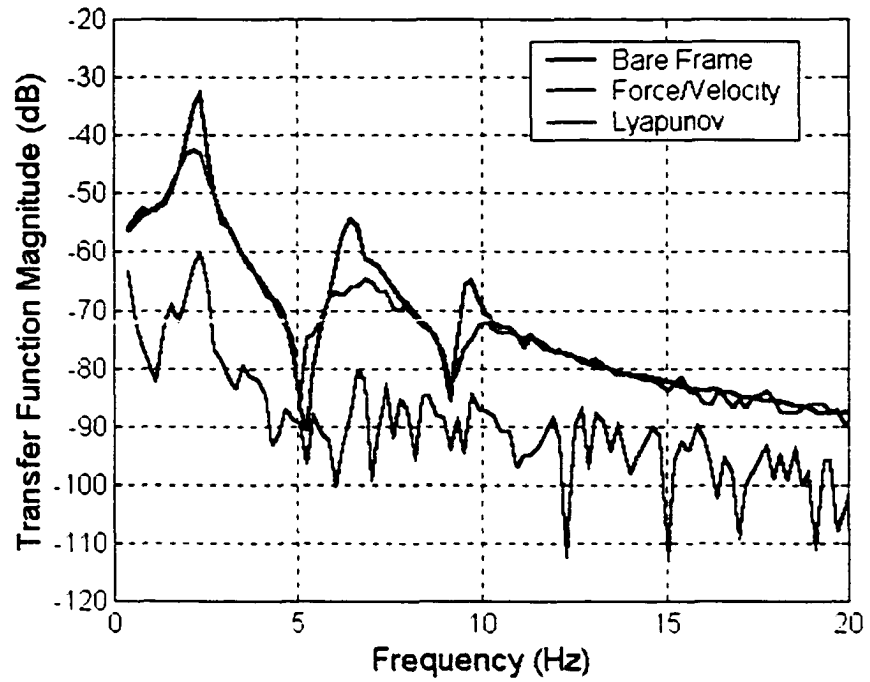


**Figure 5.25:** Frequency response function magnitude  $z_1 / d$  with semi-active control in Position 1.

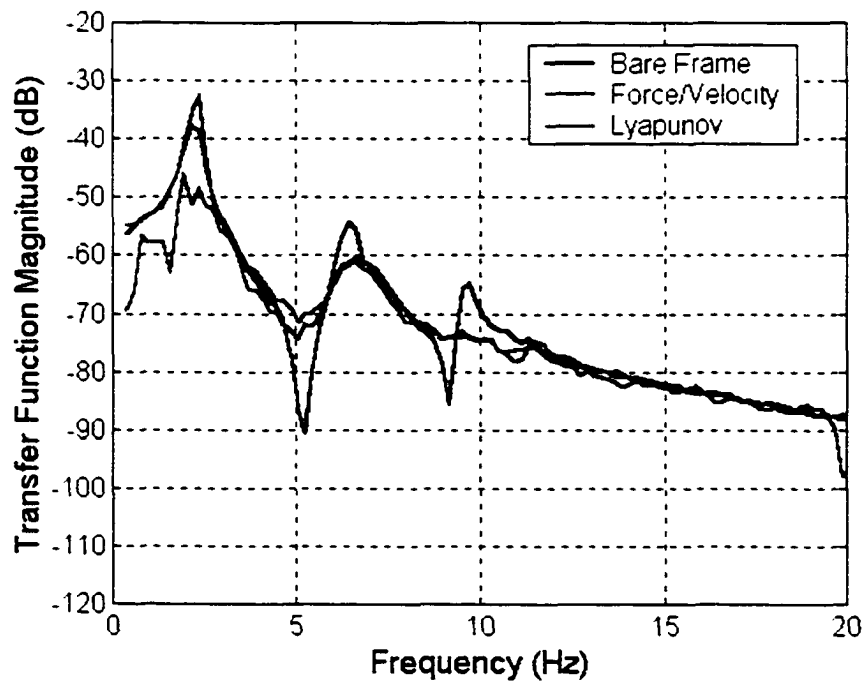


**Figure 5.26:** Frequency response function magnitude  $z_1 / d$  with semi-active control in Position 2.

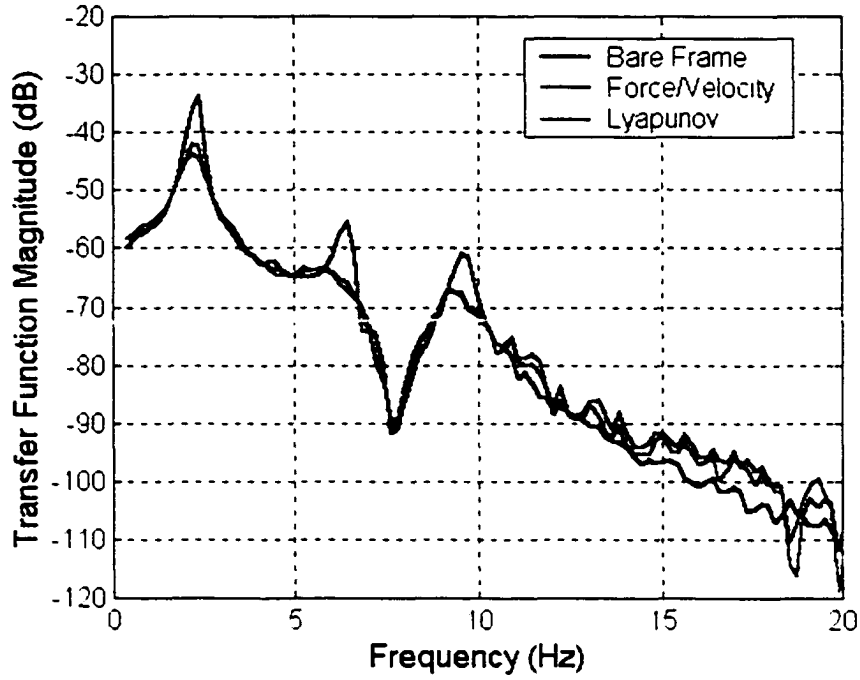


Figure 5.27: Frequency response function magnitude  $z_2/d$  with semi-active control in Position 1.

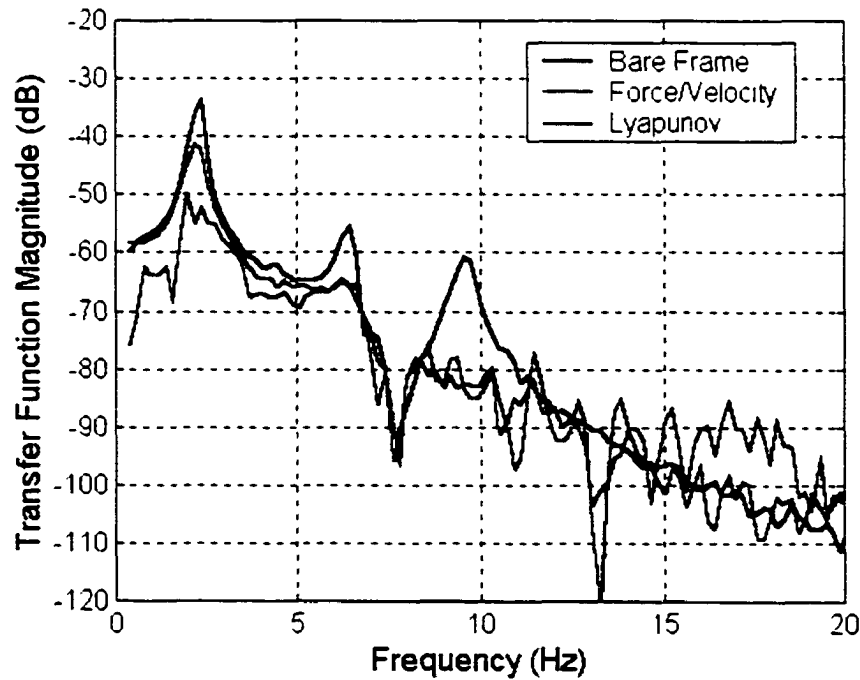
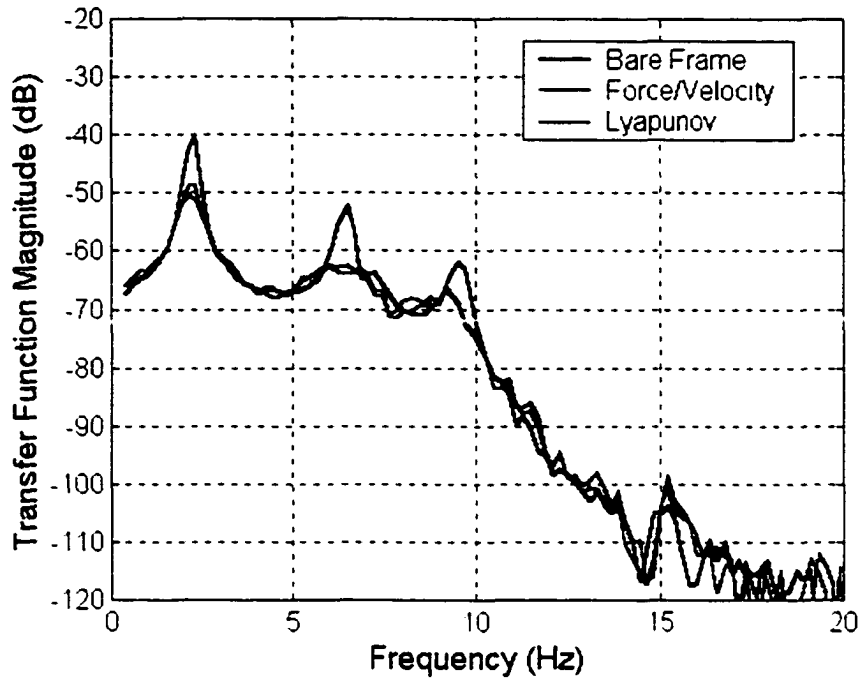
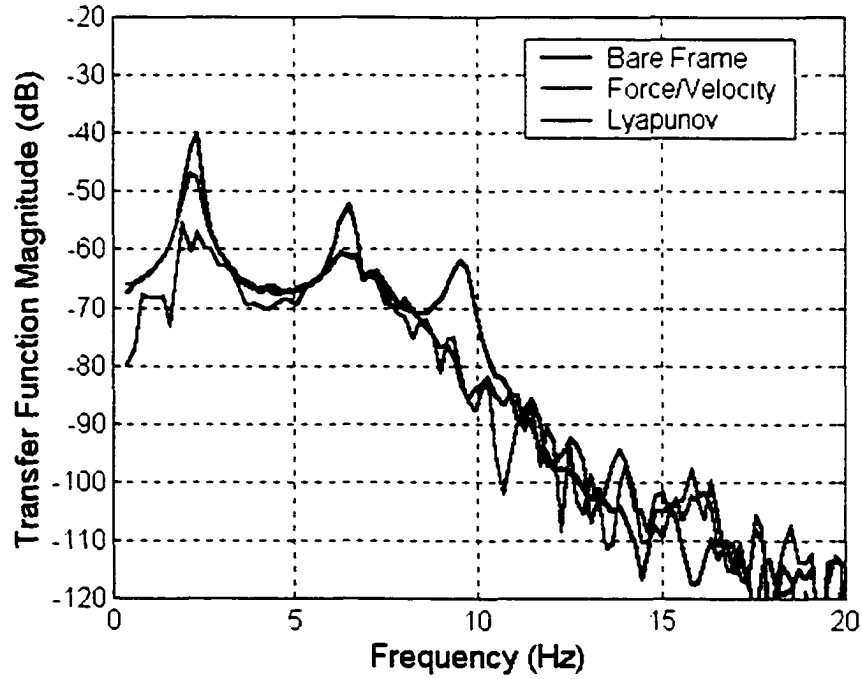


Figure 5.28: Frequency response function magnitude  $z_2/d$  with semi-active control in Position 2.



**Figure 5.29:** Frequency response function magnitude  $z_3/d$  with semi-active control in Position 1.



**Figure 5.30:** Frequency response function magnitude  $z_3/d$  with semi-active control in Position 2.

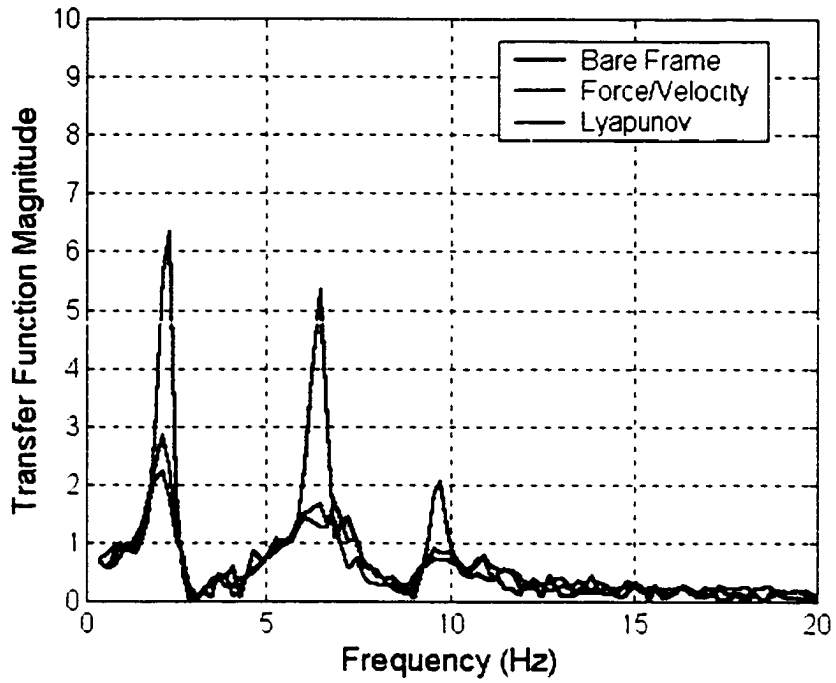


**Figure 5.31:** Frequency response function magnitude  $\ddot{x}_{11} / d$  with semi-active control in Position 1.

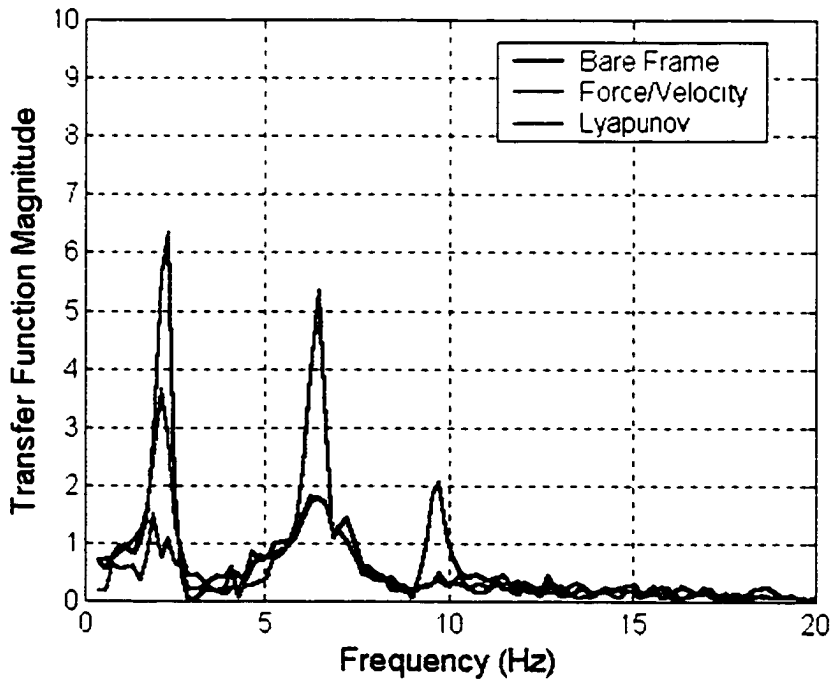


**Figure 5.32:** Frequency response function magnitude  $\ddot{x}_{11} / d$  with semi-active control in Position 2.

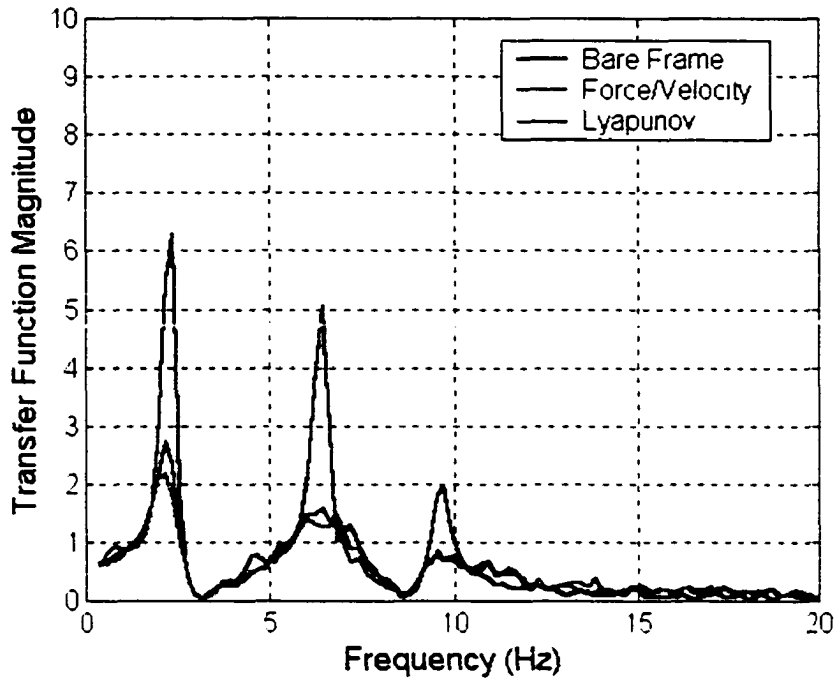


Figure 5.33: Frequency response function magnitude  $\ddot{x}_{12} / d$  with semi-active control in Position 1.

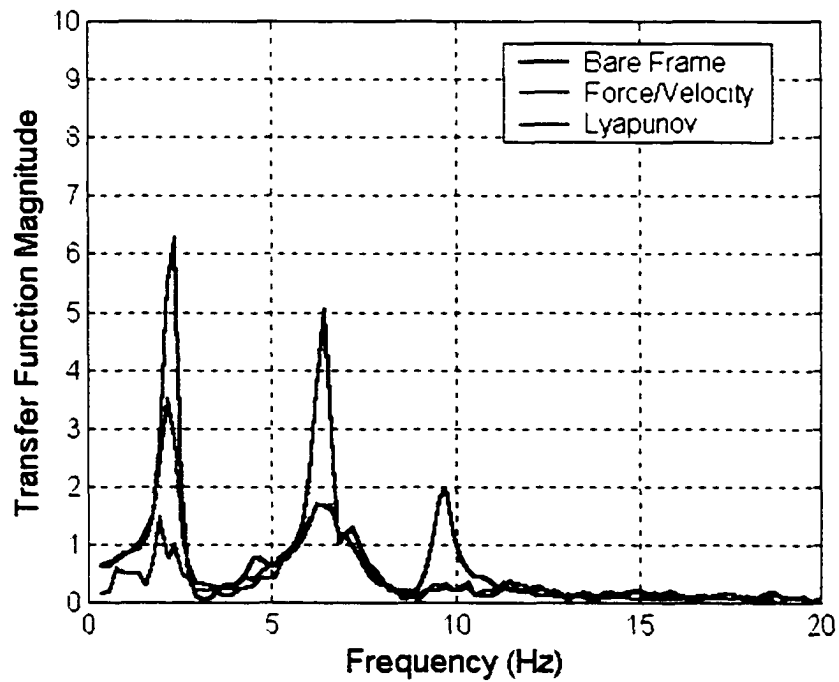
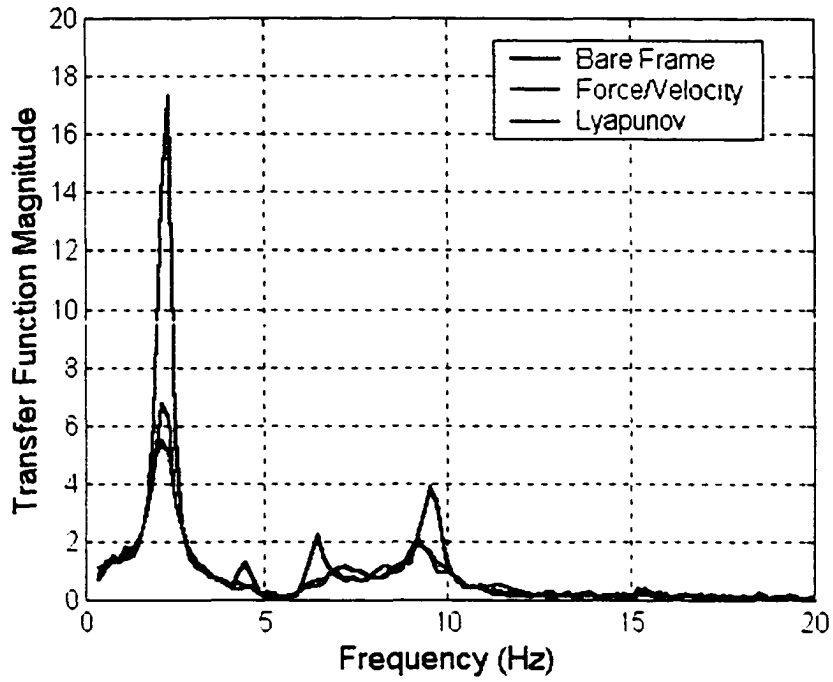
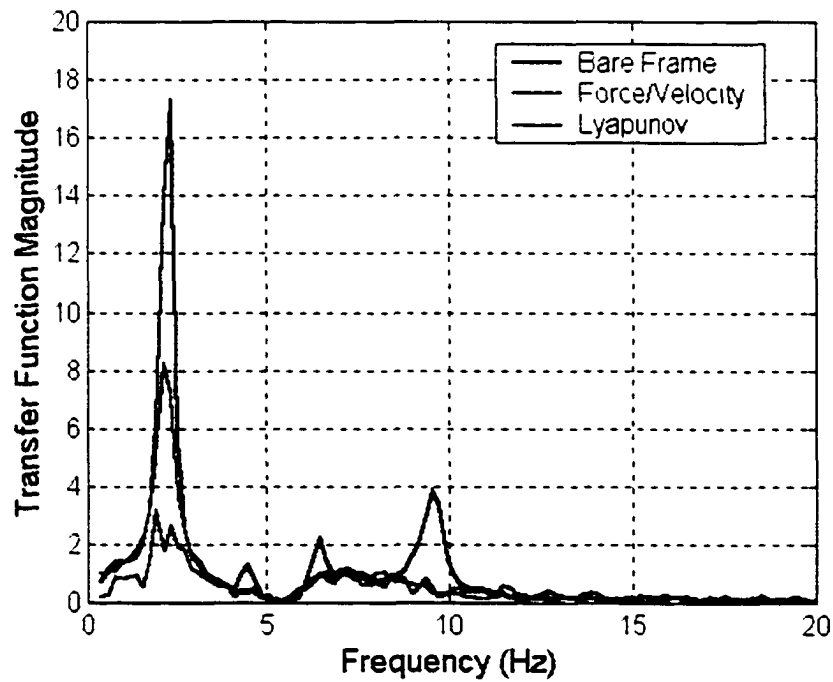


Figure 5.34: Frequency response function magnitude  $\ddot{x}_{12} / d$  with semi-active control in Position 2.



**Figure 5.35:** Frequency response function magnitude  $\ddot{x}_{21}/d$  with semi-active control in Position 1.



**Figure 5.36:** Frequency response function magnitude  $\ddot{x}_{21}/d$  with semi-active control in Position 2.

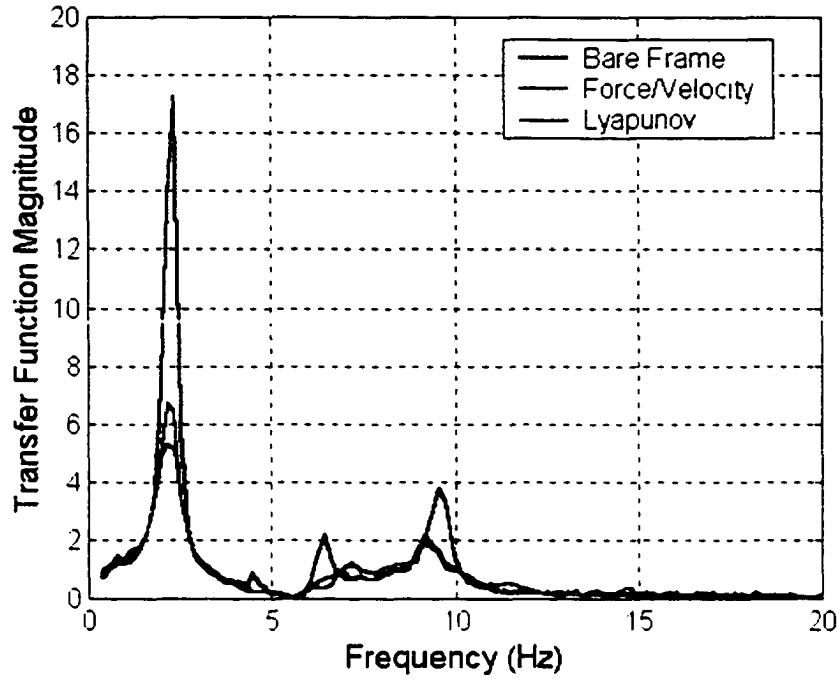


Figure 5.37: Frequency response function magnitude  $\ddot{x}_{22} / d$  with semi-active control in Position 1.

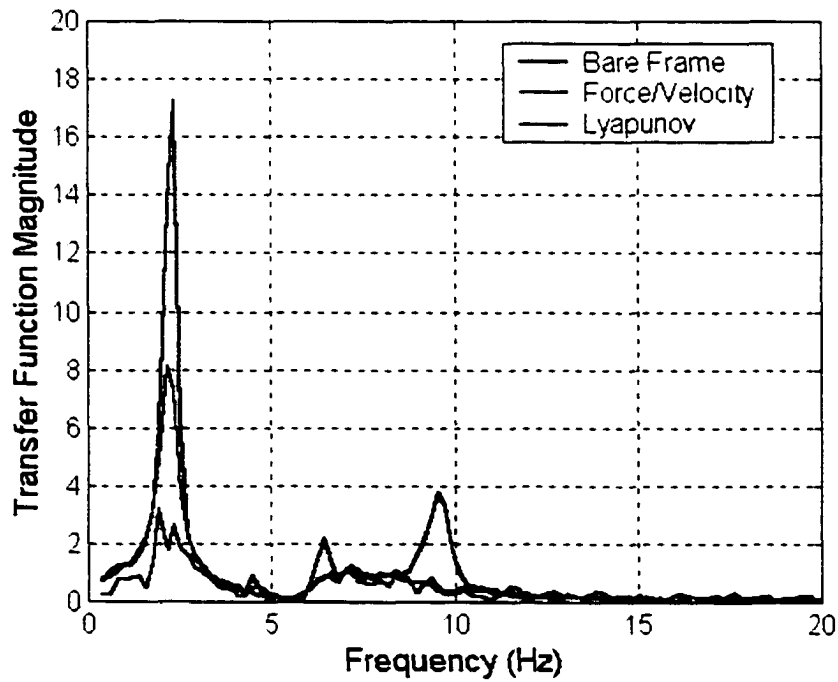
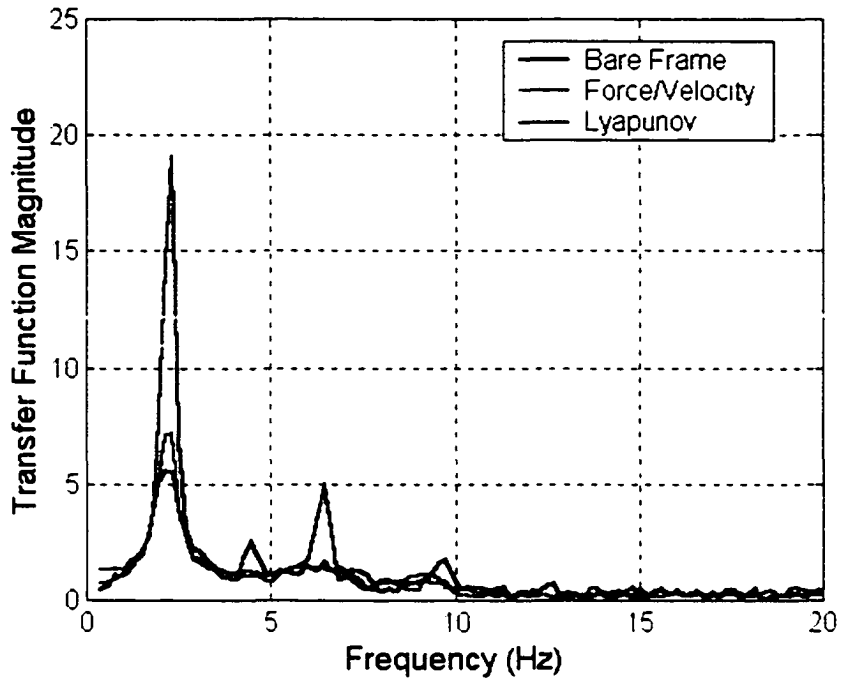
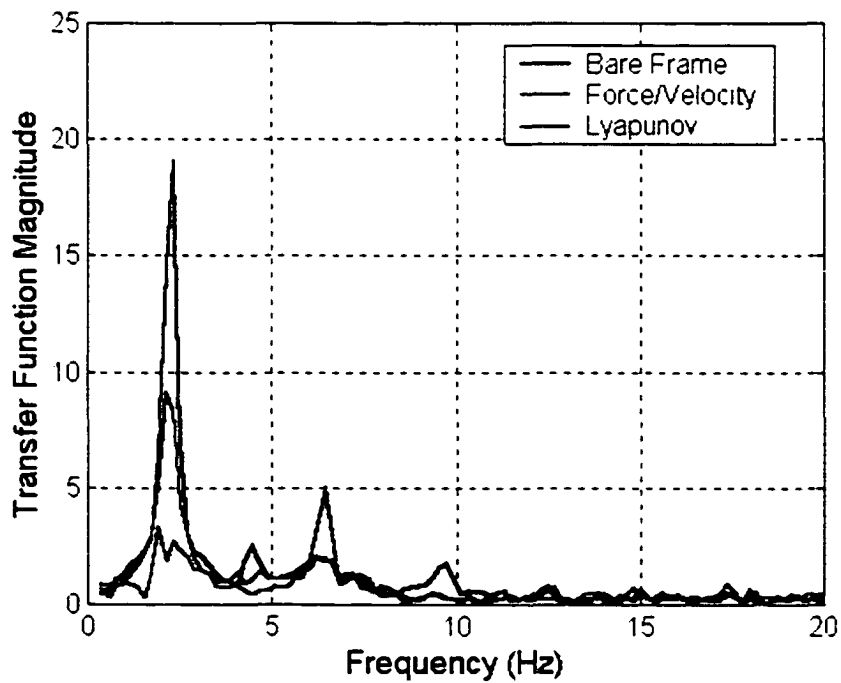


Figure 5.38: Frequency response function magnitude  $\ddot{x}_{22} / d$  with semi-active control in Position 2.



**Figure 5.39:** Frequency response function magnitude  $\ddot{x}_{31} / d$  with semi-active control in Position 1.



**Figure 5.40:** Frequency response function magnitude  $\ddot{x}_{31} / d$  with semi-active control in Position 2.

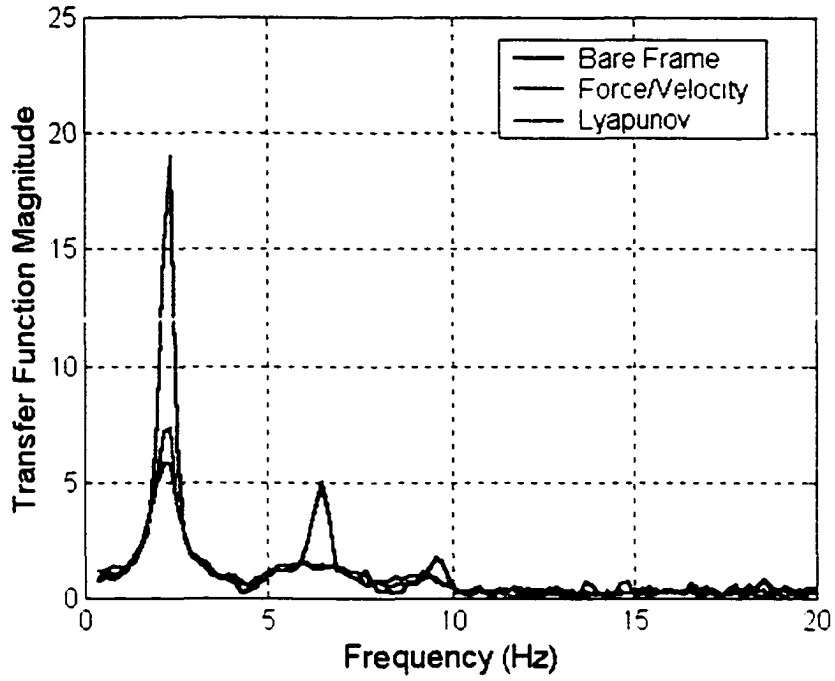


**Figure 5.41:** Frequency response function magnitude  $\ddot{x}_{32} / d$  with semi-active control in Position 1.

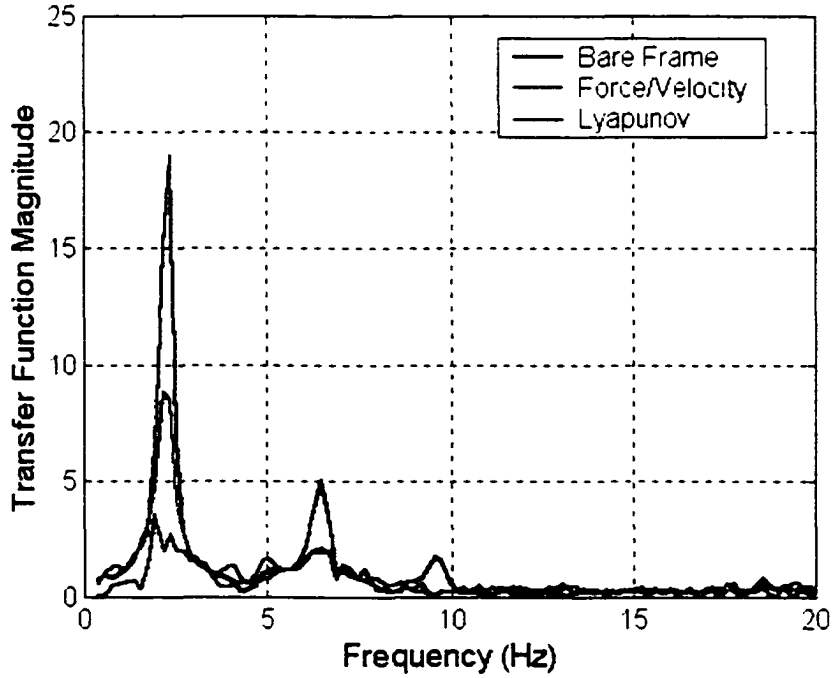


**Figure 5.42:** Frequency response function magnitude  $\ddot{x}_{32} / d$  with semi-active control in Position 2.

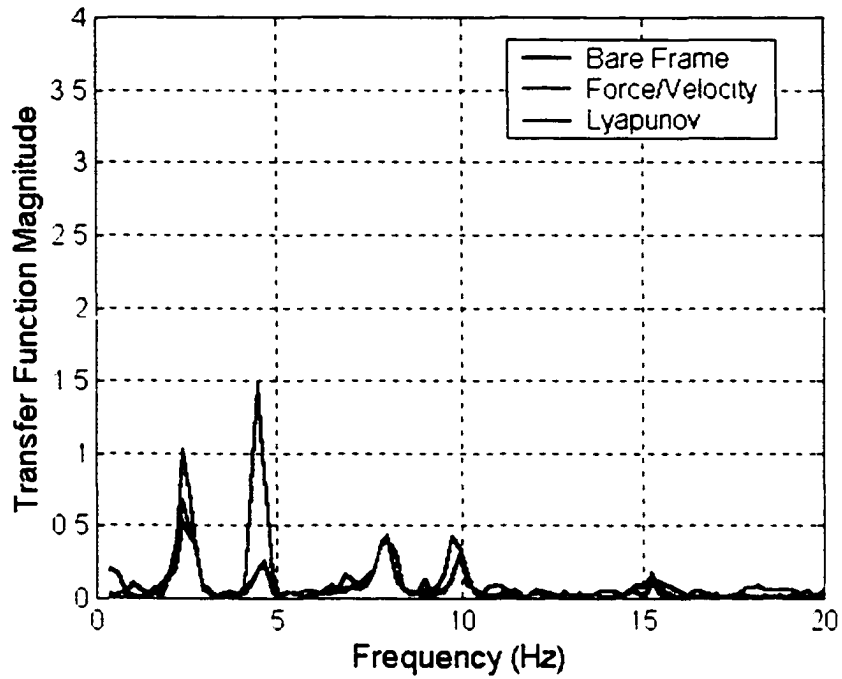


Figure 5.43: Frequency response function magnitude  $\ddot{y}_1/d$  with semi-active control in Position 1.

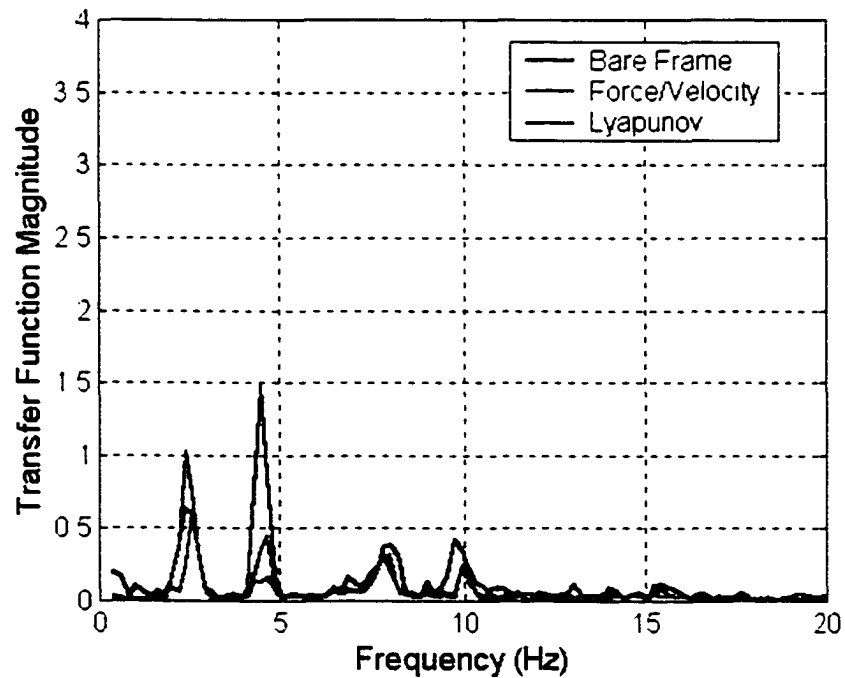


Figure 5.44: Frequency response function magnitude  $\ddot{y}_1/d$  with semi-active control in Position 2.

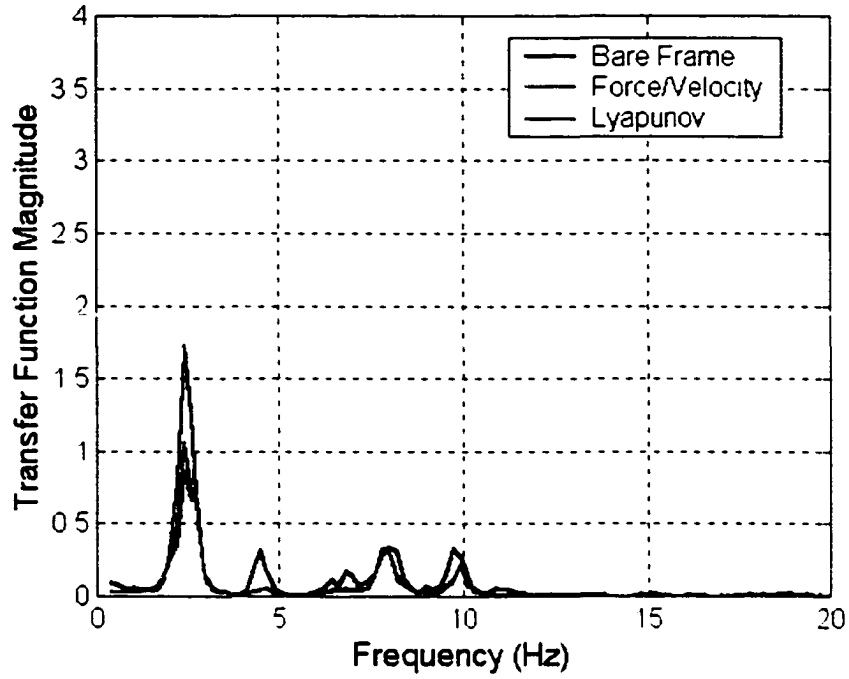


Figure 5.45: Frequency response function magnitude  $\ddot{y}_2/d$  with semi-active control in Position 1.

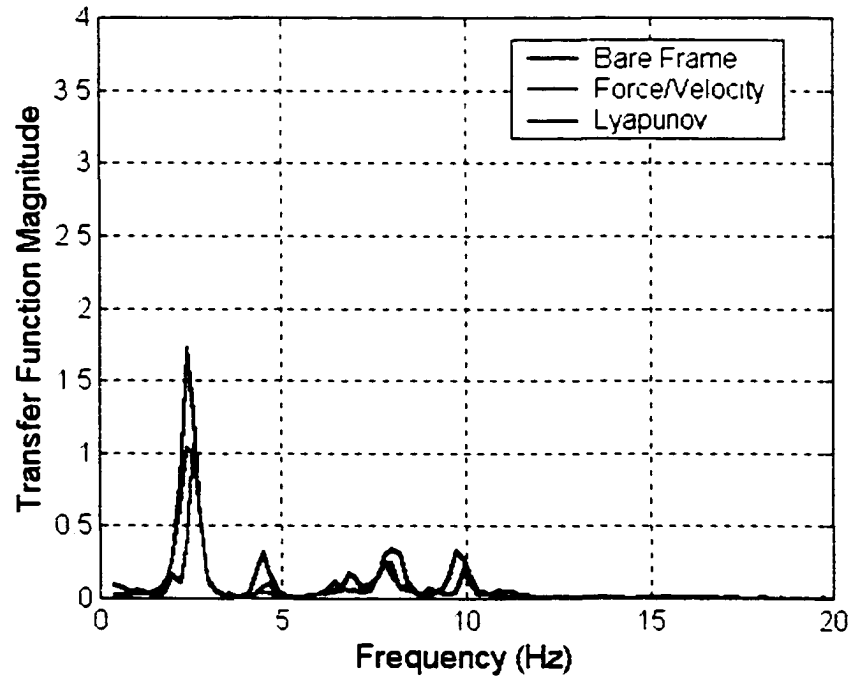


Figure 5.46: Frequency response function magnitude  $\ddot{y}_2/d$  with semi-active control in Position 2.

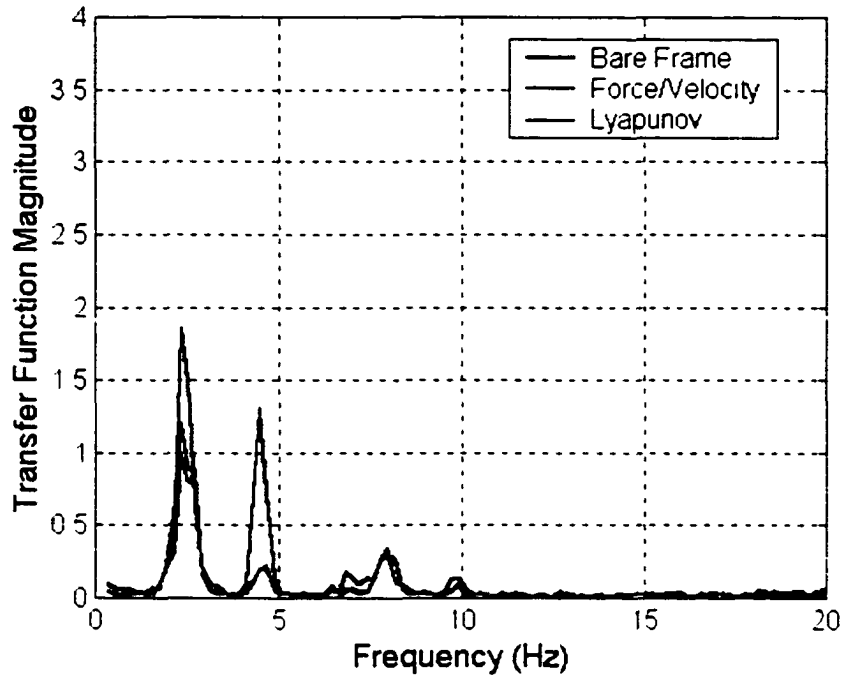


Figure 5.47: Frequency response function magnitude  $\ddot{y}_3/d$  with semi-active control in Position 1.

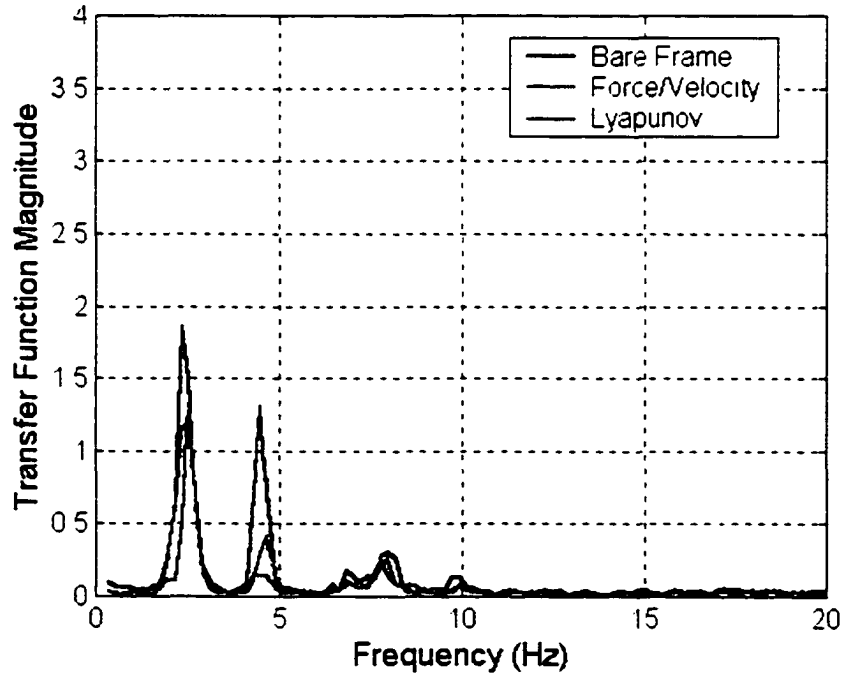


Figure 5.48: Frequency response function magnitude  $\ddot{y}_3/d$  with semi-active control in Position 2.

**Table 5.5:** RMS relative displacements and absolute accelerations for semi-active configurations subjected to a broadband input.

Actuator Position	Bare Frame	Position 1	Position 1	Position 2	Position 2
Valve Configuration	N/A	F/V	Lyapunov	F/V	Lyapunov
$z_1$ (mm)	3.30	1.40	0.20	1.80	1.70
% change	-	-57.6%	-93.9%	-45.5%	-48.5%
$z_2$ (mm)	2.70	1.20	1.20	1.20	1.20
% change	-	-55.6%	-55.6%	-55.6%	-55.6%
$z_3$ (mm)	1.40	0.60	0.60	0.70	0.60
% change	-	-57.1%	-57.1%	-50.0%	-57.1%
$\ddot{x}_1$ (m/s <sup>2</sup> )	1.92	1.01	1.03	0.99	0.97
% change	-	-47.4%	-46.4%	-48.4%	-49.5%
$\ddot{x}_2$ (m/s <sup>2</sup> )	2.54	1.33	1.39	1.41	1.39
% change	-	-47.6%	-45.3%	-44.5%	-45.3%
$\ddot{x}_3$ (m/s <sup>2</sup> )	2.99	1.51	1.59	1.68	1.65
% change	-	-49.5%	-46.8%	-43.8%	-44.8%
$\ddot{y}_1$ (m/s <sup>2</sup> )	0.46	0.40	0.44	0.21	0.29
% change	-	-13.0%	-4.3%	-54.3%	-37.0%
$\ddot{y}_2$ (m/s <sup>2</sup> )	0.31	0.24	0.25	0.22	0.22
% change	-	-22.6%	-19.4%	-29.0%	-29.0%
$\ddot{y}_3$ (m/s <sup>2</sup> )	0.52	0.33	0.34	0.30	0.33
% change	-	-36.5%	-34.6%	-42.3%	-36.5%
$\Delta p$ (MPa)	-	0.06	0.06	0.07	0.07

**Table 5.6:** Peak relative displacements and absolute accelerations for semi-active configurations subjected to a broadband input.

Actuator Position	Bare Frame	Position 1	Position 1	Position 2	Position 2
Control Logic	N/A	F/V	Lyapunov	F/V	Lyapunov
$z_1$ (mm)	11.20	5.10	2.40	6.40	5.50
% change	-	-54.5%	-78.6%	-42.9%	-50.9%
$z_2$ (mm)	8.20	3.90	4.10	4.90	4.10
% change	-	-52.4%	-50.0%	-40.2%	-50.0%
$z_3$ (mm)	4.10	2.10	2.20	2.50	2.10
% change	-	-48.8%	-46.3%	-39.0%	-48.8%
$\ddot{x}_1$ (m/s <sup>2</sup> )	8.98	4.73	4.40	5.02	5.30
% change	-	-47.3%	-51.0%	-44.1%	-41.0%
$\ddot{x}_2$ (m/s <sup>2</sup> )	9.59	5.51	5.75	6.26	5.52
% change	-	-42.5%	-40.0%	-34.7%	-42.4%
$\ddot{x}_3$ (m/s <sup>2</sup> )	9.87	6.04	6.23	6.77	6.80
% change	-	-38.8%	-36.9%	-31.4%	-31.1%
$\ddot{y}_1$ (m/s <sup>2</sup> )	1.87	1.60	1.99	1.03	1.14
% change	-	-14.4%	-6.4%	-44.9%	-39.0%
$\ddot{y}_2$ (m/s <sup>2</sup> )	1.30	0.93	1.02	0.88	0.99
% change	-	-28.5%	-21.5%	-32.3%	-23.8%
$\ddot{y}_3$ (m/s <sup>2</sup> )	2.12	1.46	1.46	1.69	1.60
% change	-	-31.1%	-31.1%	-20.3%	-24.5%
$\Delta p$ (MPa)	-	0.42	0.45	0.45	0.45

**Table 5.7:** RMS relative displacements and absolute accelerations for semi-active configurations subjected to the El Centro earthquake input.

Actuator Position	Bare Frame	Position 1	Position 1	Position 2	Position 2
Valve Configuration	N/A	F/V	Lyapunov	F/V	Lyapunov
$z_1$ (mm)	2.50	0.90	0.93	1.40	1.00
% change	-	-64.0%	-62.8%	-44.0%	-60.0%
$z_2$ (mm)	2.00	0.70	0.72	0.40	0.80
% change	-	-65.0%	-64.0%	-80.0%	-60.0%
$z_3$ (mm)	1.00	0.33	0.34	0.50	0.40
% change	-	-67.0%	-66.0%	-50.0%	-60.0%
$\ddot{x}_1$ (m/s <sup>2</sup> )	1.25	0.65	0.65	0.70	0.61
% change	-	-48.0%	-48.0%	-44.0%	-52.1%
$\ddot{x}_2$ (m/s <sup>2</sup> )	1.81	0.84	0.86	1.10	0.88
% change	-	-53.6%	-52.5%	-39.2%	-51.4%
$\ddot{x}_3$ (m/s <sup>2</sup> )	2.14	0.98	1.00	1.30	1.05
% change	-	-54.2%	-53.3%	-39.3%	-50.9%
$\ddot{y}_1$ (m/s <sup>2</sup> )	0.32	0.29	0.31	0.13	0.25
% change	-	-9.4%	-3.1%	-59.4%	-21.9%
$\ddot{y}_2$ (m/s <sup>2</sup> )	0.19	0.15	0.15	0.13	0.14
% change	-	-21.1%	-21.1%	-31.6%	-26.3%
$\ddot{y}_3$ (m/s <sup>2</sup> )	0.32	0.21	0.21	0.18	0.21
% change	-	-34.4%	-34.4%	-43.8%	-34.4%
$\Delta p$ (MPa)	-	0.04	0.04	0.05	0.05

**Table 5.8:** Peak relative displacements and absolute accelerations for semi-active configurations subjected to the El Centro earthquake input.

Actuator Position	Bare Frame	Position 1	Position 1	Position 2	Position 2
Control Logic	N/A	F/V	Lyapunov	F/V	Lyapunov
$z_1$ (mm)	12.60	7.40	7.70	9.40	7.90
% change	-	-41.3%	-38.9%	-25.4%	-37.3%
$z_2$ (mm)	10.00	5.40	5.50	5.00	6.10
% change	-	-46.0%	-45.0%	-50.0%	-39.0%
$z_3$ (mm)	5.10	2.70	2.80	4.70	2.70
% change	-	-47.1%	-45.1%	-7.8%	-47.1%
$\ddot{x}_1$ (m/s <sup>2</sup> )	7.52	6.71	8.23	6.71	9.31
% change	-	-10.8%	-9.4%	-10.8%	-23.8%
$\ddot{x}_2$ (m/s <sup>2</sup> )	10.09	7.99	9.06	9.58	7.39
% change	-	-20.8%	-10.2%	-5.1%	-26.8%
$\ddot{x}_3$ (m/s <sup>2</sup> )	11.98	6.95	6.96	10.52	7.49
% change	-	-42.0%	-41.9%	-12.2%	-37.5%
$\ddot{y}_1$ (m/s <sup>2</sup> )	1.69	1.35	1.63	1.14	6.28
% change	-	-20.1%	-3.6%	-32.5%	-271.6%
$\ddot{y}_2$ (m/s <sup>2</sup> )	1.46	0.85	1.08	0.93	0.88
% change	-	-41.8%	-26.0%	-36.3%	-39.7%
$\ddot{y}_3$ (m/s <sup>2</sup> )	1.92	1.28	1.37	1.28	1.23
% change	-	-33.3%	-28.6%	-33.3%	-35.9%
$\Delta p$ (MPa)	-	0.49	0.89	0.86	0.62

## CHAPTER 6

### CONCLUSIONS AND RECOMMENDATIONS

#### 6.1 Conclusions

In this dissertation, the open problem in the literature of designing feedback controllers that guarantee stability for seismic structures coupled with the nonlinear dynamics of semi-active actuators is investigated. There are two difficulties associated with this open problem. One was that the state matrix of the original coupled system possesses a zero eigenvalue. The zero eigenvalue made it impossible to directly construct a positive definite matrix  $P$  needed in a quadratic Lyapunov function to prove stability. A linear term was added and subtracted to the dynamics of the differential pressure state to avoid this difficulty. The resulting state matrix of the revised coupled system is Hurwitz (i.e., all eigenvalues have negative real parts), which permits the construction of a positive definite matrix  $P$  needed in the quadratic Lyapunov function.

The second difficulty encountered was the presence of the non-quadratic term in the gradient of the Lyapunov function resulting from the nonlinear dynamics of the semi-active actuator. This difficulty was addressed by establishing two general conditions (Section 4.3) to be met by the nonlinear dynamics that could help guarantee a negative gradient for the non-quadratic term and thus stability for the closed-loop semi-active control system. The nonlinear dynamics of semi-active actuators (in particular, variable-orifice hydraulic types that account for laminar, turbulent and transition flow characteristics) are shown to satisfy these two general Conditions I and II. Furthermore, the two general conditions define a wide class of semi-active control systems for which it

is possible to construct a feedback controller that guarantees stability of the closed-loop system. In a theorem, it is established that the controllers designed using the quickest descent Lyapunov method guarantee stability for this wide class of semi-active control systems with nonlinear actuator dynamics. For the zero disturbance case, it was shown that the quickest descent Lyapunov controller provides asymptotic stability to the origin within the operating range of the semi-active actuator. For the non-zero disturbance case, the controller provides asymptotic stability to a stable attractor whose size depends on the upper bound of the disturbances. This solution to the open problem in the literature is one of the major results of this dissertation. This is the first time stability has been shown for semi-active control systems with nonlinear actuator dynamics.

Simulation results are presented to demonstrate the ease of tuning the performance of our quickest descent controllers by using either state or modal penalties. Three disturbance inputs were used to assess the control performance for a variety of control designs. The modal control laws with an emphasis on the fundamental frequency of the structure and the mode associated with the semi-active actuator provided the best response characteristics with at least a 67% reduction in peak inter-story drift. The maximum simulated values of the states were much lower than the theoretical stability bounds confirming that the stability results are relatively conservative in that they do not take into consideration the effect of the semi-active actuator.

Experiments were also conducted to verify the performance of the control law. The three-story structure was subjected to both a banded white noise input and a component of the 1940 El Centro earthquake. For the white noise acceleration input with the actuator in Position 1, the Lyapunov control law achieved a 78% reduction in

maximum relative displacement between the ground and first floor compared to the bare frame response while a generic minimum force/velocity control provided a 54% reduction. In Position 2, the Lyapunov control law reduced the maximum relative displacement between the ground and first floor by 48% and the force/velocity control afforded a 39% reduction. Both controllers provided similar reductions in RMS acceleration. For the El Centro input, both control laws provided similar performance gains indicating that performance is input specific. Even though the force/velocity control is simple to implement, the ability to tune the performance of the Lyapunov controller along with the stability results make it a much more desirable alternative.

## **6.2 Recommendations**

There are a number of obstacles that must be overcome before semi-active control systems become a feasible solution to the seismic response problem. For instance, a systematic approach is needed to optimize the performance of the semi-active control system. At the present time, numerical simulations must be conducted for each set of control gains to assess performance. The time and computer power required to optimize the control performance over the entire set of possible penalties is prohibitive for higher order systems. An effort should be made to develop control synthesis and analysis tools to aid in designing controllers for semi-active systems with nonlinear dynamics.

There is a need to improve methods for designing semi-active actuators for specific applications. This also would require the development of more efficient analysis techniques for nonlinear systems.

Future work should also attempt to develop more complete system models. For instance, thermal effects have a significant effect on the behavior of the hydraulic fluid properties and additional performance gains may be possible if such variations are taken into account.

The stability bounds developed in Chapter 4 were typically much larger than the maximum values obtained in simulation. Tighter stability bounds might be obtained if the contribution of the control was incorporated into the analysis. Alternative Lyapunov functions might also provide tighter stability bounds.

In the interest of occupant safety, design codes need to be developed for controlled structures as well as control actuators and fixtures. Such codes should also require a stability analysis be conducted before any control system is implemented in an occupied structure.

## REFERENCES

- [1] Akbay, Z., and Aktan, H., "Intelligent Energy Dissipation Devices," *Proceedings, US National Conference on Earthquake Engineering*, Palm Springs, CA, pp. 427-435, 1990.
- [2] Blondet, M., and Esparza, C., "Analysis of Shaking Table-Structure Interaction Effects During Seismic Simulation Tests." *Earthquake Engineering and Structural Dynamics*, Vol. 16, pp. 473-490, 1988.
- [3] Bobrow, J., Jabbari, F., and Thai, K., "Active Truss Element and Control Law for Vibration Suppression," *Smart Materials and Structures*. Vol. 4, pp. 264-269, 1995.
- [4] Brock, G., *Design and Experimental Validation of a Feedback/Feedforward Controller for a Seismic Simulator*. Masters Thesis, University of Oklahoma, School of Aerospace and Mechanical Engineering, 2000.
- [5] Cao, Y., *Design Sensitivity Analysis of a Hydraulic Structural Control System*. Masters Thesis, University of Oklahoma, School of Aerospace and Mechanical Engineering, 1999.
- [6] Chung, L., Reinhorn, A., and Soong, T., "Experiments on Active Control of Seismic Structures." *Journal of Engineering Mechanics*, Vol. 114, pp. 241-256, 1988.
- [7] Corless, M., and Leitmann, G., "Destabilization via Active Stiffness." *Dynamics and Control*, Vol. 7, pp. 263-268, 1997.
- [8] Dai, H., Sain, M., and Spencer, B., "Using Tensors to Track Earthquakes on Hydraulic Shaker Tables," *Proceedings, American Controls Conference*, Albuquerque, NM, 1997.

- [9] Dowdell, D., and Cherry, S., "Structural Control Using Semi-active Friction Dampers," *Proceedings, First World Conference on Structural Control*, Los Angeles, CA, Vol. FA1, pp. 59-68 1994.
- [10] Dulay, I., Fűrész, F., Harkay, G., and Lukács, J., *Fundamentals of Hydraulic Power Transmission*. Elsevier Science. NY, 1988.
- [11] Dyke, S., *Acceleration Feedback Control Strategies for Active and Semi-active Control Systems: Modeling, Algorithm Development, and Experimental Verification*, Doctoral Dissertation, University of Notre Dame, Department of Civil Engineering and Geological Sciences. 1996.
- [12] Dyke, S., Spencer, B., Quast, P., Kaspari, D., and Sain, M., "Implementation of an Active Mass Driver Using Acceleration Feedback Control." *Microcomputers in Civil Engineering*, Vol. 11, pp. 305-323, 1996a.
- [13] Dyke, S., Spencer, B., Sain, M., and Carlson, J., "Modeling and Control of Magnetorheological Dampers for Seismic Response Reduction." *Smart Materials and Structures*, Vol. 5, pp. 565-575, 1996b.
- [14] Dyke, S., Spencer, B., Sain, M., and Carlson, J., "An Experimental Study of MR Dampers for Seismic Protection." *Smart Materials and Structures*, Vol. 7, pp. 693-703, 1998.
- [15] Ehergott, R., and Masri, S., "Experimental Characterization of an Electrorheological Material Subjected to Oscillatory Shear Strains," *Journal of Vibration and Acoustics*, Vol. 116, pp. 53-60, 1994.
- [16] Feng, M., Shinozuka, M., and Fujii, S., "Friction Controllable Sliding Isolation System," *Journal of Engineering Mechanics*, Vol. 119, pp. 1845-1864, 1993.
- [17] Gavin, H., *Electrorheological Dampers for Structural Vibration Suppression*, Doctoral Dissertation, University of Michigan, Department of Civil Engineering, 1994.

- [18] Gavin, H., Hanson, R., and Filisko, F., "Electrorheological Dampers Part 1: Analysis and Design," *Journal of Applied Mechanics*, Vol. 63, pp. 669-682, 1996.
- [19] Housner G., Bergman, L., Caughey, T., Chassiakos, A., Claus, R., Masri, S., Skelton, R., Soong, T., Spencer, B., and Yao, J., "Structural Control: Past, Present and Future," *Journal of Engineering Mechanics*, Vol. 123, pp. 897-971, 1997.
- [20] Hrovat, D., Barak, P., and Rabbins, M., "Semi-active versus Passive or Active Tuned Mass Dampers for Structural Control," *Journal of Engineering Mechanics*, Vol. 109, pp. 691-705, 1983.
- [21] Jansen, L., and Dyke, S., "Semi-Active Control Strategies for MR Dampers: A Comparative Study," *Journal of Engineering Mechanics*, Vol. 126, pp.795-803, 2000.
- [22] Kalman, R., and Bertram, J., "Control System Analysis and Design via the Second Method of Lyapunov," *ASME Journal of Basic Engineering*, Vol. 82, pp. 371-399, 1960.
- [23] Kamagata, S., and Kobori, T., "Autonomous Adaptive Control of Active Variable Stiffness System for Seismic Ground Motion," *Proceedings, First World Conference on Structural Control*, Los Angeles, CA, Vol. TA4, pp. 33-42, 1994.
- [24] Karnopp, D., Crosby, M., and Harwood, R., "Vibration Control Using Semi-active Force Generators," *Journal of Engineering for Industry*, Vol. 96, pp. 619-626, 1974.
- [25] Kasturi, P., and Dupont, P., "Constrained Optimal Control of Vibration Dampers," *Journal of Sound and Vibration*, Vol. 215, pp. 499-509, 1998.
- [26] Kobori, T., Takahashi, M., Nasu, T., Niwa, N., and Ogasawara, K., "Seismic Response Controlled Structure with Active Variable Stiffness System," *Earthquake Engineering and Structural Dynamics*, Vol. 22, pp. 925-941, 1993.

- [27] Kuehn, J., Epp, D., and Patten, W.N., "A High Fidelity Control for Seismic Shake Tables," *Proceedings, ASCE 12<sup>th</sup> Engineering Mechanics Conference*, San Diego, CA, pp. 783-786, 1998.
- [28] Kuehn, J., Epp, D., and Patten, W.N., "High-fidelity Control of a Seismic Shake Table," *Earthquake Engineering and Structural Dynamics*, Vol. 28, pp. 1235-1254, 1999.
- [29] Kuehn, J., Sun, J., and Song, G., "Experimental Verification of a Non-protruding Intelligent Stiffener for Bridges," *International Post-SmiRT Conference on Seismic Isolation, Passive Energy Dissipation and Active Control of Vibrations of Structures*, Cheju, Korea, 1999.
- [30] Kurata, N., Kobori, T., Takahashi, M., Ishibashi, T., Niwa, N., Tagami, J., and Midorikawa, H., "Forced Vibration Test of a Building with Semi-Active Damper System," *Earthquake Engineering and Structural Dynamics*, Vol. 29, pp. 629-645, 2000.
- [31] Lee, J., *A Study of Semiactive Controls and Applications*, Doctoral Dissertation, University of Oklahoma, School of Aerospace and Mechanical Engineering, 1998.
- [32] Leitmann, G., "Semiactive Control for Vibration Attenuation," *Journal of Intelligent Material Systems and Structures*, Vol. 5, pp. 841-846, 1994.
- [33] Loh, C., and Ma, M., "Active Damping or Active Stiffness Control for Seismic Excited Buildings," *Proceedings, First World Conference on Structural Control*, Los Angeles, CA, Vol. TA2, pp. 11-20, 1994.
- [34] Merritt, H., *Hydraulic Control Systems*, John Wiley and Sons, Inc., NY, 1967.
- [35] Mo, C., Lee, J., Kuehn, J., Khaw, C., and Patten, W.N., "Fluid Compressibility Effects in Semiactive Vibration Absorbers (SAVA)," *Active Control of Vibration and Noise*, ASME Winter Annual Meeting, Atlanta, GA, DE Vol. 93, pp. 197-204, 1996.

- [36] Mo, C., *Semiactive Vibration Absorbers (SAVA) for Auto Seat/Suspension*, Doctoral Dissertation, University of Oklahoma, School of Aerospace and Mechanical Engineering, 1996.
- [37] Mohler, R., *Nonlinear Systems, Volume 1, Dynamics and Control*, Prentice Hall, NJ, 1991.
- [38] Nagarajaiah, S., and Mate, D., "Semi-active Control of Continuously Variable Stiffness System," *Proceedings, Second World Conference on Structural Control*, Kyoto, Japan, pp. 397-405, 1998.
- [39] Newell, D., Dai, H., Sain, M., Quast, P., and Spencer, B., "Nonlinear Modeling and Control of a Hydraulic Seismic Simulator," *Proceedings, American Controls Conference*, Seattle, WA, pp. 801-805, 1995.
- [40] Niwa, N., Kobori, T., Takahashi, M., Matsunaga, Y., Kurata, N., and Mizuno, T., "Applications of a Semi-active Damper System to an Actual Building," *Proceedings, Second World Conference on Structural Control*, Kyoto, Japan, pp. 815-824, 1998.
- [41] Patten, W.N., Kuo, C., He, Q., Liu, L., and Sack, R., "Seismic Structural Control via Hydraulic Semiactive Vibration Dampers (SAVD)," *Proceedings, First World Conference on Structural Control*, Los Angeles, CA, Vol. FA2, pp. 83-89, 1994.
- [42] Patten, W.N., "The I-35 Walnut Creek Bridge: An Intelligent Highway Bridge via Semi-Active Structural Control," *Proceedings, Second World Conference on Structural Control*, Kyoto, Japan, pp. 427-436, 1998.
- [43] Patten, W.N., Mo, C., Kuehn, J., and Lee, J., "A Primer on Design of Semiactive Vibration Absorbers (SAVA)," *Journal of Engineering Mechanics*, Vol. 124, pp. 61-68, 1998.
- [44] Patten, W.N., Sun, J., Li, G., Kuehn, J., and Song, G., "Field Test of an Intelligent Stiffener for Bridges at the I-35 Walnut Creek Bridge," *Earthquake Engineering and Structural Dynamics*, Vol. 28, pp. 109-126, 1999.

- [45] Sadek, F., and Mohraz, B., "Semiactive Control Algorithms for Structures with Variable Dampers," *Journal of Engineering Mechanics*, Vol. 124, pp. 981-990, 1998.
- [46] Sakamoto, M., Kobori, T., Yamada, T., and Takahashi, M., "Practical Applications of Active and Hybrid Response Control Systems and Their Verifications by Earthquake and Strong Wind Observations." *Proceedings, First World Conference on Structural Control*, Los Angeles, CA, Vol. WP2, pp. 90-99, 1994.
- [47] Singh, M., Matheu, E., and Suarez, L., "Active and Semi-active Control of Structures Under Seismic Excitation." *Earthquake Engineering and Structural Dynamics*, Vol. 26, pp. 193-213, 1997.
- [48] Soong, T., Reinhorn, A., and Yang, J., "A Standardized Model for Structural Control Experiments and Some Experimental Results." *Proceedings, 2<sup>nd</sup> International Symposium on Structural Control*, Waterloo, Canada, pp. 669-693, 1987.
- [49] Spencer, B., and Sain, M., "Controlling Buildings: A New Frontier in Feedback." *IEEE Control System*, Vol. 6, pp.19-35, 1997.
- [50] Spencer, B., Dyke, S., Sain, M., and Carlson, J., "Phenomenological Model of a Magnetorheological Damper," *Journal of Engineering Mechanics*, Vol. 123, pp. 230-238, 1997.
- [51] Spencer, B., and Yang, G., "Earthquake Simulator Control by Transfer Function Iteration." *Proceedings, ASCE 12<sup>th</sup> Engineering Mechanics Conference*, San Diego, CA, pp. 766-769, 1998.
- [52] Spencer, B., Yang, G., Carlson, J., and Sain, M., "'Smart' Dampers for Seismic Protection of Structures: A Full-Scale Study," *Proceedings, Second World Conference on Structural Control*, Kyoto, Japan, pp. 417-426, 1998.

- [53] Symans, M., *Development and Experimental Study of Semi-active Fluid Damping Devices for Seismic Protection of Structures*, Doctoral Dissertation, State University of New York at Buffalo, 1995.
- [54] Symans, M., and Constantinou, M., "Seismic Testing of a Building Structure with a Semi-active Fluid Damper Control System." *Earthquake Engineering and Structural Dynamics*, Vol. 26, pp. 759-777, 1997.
- [55] Symans, M., and Twitchell, B., "System Identification of a Uniaxial Seismic Simulator." *Proceedings, ASCE 12<sup>th</sup> Engineering Mechanics Conference*, San Diego, CA, pp. 758-761, 1998.
- [56] Symans, M., and Constantinou, M., "Semi-active Control Systems for Seismic Protection of Structures: a State-of-the-art Review." *Engineering Structures*, Vol. 21, pp. 469-487, 1999.
- [57] Symans, M., and Kelly, S., "Fuzzy Logic Control of Bridge Structures Using Intelligent Semi-active Seismic Isolation Systems." *Earthquake Engineering and Structural Dynamics*, Vol. 28, pp. 37-60, 1999.
- [58] Trombetti, T., and Conte, J., "Actuator-Foundation-Specimen Interaction in a Small Shaking Table." *Proceedings, ASCE 12<sup>th</sup> Engineering Mechanics Conference*, San Diego, CA, pp. 770-773, 1998.
- [59] Vincent, T., and Grantham, W., *Nonlinear and Optimal Control Systems*, John Wiley and Sons, Inc., NY, 1997.
- [60] Yao, J., "Concept of Structural Control," *ASCE Journal of Structural Division*, Vol. 98, pp. 1567-1574, 1972.
- [61] Zhuang, W., *Optimal Design Analysis of a Semi-active Tuned Mass Hydraulic Damper for Structural Control*, Masters Thesis, University of Oklahoma, School of Aerospace and Mechanical Engineering, 1999.